Doctoral Dissertation

Design of Boron-Rich Cathodic Electrolyte Interphase to Enhance the Performance of Li-ion Secondary Batteries

LIU Zhaohan

Supervisor: Noriyoshi Matsumi

Graduate School of Advanced Science and Technology

Japan Advanced Institute of Science and Technology

Materials Science

March 2025

Abstract

LIU Zhaohan (2220032)

Lithium-ion batteries (LIBs) are pivotal in modern energy storage systems, powering applications ranging from portable electronics to electric vehicles (EVs) and grid-scale storage. Despite their widespread use, challenges such as limited energy density, performance degradation under high rates, and reduced stability at extreme conditions hinder their full potential. This study focuses on addressing these limitations through advanced electrolyte design and cathode optimization, emphasizing the integration of boron-containing additives and the development of stable interphases.

The research highlights the importance of cathode-active materials (CAMs) such as layered oxides, including $LiNi_{0.33}Mn_{0.33}Co_{0.33}O_2$ (NMC111) and nickel-rich variants like $LiNi_{0.8}Mn_{0.1}Co_{0.1}O_2$ (NMC811), in achieving high energy densities. While these materials offer excellent performance, they face challenges such as transition metal dissolution, interfacial instability, and structural degradation during prolonged cycling. These issues underscore the need for optimized electrolytes capable of forming robust cathode-electrolyte interphases (CEIs) to mitigate degradation and enhance overall battery performance.

To address these challenges, boron-containing compounds were investigated as key components in electrolyte formulations. Mesityldimethoxyborane (MDMB) was introduced as a multifunctional electrolyte component to improve lithium-ion transport and interfacial stability. By modifying the solvation structure and reducing anion mobility, MDMB enhanced ionic conductivity and facilitated the formation of a boron-rich CEI. This interphase effectively stabilized the cathode, minimized side reactions, and improved cycling performance under high current densities. Electrochemical impedance spectroscopy (EIS) and computational modeling validated MDMB's role in optimizing electrolyte dynamics, demonstrating reduced overpotential and enhanced lithium-ion transference.

Building on this foundation, ethylene glycol mesityl borane (EGMB), a novel cyclic boric ester, was synthesized and incorporated as a functional additive to improve battery performance under extreme conditions. EGMB exhibited significant benefits, forming a CEI enriched with boron and fluorine. This robust interphase not only improved mechanical and chemical stability but also mitigated oxygen release and transition metal dissolution, which are common issues with Ni-rich cathodes. The enhanced CEI facilitated high lithium-ion conductivity, resulting in improved discharge capacities and extended cycle life, even under ultrahigh voltages (up to 4.8 V), fast charging, and wide temperature ranges. Electrochemical evaluations confirmed EGMB’s ability to enhance compatibility with NMC cathodes, achieving high capacity retention and Coulombic efficiency over extended cycling.

The research demonstrates that boron-based additives or electrolyte component can effectively address critical issues in LIBs, including interfacial instability and poor lithium-ion transport. By tailoring electrolyte formulations to incorporate boron-containing compounds, this work provides a pathway to enhance the durability, safety, and performance of LIBs in demanding applications. These findings contribute to the advancement of next-generation LIBs capable of meeting the growing energy demands of modern technology while maintaining operational stability across diverse conditions.

This study underscores the transformative potential of electrolyte engineering in overcoming the limitations of current LIB technologies. By integrating innovative boron chemistry and interfacial design strategies, this research paves the way for the development of high-performance energy storage systems suitable for a broad range of applications, from consumer electronics to electric mobility and renewable energy solutions.

Keywords: Lithium-ion battery, electrolyte, additive, boron compounds, high voltage.

Referee-In-Chief: Professor Noriyoshi Matsumi
Japan Advanced Institute of Science and Technology

Referees: Professor Yoshifumi Oshima
Japan Advanced Institute of Science and Technology

Professor Toshiaki Taniike
Japan Advanced Institute of Science and Technology

Professor Kazuma Gotoh
Japan Advanced Institute of Science and Technology

Professor Kaoru Adachi
Kyoto Institute of Technology

Acknowledgements

First and foremost, I would like to express my heartfelt gratitude to my advisor, Professor Matsumi, for his steadfast guidance, invaluable insights, and unwavering support throughout my research journey. His expertise and encouragement have been pivotal in shaping this thesis and fostering my academic growth. I am deeply grateful for the opportunity to work under his mentorship, which allowed me to embark on fascinating research into the electrolytes of lithium-ion batteries—work that aligns with my passions and aspirations. Prof. Cui, Prof. Zhao and Dr. Ren also supported me a lot in the minor research studies.

I am also profoundly grateful to my friends and colleagues, especially Dr. Amarshi, whose collaboration and daily discussions over the past three years have been invaluable. Our shared enthusiasm for research has not only enriched my academic experience but also made the journey more enjoyable. I sincerely hope we can continue to collaborate in the future.

To my family, I owe my deepest thanks for their unconditional love, encouragement, and unshakable belief in me. They have been my anchor during challenging times, standing by my side and giving me the strength to overcome difficulties. Their unwavering support and understanding have meant the world to me, and I cherish them deeply. No matter what, my love for them will endure forever.

I would like to extend a special note of gratitude to my husband, Du Wentao, and his family, for their patience, understanding, and steadfast support. His encouragement and faith in me have been a constant source of strength and inspiration. Having him by my side has made this journey immeasurably more meaningful, and I feel truly fortunate to have him in my life.

I am also deeply appreciative of Dr. Wu, Dr. Xu and Ms. Lu, whose exceptional support and the care provided by their team helped me both physically and mentally. Without their help,

completing my studies and research would have been much more challenging.

To all who have contributed to this work, directly or indirectly, I extend my sincere thanks. This accomplishment would not have been possible without each and every one of you.

LIU Zhaohan

Graduate School of Advanced Science and Technology

Japan Advanced Institute of Science and Technology

March 2025

Table of Contents

Chapter 1 General Introduction

1.1 Introduction to highly efficient energy device-lithium battery

A battery is a device composed of electrochemical cells, which convert stored chemical energy into electrical energy through specific electrochemical reactions. These reactions, typically involving reduction-oxidation (redox) processes, result in the transfer of electrons between two materials through an external circuit. Based on the nature of the redox reaction, batteries can be classified into primary (non-rechargeable) [1-4] and secondary (rechargeable) types [5-9].

Primary batteries undergo irreversible redox reactions, meaning the active materials are permanently altered and cannot be restored to their original state. As a result, they can only be used once before disposal. These batteries generally offer higher energy densities and are advantageous for applications requiring simplicity, portability, long shelf life, and convenient design flexibility [10].

In contrast, secondary (rechargeable) batteries feature reversible redox reactions, allowing them to be recharged and reused multiple times. The electrochemical reactions in these batteries can be reversed by applying an external electric current, enabling repeated charge-discharge cycles, depending on the stability of the materials used [11]. The lead-acid battery, one of the earliest examples of rechargeable batteries, is known for its durability and long lifespan [12]. However, its use has declined due to factors such as high cost, maintenance requirements, and lower specific energy compared to newer battery technologies. Thus, while primary batteries excel in single-use applications, secondary batteries provide a more sustainable and long-term energy solution through reusability [13].

The rapid advancement of battery technology began in the 20th century, driven in part by the environmental and resource concerns associated with gasoline-powered automobiles. In the mid-20th century, the global rise in automobile use led to an increase in harmful smog, particularly in major cities, exacerbated by the emissions from internal combustion engines.

This, combined with growing awareness of the finite nature of oil reserves, prompted a shift in focus toward alternative energy and electric vehicles (EVs). To support these innovations, there was a pressing need for efficient, high-capacity batteries capable of storing significant amounts of energy.

At that time, the available rechargeable batteries were limited to two main types: the lead-acid battery, first invented in 1859 and still used as a starter battery in gasoline vehicles, and the nickel-cadmium (NiCd) battery, developed earlier in the 20th century. In the early 1970s, Stanley Whittingham made a breakthrough by leveraging the high energy potential of lithium, which can release electrons from its outer layers. His work led to the development of the first functional lithium battery.

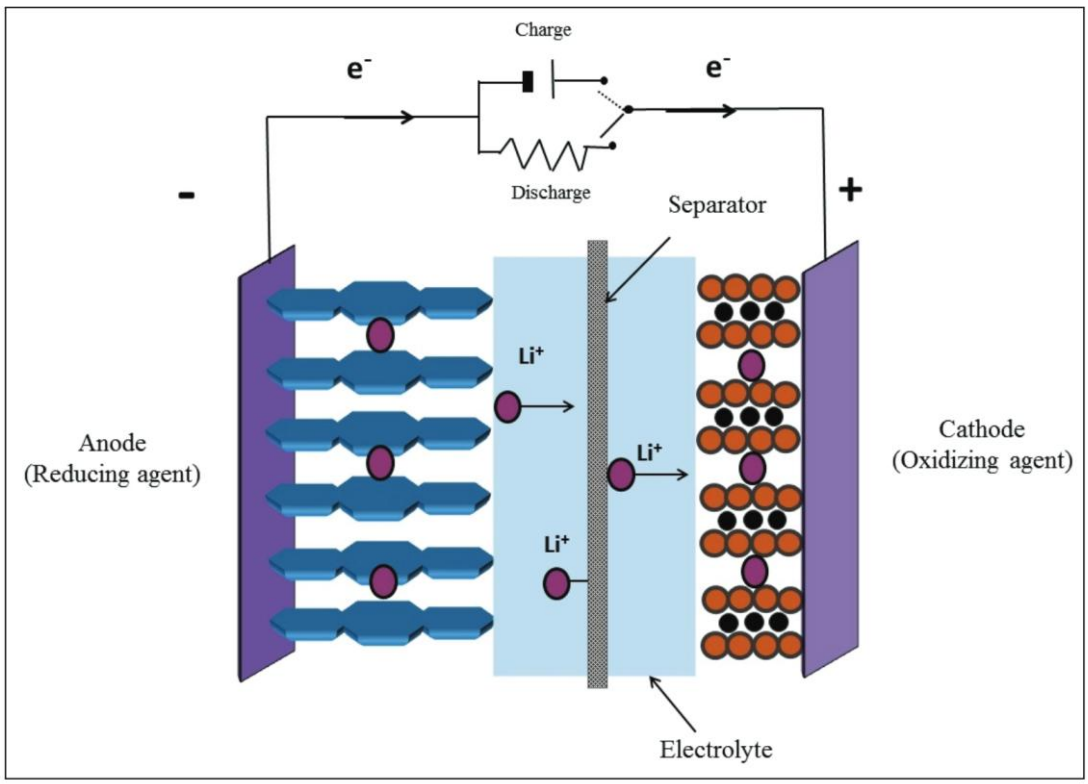

Figure 1. Schematic graph of Lithium-ion battery [14].

In 1980, John Goodenough advanced this technology further, doubling the battery's potential and laying the groundwork for more powerful and practical energy storage solutions.

By 1985, Akira Yoshino improved upon these developments by replacing pure lithium with graphite anode, as shown in **Figure 1**, which are safer and more stable, making lithium-ion batteries viable for commercial use [14-15]. Lithium-ion batteries have revolutionized energy storage and powered the development of portable electronics, such as laptops and smartphones, as well as electric vehicles. They have also played a crucial role in enabling the storage of renewable energy from sources like solar and wind power, marking a significant leap forward in both energy efficiency and sustainability.

As lithium battery technology has evolved from its inception in the last century to the present day, researchers have continuously pushed the boundaries to develop next-generation batteries capable of meeting diverse and increasing human demands [16]. The goal is to create energy storage solutions that are not only powerful and efficient but also safer, more sustainable, and adaptable to various applications [17]. By improving energy density [18], accelerating charging speeds [19], enhancing recycling [20] and sustainability practices [21], and ensuring stability across temperature ranges [22-24], researchers aim to address the limitations of current lithium-ion technology. These advancements promise to make batteries more suitable for high-demand applications, from electric vehicles and consumer electronics to renewable energy storage, ultimately supporting a cleaner and more energy-efficient future [25]

(1) Higher Energy Density

Higher energy density in lithium batteries means increasing the amount of energy stored per unit mass or volume, allowing for longer usage times between charges [26-28]. This is especially important for applications requiring compact and lightweight power sources, such as electric vehicles (EVs) and portable electronics. Increasing the energy density of lithium batteries is crucial to meet the growing demands for longer battery life and higher power in a limited space. For EVs, higher energy density translates to extended driving range, reducing 'range anxiety' and making EVs more viable for consumers [29]. In consumer electronics, it

allows devices to become smaller, lighter, and more efficient, all while providing more operational hours.

Increasing the cut-off voltage of batteries is an effective approach to achieving higher energy density [30]. The cut-off voltage is the maximum voltage to which a battery cell can be charged before it risks degradation or safety issues. By raising this voltage limit, the energy stored in the battery increases, as the total energy output is directly related to both the capacity and the operational voltage range.

However, higher cut-off voltages place greater demands on the battery's materials, especially on the electrolyte and cathode, as they need to withstand more intense oxidative and thermal stress [31-33]. To enable higher voltage operation without compromising safety or cycle life, researchers are developing advanced electrolyte formulations that are more resistant to high-voltage decomposition. These include high-voltage-tolerant electrolytes, such as those with fluorinated solvents or solid-state components, which provide improved oxidative stability [34].

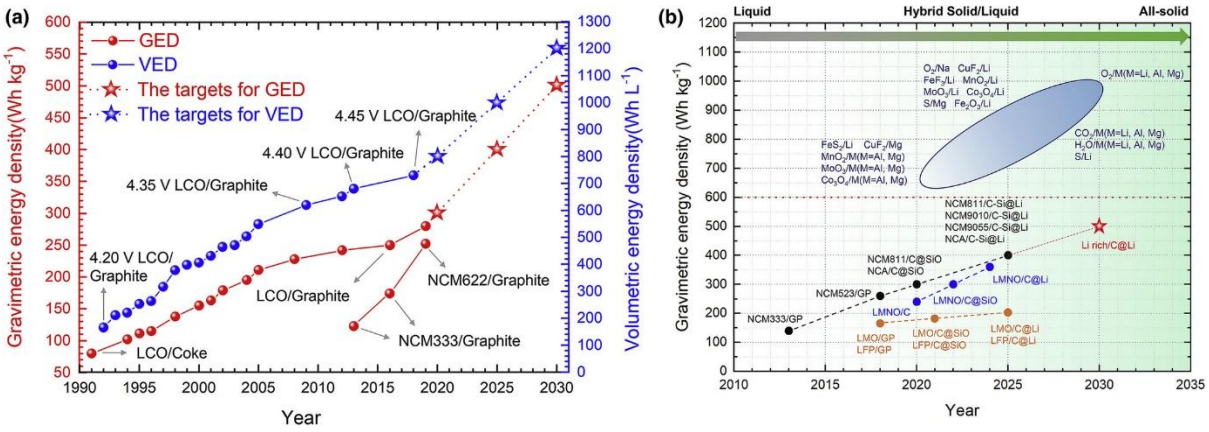

Figure 2. (a) Gravimetric energy density (GED) and volumetric energy density (VED) of currently commercialized LIBs with $LiCoO_2$ and high-nickel materials as cathodes; b) development of high-energy-density LIBs on the basis of present cathode and anode materials for the next decade [27].

Cathode materials with higher structural integrity at elevated voltages, such as nickel-rich

layered oxides and lithium cobalt nickel oxide, as shown in **Figure 2a,** are also being explored to sustain performance at higher voltages [35]. Protective coatings on both electrodes are another promising strategy, as they prevent direct contact between reactive species in the electrolyte and the electrode surface, reducing side reactions and prolonging battery life.

As presented in **Figure 2b**, by combining these material innovations with advanced electrolyte and electrode designs, increasing the cut-off voltage can unlock substantial energy density gains, making lithium batteries more powerful and versatile for applications requiring compact, high-energy solutions.

(2) Faster Charging

Faster charging refers to reducing the time it takes to fully charge a lithium battery, making it comparable to or faster than refueling conventional vehicles with gasoline [36]. This is particularly critical for EV applications where charging times are still significantly longer than gas refueling times. Rapid charging is essential for enhancing the user experience and practicality of lithium batteries in consumer electronics and EVs. In the context of EVs, faster charging reduces downtime and improves convenience, helping drive adoption [37]. For consumer devices, rapid charging supports high-performance lifestyles where users need devices quickly recharged.

Developing electrolytes with higher ionic conductivity is crucial for enabling quicker lithium-ion transport, which directly facilitates faster charging rates [38]. The ionic conductivity of an electrolyte determines how easily lithium ions can move between the anode and cathode during the charge and discharge processes[39]. When ionic conductivity is enhanced, lithium ions can travel more rapidly through the electrolyte, reducing the time required for a full charge [40].

To achieve higher ionic conductivity, researchers are exploring a variety of advanced electrolyte formulations. One approach is to modify liquid electrolytes by adding lithium salts

with specific anions that increase ionic mobility [41]. Another promising avenue involves solid-state electrolytes, such as lithium garnets and sulfide-based materials, which can achieve high ionic conductivities and enable fast charging while improving overall safety. Gel polymer electrolytes, which combine liquid-like ionic mobility with the stability of a solid matrix, are also being developed as a middle ground between traditional liquid and solid electrolytes [42].

Additionally, enhancing electrolyte conductivity can be achieved by optimizing the electrolyte's solvent composition to reduce viscosity and by adjusting the concentration of lithium salts to create a more favorable environment for ion movement [43-44]. By employing these strategies, researchers aim to create electrolytes that support rapid charging without compromising the battery's safety, stability, or lifespan, making fast-charging lithium batteries a feasible reality for electric vehicles and other high-power applications [45].

(3) Temperature Stability

Temperature stability in lithium-ion batteries is crucial to ensure that they operate safely and effectively across a broad temperature range without degradation or risk of failure, as shown in **Figure 3** [46]. This requirement is especially critical in applications subject to extreme or fluctuating temperatures, such as electric vehicles, grid energy storage, and aerospace systems. Lithium-ion batteries are particularly sensitive to temperature variations [47], which can negatively impact their performance, reduce their lifespan, and, in severe cases, lead to safety risks such as thermal runaway—a condition where excessive heat accumulation results in uncontrollable reactions and potential battery failure.

Enhancing temperature stability is essential to achieve the reliability and safety standards necessary for widespread adoption, especially in fields like automotive and energy storage, which demand high safety margins. Developing thermally robust electrolyte formulations is a key strategy to address this need [48]. Emerging electrolyte chemistries, including fluorinated and

solid-state electrolytes, show promise in resisting thermal decomposition and sustaining performance under high temperatures [49]. Similarly, selecting electrode materials that retain their structural integrity at elevated temperatures can mitigate thermal degradation risks [50]. Advances in materials science, such as incorporating temperature-resistant polymers or applying ceramic coatings, further help extend the safe operational range of lithium-ion batteries by providing additional protection against heat-induced damage [51].

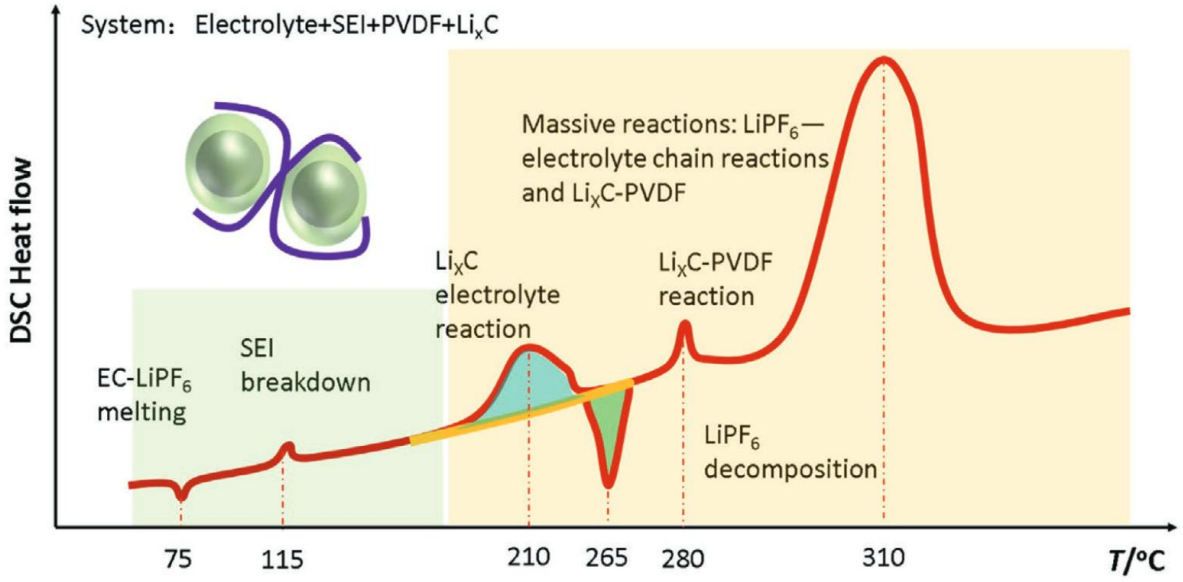

Figure 3. Schematic DSC profile of anode thermal stability [51].

Together, these efforts target fundamental aspects of lithium battery technology—including energy density, charging speed, and safety—to meet the growing demands across diverse applications, from consumer electronics to EVs and large-scale energy storage solutions.

1.2 Various cathodes in lithium battery

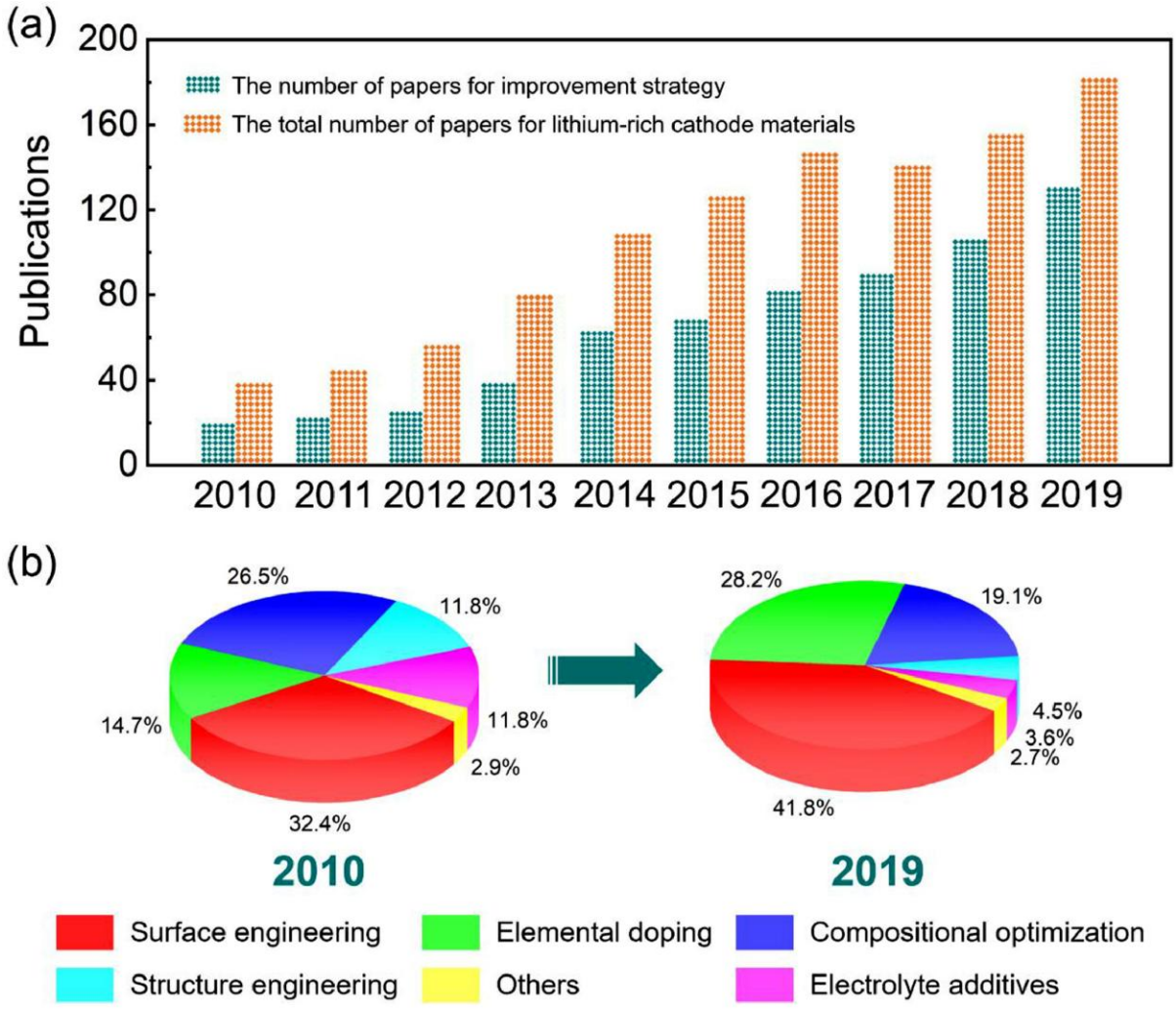

Figure 4. (a) The number of publications on LRCMs sorted by year. (b) The percentage of various improvement strategies between 2010 and 2019 [52].

Selecting appropriate cathode-active materials (CAMs) is vital for advancing lithium-ion battery (LIB) performance, particularly in terms of energy density, lifespan, safety, and cost-efficiency, as shown in **Figure 4** [52]. LIBs employ a variety of cathode chemistries, each with distinct advantages and drawbacks. The most widely studied CAMs fall into three main categories: (a) polyanionic compounds, (b) spinel oxides, and (c) layered oxides [53].

(a) The symbol of **polyanionic compounds** is Lithium Iron Phosphate ($LiFePO_4$). It stands out for its excellent safety and long cycle life, characteristics that are particularly

desirable in heavy-duty applications like electric vehicles and renewable energy storage [54]. $LiFePO_4$'s thermal and chemical stability reduces risks associated with thermal runaway, and it is environmentally friendlier than cobalt-based cathodes. However, its lower energy density and operating voltage mean that it may not be suitable for compact, high-capacity storage needs, as it delivers less energy per charge [55].

(b) The symbol of **spinel oxides**. Lithium Manganese Oxides ($LiMn_2O_4$) are another commonly used cathode materials valued for its thermal stability and cost-effectiveness, as manganese is more abundant and affordable than cobalt [56]. It also provides high power output, beneficial for fast-charging applications. However, its energy density is lower compared to $LiCoO_2$, limiting its use in applications where extended battery life is crucial [57]. $LiMn_2O_4$ also has a relatively short cycle life, with faster degradation at high temperatures, making it more suitable for power tools and medical devices, where safety and cost considerations are prioritized [58].

(c) **Layered oxide cathodes** come in a range of compositions, each with specific advantages and limitations tailored for distinct applications. $LiCoO_2$ offers high energy density, making it particularly suitable for portable electronics like smartphones and laptops [59]. Its stable cycling performance is advantageous, but due to cobalt's scarcity, $LiCoO_2$ is expensive and poses environmental and ethical concerns related to mining practices [60]. Furthermore, its thermal instability at high temperatures raises safety issues, especially in larger applications such as electric vehicles.

Nickel Manganese Cobalt Oxide (NMC) cathodes, with varying ratios of nickel, manganese, and cobalt, offer a balanced performance profile that makes them ideal for use in electric vehicles and power tools [61]. Within the NMC family, compositions such as NMC111 (1:1:1 ratio) and NMC811 (8:1:1 ratio) provide options for adjusting capacity, stability, and cost-effectiveness. NMC111 strikes a practical balance between energy density, power density,

and cycle life, making it a versatile and relatively affordable choice [62]. It is safer than $LiCoO_2$, though less thermally stable than $LiFePO_4$, and has a lower energy density than newer formulations like NMC811. NMC811, a nickel-rich formulation, offers higher capacity and operating voltage since nickel (Ni) serves as the primary redox-active species ($Ni^{2+} \leftrightarrows Ni^{4+}$) [63]. However, it requires precise manufacturing controls to maintain performance and exhibits lower thermal stability than NMC111, necessitating careful battery management.

Table 1: Theoretical capacity and practical capacity of various cathodic materials

Cathodic material	$LiCoO_2$	$LiNi_xCo_yMn_{1-x-y}O_2$	$LiMn_2O_4$	$LiFePO_4$
Theoretical Capacity (mAh/g)	274	275	148	170
Practical Capacity (mAh/g)	140	160-220	120	150
Voltage Platform(V)	3.7	3.5-4.0	4.0	3.3
Cyclability	Good	Fair	Poor	Excellent
Metal Resource Reserves	Poor	Fair	Abundant	Abundant

NMC materials achieve a balance of stability, cost, and energy density, with manganese (Mn) providing long cycle life and cobalt (Co) enhancing electronic conductivity, which improves rate capability. These characteristics have led to widespread commercialization of NMC, with major producers like Panasonic, Toshiba, and LG Chem advancing its use. NMC cathodes theoretically offer capacities around 275 mAh g^{-1}, though actual capacity depends on the transition metal composition and formulation, as shown in **Table 1 and Figure 5** [64]. While Ni-rich NMC variants like NMC811 offer higher capacities, they are also more prone to

degradation mechanisms, including cation mixing, surface reconstruction into rock salt phases, phase transformations, particle cracking, transition metal dissolution, and undesirable side reactions with the electrolyte [65].

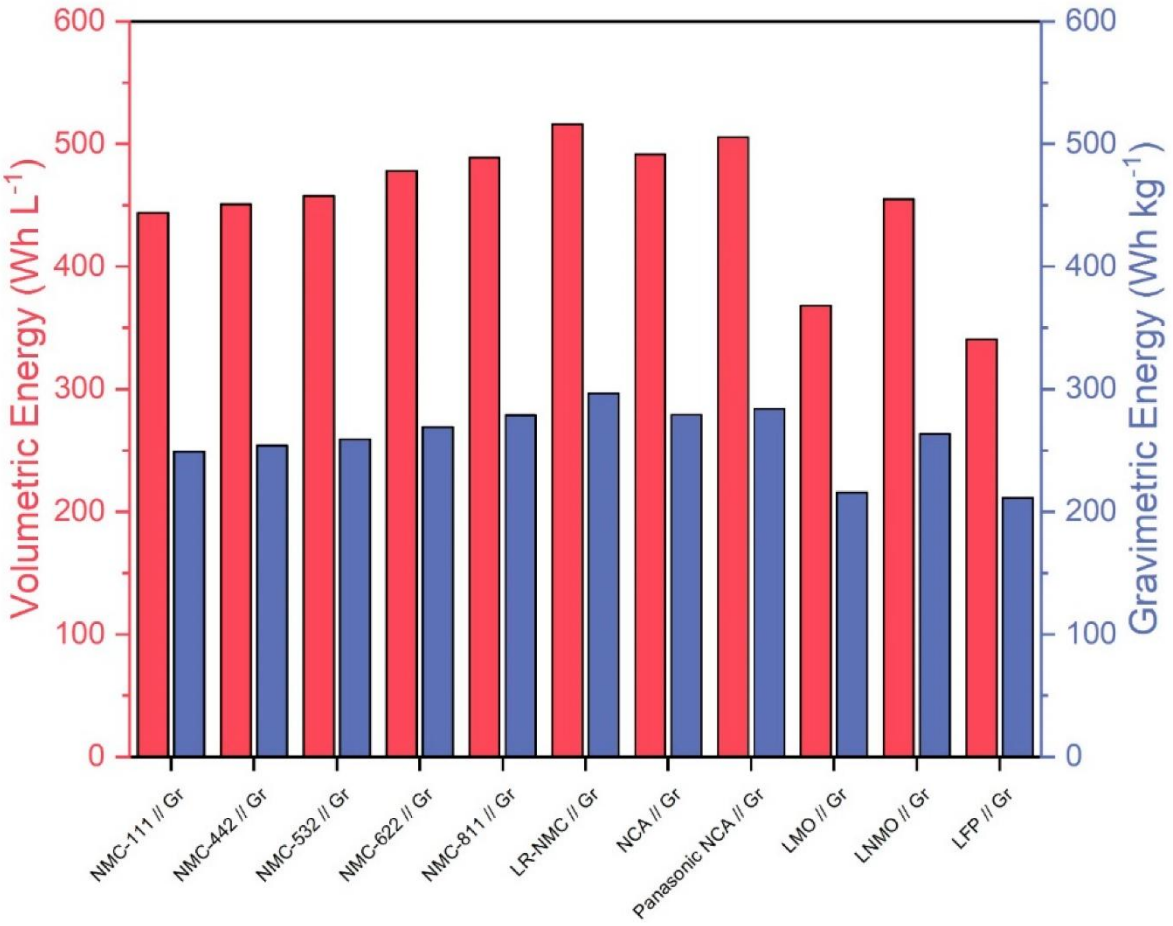

Figure 5. Volumetric energy in (Wh L^{-1}) based on used material volume and gravimetric energy in (Wh kg^{-1}) of the 10 considered cell chemistries plus the Panasonic NCA Use Case [65].

The performance of lithium-ion batteries (LIBs) at high voltages also depends on the stability of the electrolyte. At voltages above 4.4 V, the electrolyte is susceptible to oxidative degradation, which can lead to oxygen release from the cathode, increased reactivity of the de-lithiated phase, and transition metal dissolution due to structural instability [66]. A common solution is the addition of electrolyte additives. These additives stabilize the cathode-electrolyte

interface, reduce interfacial resistance, and limit transition metal dissolution by forming a protective layer on the cathode surface [67]. This approach preserves capacity and prolongs battery life, especially for high-voltage applications. Through these innovations, layered oxide cathodes enable LIBs to meet diverse energy, safety, and cost requirements across a broad spectrum of applications, from consumer electronics to electric vehicles and grid storage solutions.

In conclusion, selecting the appropriate cathode-active materials (CAMs) is essential to optimize lithium-ion battery performance, balance energy density, cycle life, safety, and cost. Polyanionic compounds, spinel oxides, and layered oxides each brings unique benefits suited to different applications. Continued advancements in CAMs are key to enhance lithium-ion batteries for diverse energy storage needs, from consumer electronics to electric vehicles.

1.3 Introduction to components of electrolyte

The electrolyte in lithium-ion batteries (LIBs) plays a crucial role in determining the battery's performance, stability, and safety, making it a central focus in advancing next-generation energy storage, as shown in **Figure 6** [68]. As an ionic conductor, the electrolyte facilitates lithium-ion transport between the anode and cathode during charge and discharge cycles, directly influencing charge rate, energy density, and cycle life [69]. An ideal electrolyte must exhibit high ionic conductivity, chemical stability, and compatibility with both electrodes across a range of temperatures and voltages, all while minimizing side reactions that could degrade battery performance or safety [70]. The main components of LIB electrolytes are organic solvents, lithium salts, and functional additives, each contributing distinct properties to optimize electrolyte behavior.

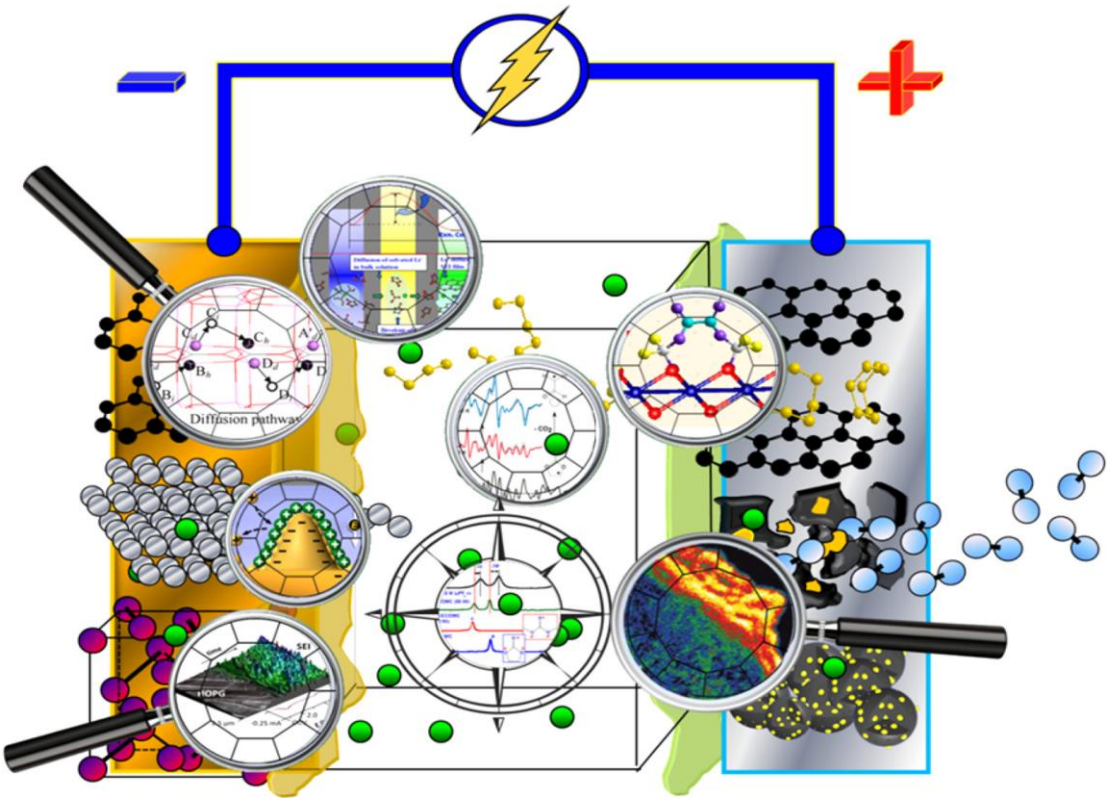

Figure 6. During 2003–2014, significant advances have been made in the development of new electrolyte components (lithium salts, solvents, and additives) and fundamental understanding of the related interphasial chemistry in both lithium ion and advanced rechargeable batteries [68].

Solvents in LIB electrolytes are typically organic carbonates that dissolve lithium salts and facilitate ion movement. Commonly used solvents include ethylene carbonate (EC), dimethyl carbonate (DMC), and propylene carbonate (PC) [71]. Ethylene carbonate is essential in LIB electrolytes due to its high dielectric constant, which supports effective salt dissociation, enhancing ionic conductivity. EC, however, is solid at room temperature, so it is often combined with low-viscosity solvents like dimethyl carbonate (DMC) or diethyl carbonate (DEC) to reduce viscosity and improve the low-temperature performance of the electrolyte [72]. Propylene carbonate, while highly polar and thermally stable, is less commonly used in commercial LIBs due to its reactivity with graphite anodes, although it remains a valuable component in high-temperature applications [73]. The appropriate combination of these solvents is vital to achieve a balance of ionic conductivity, stability, and compatibility with both

electrodes.

The **lithium salt** used in LIB electrolytes also profoundly impacts battery performance. The most widely used lithium salt is lithium hexafluorophosphate ($LiPF_6$), prized for its high ionic conductivity and compatibility with typical carbonate solvents [74]. $LiPF_6$, however, is thermally unstable and can decompose to form HF under high-temperature conditions, which can accelerate degradation and safety risks. To address these limitations, alternative salts such as lithium bis(trifluoromethanesulfonyl)imide (LiTFSI) [75] and lithium bis(fluorosulfonyl)imide (LiFSI) [76] are gaining attention due to their superior thermal stability, enhanced conductivity, and ability to stabilize the electrode-electrolyte interface. Both LiTFSI and LiFSI are also less prone to HF formation, thereby reducing corrosive effects on battery components and extending cycle life, making them attractive for high-performance LIB applications.

Electrolyte additives are another key component, introduced in small amounts to improve specific performance aspects of the electrolyte. In lithium-ion batteries, additives such as vinylene carbonate (VC) and fluoroethylene carbonate (FEC) are commonly used to enhance electrolyte stability, protect electrode surfaces, and improve overall battery performance [77]. These additives are particularly valuable because they contribute to the formation of a stable and robust solid electrolyte interphase (SEI) layer on the anode, a critical factor for maintaining battery longevity and safety, especially at high voltages and low temperatures [78]. Vinylene Carbonate (VC) is one of the earliest and most widely used electrolyte additives for lithium-ion batteries. VC is known for its ability to improve the SEI layer on the anode, particularly in graphite-based systems [79]. When added to the electrolyte in small concentrations, VC undergoes reduction reactions at the anode during the initial charging cycles, forming a protective SEI layer that is both stable and effective in preventing further decomposition of the electrolyte. This SEI layer acts as a barrier, significantly reducing continuous electrolyte decomposition, which improves cycle life and reduces capacity fade. VC also helps to stabilize

the battery during high-temperature operation, reducing the risk of thermal runaway and enhancing battery safety. However, VC has limited solubility in many electrolyte solvents, which restricts the concentration that can be used, and it can increase the internal resistance of the battery under certain conditions.

Fluoroethylene Carbonate (FEC) is another important additive, particularly advantageous in systems using silicon-based anodes, which tend to experience significant volume expansion during cycling [80]. FEC, like VC, helps in forming a stable SEI layer, but with even greater effectiveness in high-stress environments. FEC's molecular structure, which includes a fluorine atom, enhances its stability under electrochemical conditions. This structure allows FEC to form a more flexible and resilient SEI layer, which can accommodate the mechanical strain from silicon anodes, thereby reducing cracking and degradation. FEC has also shown benefits in low-temperature performance by preventing electrolyte freezing and enhancing lithium-ion transport, making it valuable for applications in cold environments [81]. Additionally, FEC provides improved oxidation stability at the cathode, extending the electrolyte's voltage window and supporting higher-voltage operations without significant side reactions [82]. VC and FEC play a crucial role in improving lithium-ion battery performance by stabilizing the electrolyte, enhancing the durability of the SEI layer, and supporting high-energy-density applications. While VC is generally more suited for graphite anodes, FEC is preferred for systems with silicon anodes or applications requiring high-voltage or low-temperature stability. These additives are fundamental in the ongoing development of lithium-ion battery technology, enabling safer, longer-lasting batteries that are increasingly suitable for demanding applications such as electric vehicles and energy storage systems.

Other additive, like lithium bis(oxalato)borate (LiBOB) [83], for example, acts as a film-forming additive that enhances the stability of the solid electrolyte interphase (SEI) on the anode. This protective SEI layer helps to minimize undesirable reactions between the

electrolyte and the electrode, thus improving the cycle life and thermal stability of the battery. LiBOB is particularly effective in high-voltage systems, where it forms a robust, stable interface that can prevent decomposition reactions at elevated voltages [85]. **Table 2** summarizes various common additives and their performance in battery.

Table 2. Different types of electrolyte additives species [52].

Type of electrolyte additives	Initial Coulombic efficiency	Discharge capacity (mAh g^{-1})	Capacity retention
Trimethyl phosphite (TMP)	92.2%	~270 (0.1 C)	81.3% (100 cycles, 0.5 C)
Triphenyl phosphite (TPPi)	–	204.3 (0.5 C)	90.8% (100 cycles, 0.5 C)
Tri(hexafluoro-isopropyl)phosphate (HFiP)	78.9%	250 (0.07 C)	72.3% (130 cycles, 0.72 C)
Trimethylsilyl (trimethylsiloxy) acetate (bi-TMSA)	70.2%	237.56 (0.1 C)	80.1% (374 cycles, 1 C)
Tris(2,2,2-trifluoroethyl) phosphite (TTFP)	81.4%	280 (0.2 C)	82.1% (110 cycles, 0.2 C)
Tris(trimethylsilyl)borate (TMSB)	80.3%	213 (0.5 C)	73.6% (220 cycles, 0.5 C)
Tris(pentafluorophenyl)borane (TPFPB)	~79.5%	245 (0.1 C)	76.8% (500 cycles, C/3)
Tris(trimethylsilyl)phosphate (TMSP)	76.2%	225 (0.08 C)	91.1% (50 cycles, 0.08 C)
3-hexylthiophene (3HT)	~85%	~280 (0.1 C)	90% (70 cycles, 0.1 C)
$LiF_2BC_2O_4$ (LiDFOB)	~91.2%	251 (0.06 C)	65% (200 cycles, 0.06 C)
Lithium bis(oxalato)borate (LiBOB)	88.4%	284 (0.1 C)	98.1% (120 cycles, 0.5 C)
Lithium difluoro(bisoxalato)phosphate (LiDFBP)	~82.5%	~246 (0.1 C)	90% (100 cycles, 0.5 C)
Ethylene glycol bis (propionitrile) ether (EGBE)	–	203.5 (0.1 C)	89% (150 cycles, 0.5 C)
Methyl diphenylphosphinite (MDP)	88.5%	230 (0.1 C)	93.9% (80 cycles, 0.1 C)
Phenyl vinyl sulfone (PVS)	74%	~260 (0.1 C)	80% (240 cycles, 0.5 C)
Fluoroethylene carbonate (FEC)	70%	~280 (0.1 C)	92.5% (100 cycles, 0.5 C)

Overall, optimizing the electrolyte composition—balancing the properties of solvents, salts, and additives—remains essential for advancing LIB technology. By addressing challenges such as thermal instability, limited voltage window, and electrolyte decomposition, ongoing research into novel electrolyte systems aims to enable safer, more efficient, and longer-lasting lithium-ion batteries suitable for a range of applications from consumer electronics to electric vehicles and grid storage. This thesis investigates the role of electrolyte formulation in enhancing lithium-ion battery performance, focusing on the interactions and synergies between solvents, salts, and additives in the quest for next-generation energy storage solutions.

1.4 A significant interphase between cathode and electrolyte - solid cathode-electrolyte interface (CEI)

The development of high-performance lithium-ion batteries (LIBs) has placed an

increasing focus on interfacial stability, particularly at the cathode-electrolyte boundary. A critical component of this stability is the solid cathode-electrolyte interface (CEI), a protective layer that forms on the surface of the cathode during electrochemical cycling [86-88]. Similar to the solid electrolyte interphase (SEI) on the anode, the CEI plays a pivotal role in protecting the cathode from electrolyte decomposition and in maintaining the electrochemical integrity of the system. The structure, formation, and components of the CEI could be used for optimizing this interphase in next-generation lithium-ion batteries.

In lithium-ion batteries, the cathode is often exposed to oxidative environments, especially at high voltages, which can lead to instability and degradation of the electrolyte and cathode materials. Unlike the SEI at the anode, the CEI must withstand oxidizing conditions rather than reducing reactions [89]. As cathode materials are pushed to higher voltages to increase energy density, the electrolyte is more prone to oxidation, which can lead to the formation of reactive oxygen species and other byproducts that attack both the electrolyte and the cathode structure [90-91]. The CEI forms as a result of electrolyte decomposition at the cathode surface, creating a thin, solid layer that serves as a barrier against further degradation.

The CEI is formed through complex electrochemical reactions that involve both the electrolyte solvents and the lithium salt. During the initial cycling of the battery, these components undergo partial decomposition, generating products that adhere to the cathode surface. Key decomposition products include inorganic compounds like lithium carbonate (Li_2CO_3), lithium fluoride (LiF), and other lithium-containing oxides, as well as organic compounds derived from electrolyte solvents [92]. The exact composition and morphology of the CEI depend on the electrolyte chemistry, the cathode material, and operating conditions, including temperature and applied voltage.

The components of electrolyte decide the composition of CEI. For example, in electrolytes containing $LiPF_6$, the presence of fluorine-containing species encourages the formation of LiF,

which is beneficial due to its high ionic conductivity and chemical stability. Similarly, electrolytes containing fluorinated solvents or specific additives like FEC contribute additional fluorinated decomposition products that can further enhance CEI stability and functionality [80-82].

The primary function of the CEI is to act as a protective barrier, reducing direct contact between the electrolyte and the cathode. This barrier minimizes continuous electrolyte decomposition, thereby enhancing battery longevity. The CEI also improves the stability of the lithium-ion conduction pathway by preventing unwanted side reactions between reactive oxygen species and electrolyte components, which can damage both the electrolyte and the cathode's crystal structure.

A well-formed CEI can mitigate issues such as transition metal dissolution, which is particularly significant in high-nickel and high-cobalt cathodes. Transition metals, if not stabilized by a protective layer, can dissolve into the electrolyte and migrate to the anode, where they catalyze undesirable side reactions that ultimately degrade battery capacity [93-94]. Additionally, the CEI reduces gas generation at the cathode, which is common at high voltages and can lead to cell swelling, increased internal resistance, and safety risks.

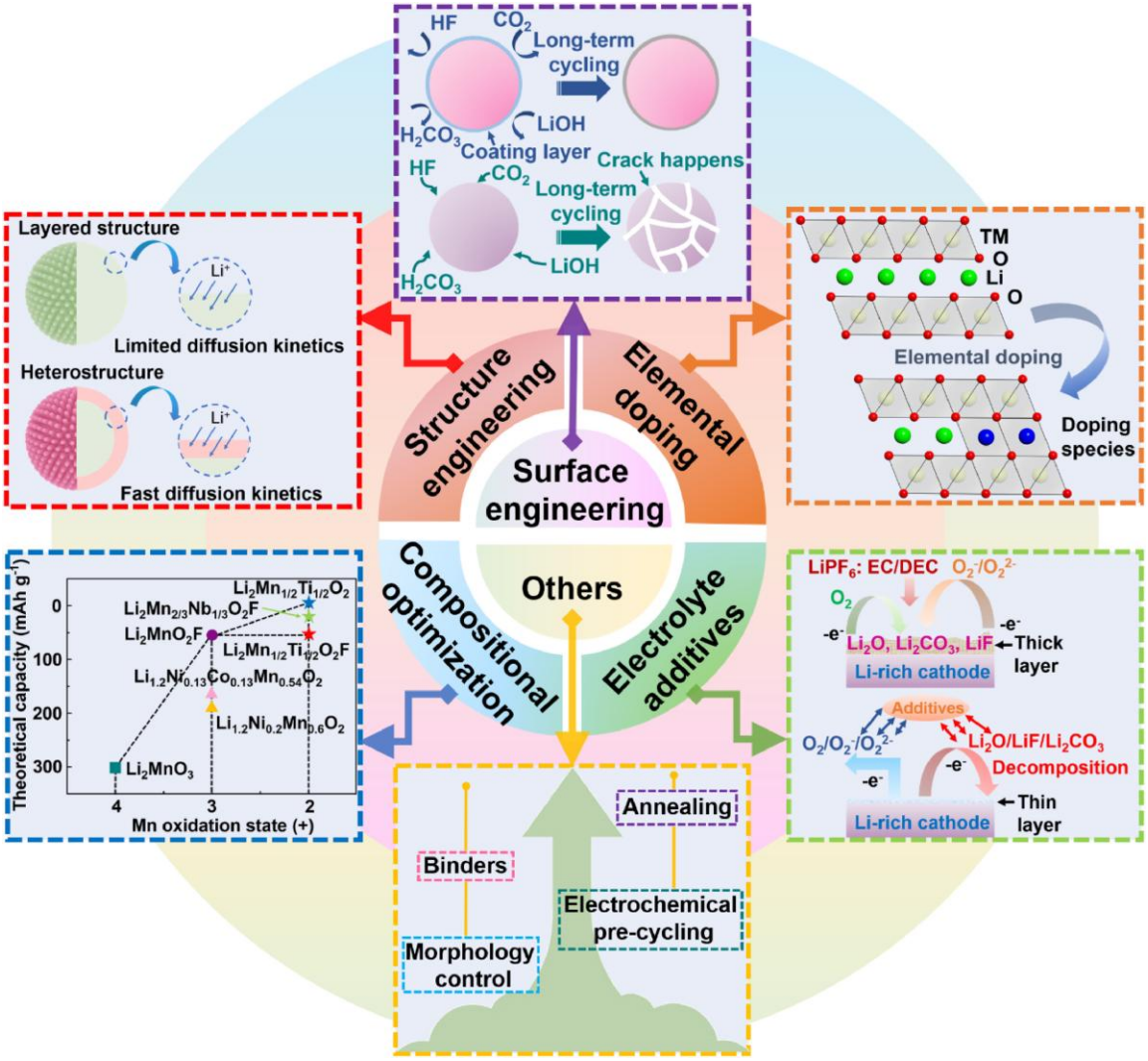

Figure 7. Strategies for improving performances of layered LRCMs through surficial modification [52].

While the CEI provides critical protection, there are several challenges in developing an ideal CEI. Firstly, achieving a robust and stable CEI layer is difficult, particularly for high-voltage cathodes. The CEI should ideally be ionically conductive to lithium ions but electronically insulating to prevent further electron transfer reactions at the cathode surface. Ensuring these properties across the entire cathode surface is challenging, as inhomogeneities can result in uneven lithium-ion distribution, leading to localized degradation.

Another challenge is the inherent instability of some CEI components under cycling conditions. For example, Li_2CO_3 and organic components in the CEI can undergo further

decomposition at high voltages, which can limit the CEI's effectiveness over extended cycles. Furthermore, the high-voltage conditions at the cathode can exacerbate CEI breakdown, leading to cumulative degradation over time, particularly in high-energy-density applications such as electric vehicles.

Numerous strategies have been proposed to enhance CEI stability, performance, and uniformity, as presented in **Figure 7**. Electrolyte additives have shown considerable promise in this area. Certain additives, such as VC and FEC, decompose at the cathode surface to form stable, protective layers that help reinforce the CEI. Additives like LiBOB can also enhance the formation of a robust CEI by introducing boron-containing compounds, which improve film integrity and resist degradation at high voltages.

Another promising approach is surface coating on the cathode itself. Thin layers of materials such as Al_2O_3, Li_3PO_4, or other ceramic coatings are applied to the cathode surface to physically separate it from the electrolyte [95-97]. These coatings not only improve the CEI's stability by preventing direct contact with the electrolyte but also support lithium-ion diffusion, enhancing both cycle life and rate capability.

Ultimately, the development of a stable, effective CEI will be instrumental in advancing lithium-ion batteries for applications requiring long life, high capacity, and safety, such as electric vehicles, grid storage, and portable electronics. By focusing on both the material and interfacial properties of the CEI, researchers aim to unlock the full potential of LIBs, addressing challenges in cycle stability, energy density, and operational safety.

1.5 Organoboron compounds in batteries

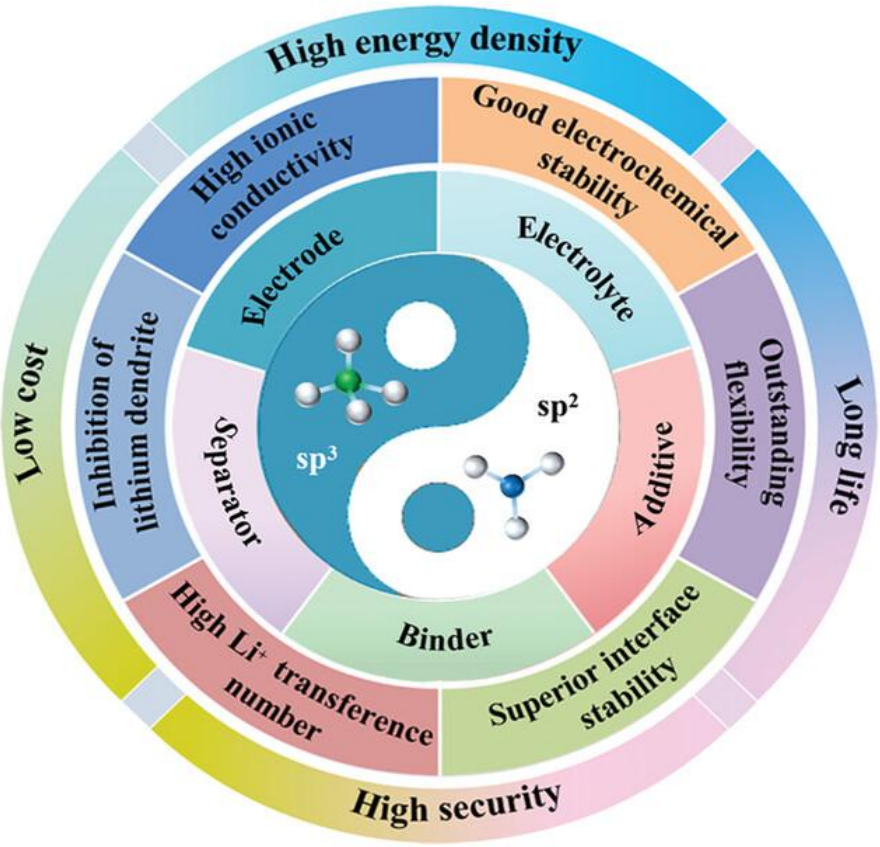

Figure 8. Applications and characteristics of boron in LBs [98].

In hybrid orbital theory, boron can exhibit two distinct hybridization states: sp^3 and sp^2. Each hybridization form influences the electronic environment around boron atoms, enabling them to form four covalent bonds (sp^3) or three covalent bonds (sp^2) with other atoms. In the sp^2 hybridized state, boron retains an empty p orbital, imparting electron-deficient characteristics. This electron deficiency makes three-coordinate boron atoms effective electrophilic reagents or Lewis acids, allowing them to interact with atoms bearing lone pairs of electrons. Conversely, in the sp^3 hybridized state, boron exhibits a negatively charged electronic structure. These versatile hybridization states of boron contribute to the unique physical and chemical properties of boron-containing compounds, which have become valuable in applications such as cathode, electrolyte additive, salt, binder and so on, as shown in **Figure 8**.

(1) Cathode

In recent years, certain polyanionic materials have garnered significant attention due to their excellent thermal stability and inherent safety characteristics. Among these, borate-based materials stand out as promising cathode candidates, offering advantages such as low molar mass, high theoretical capacity, superior conductivity, structural stability, and environmental compatibility.

$LiMBO_3$-type borates have been particularly noteworthy, as the light polyanionic BO_3^{3-} group enables a higher theoretical energy density compared to other polyanionic cathode materials. In foundational work [98], Legagneur et al. first explored the electrochemical properties of $LiMBO_3$ (where M = Mn, Fe, Co), demonstrating that up to 0.04 Li could be reversibly deinserted from each compound. This study paved the way for borates in lithium battery cathodes. Further research by Yamada et al. provided insights into the crystal structure of $LiFeBO_3$, advancing the understanding of borate-based cathodes and their potential applications in energy storage [99].

(2) Polymer electrolyte

Adding nanofillers, single-ion conductors, porous structures, and boron-based groups into polymer matrices has been demonstrated to raise the Li-ion transference number in electrolyte systems. Among these methods, the inclusion of boron-containing groups offers a particularly simple and efficient way to boost the Li-ion transference number, providing an accessible means to enhance electrolyte functionality. Ma et al. developed a boron-containing solid polymer electrolyte (SPE), designated as P(V–B), through in situ polymerization of vinylene carbonate (VC) and poly(ethylene glycol) methyl ether methacrylate, which incorporates cyclic boroxane groups on a cellulose membrane[100]. The resulting flexible P(V–B) electrolyte demonstrates excellent physical, mechanical, and electrochemical properties. It exhibits a notably high ionic conductivity of $9.11*10^{-4}$ S cm^{-1} at room temperature, alongside a substantial

Li-ion transference number of 0.68 and strong interfacial stability, making it a promising candidate for advanced lithium-ion battery applications.

(3) Additive

Boron-containing additives have been extensively utilized in LIBs due to the unique property of sp^2-hybridized boron to complex anions, enabling the formation of a protective film on the cathode surface during cycling. This stabilization of the electrode/electrolyte interface enhances the electrochemical performance of the battery. In contrast, conventional additives like VC, tris(trimethylsilyl)phosphate, and phenyl vinyl sulfone typically benefit only one electrode and cannot simultaneously form protective films on both electrodes. To overcome these limitations, Yue et al. introduced tris(pentafluorophenyl)borane (TPFPB)[101], a boron-based additive featuring a central boron atom surrounded by pentafluorophenyl groups, as a dual-effect additive. Electrochemical analysis demonstrated that the LNMO/Li cell containing 1% TPFPB retained a discharge capacity of 111.8 $mAhg^{-1}$ at 0.5 C. After 500 cycles, the cell achieved a capacity retention of 90% and an average Coulombic efficiency of 99%, highlighting its excellent cycling stability and efficiency.

(4) Lithium salt

Common lithium borate salts include lithium bis(oxalate)borate (LiBOB) [85], lithium difluoro(oxalate)borate (LiDFOB), and lithium trifluoro(perfluoro-tert-butyloxyl)borate (LiTFPFB), all of which exhibit high thermal and chemical stability. Xu et al. demonstrated that an electrolyte formulated with LiBOB effectively passivates aluminum substrates and maintains stability on both carbonaceous and metal oxide cathodes. Moreover, LIBs utilizing LiBOB as the lithium salt show outstanding rate capabilities, enhanced cycling stability, and strong capacity retention at room temperature.

(5) Separator

Boron nitride (BN) materials have recently gained significant attention for modifying LIB

separators, attributed to their ultrahigh Young's modulus, excellent electrical insulation properties, and exceptional chemical stability. Luo et al. developed a straightforward and effective approach to enhance the cycling stability of LMBs by coating thermally conductive BN nanosheets onto commercial separators. This innovative method demonstrates the potential of BN-based materials in improving battery performance and durability[102].

(6) Binder

Poly(vinylidene fluoride) (PVDF) has long served as the primary binder for electrochemical energy storage devices, valued for its robust mechanical properties and excellent electrochemical stability. However, its broader applicability is constrained by drawbacks such as low electrical and ionic conductivity, susceptibility to volume expansion, and reliance on N-methyl-2-pyrrolidone (NMP)—a solvent with significant environmental impact—for slurry preparation. To address these challenges, Pradhan et al. developed a lithium-borate-based aqueous polyelectrolyte binder (CAB) for graphite anodes[103]. This innovative binder facilitates SEI film formation, enhances Li-ion diffusion, and reduces impedance, offering a promising alternative to PVDF for sustainable and efficient energy storage systems. Cells using CAB demonstrated a discharge capacity of up to 343 mAh g^{-1} at 1 C, with a capacity retention of 87% after 750 cycles. Additionally, the binder exhibited strong cycling stability and Coulombic efficiency (CE) at high current densities, achieving 93% capacity retention and a CE of 99.6% after 1200 cycles at 10 C.

1.6 Objectives

In this thesis, the primary focus is to modify the electrolyte composition by incorporating various boron-containing components, including (a) solvents, (b) additives, to enhance the performance of lithium-ion batteries with NMC-type cathodes. While previous studies have extensively investigated the role of boron in stabilizing the SEI, there is a notable gap in understanding the impact of boron-containing compounds on the CEI. This research aims to

address this gap by exploring how boron-based products influence the formation and properties of the CEI, thereby contributing to improved battery stability and performance.

Boric ester as a component of electrolyte to increase the stability and durability of battery are explored with the anodic materials like graphite and silicon, however its application in lithium-ion battery cathode has not been studied yet. In **Chapter 2**, different ratio of mesityldimethoxyborane (MDMB) is used into conventional carbonate-based electrolyte (1M LiTFSI in EC-DEC) to investigate the Boron-rich electrolyte's influence on cathodic material $LiNiCoMnO_2$. The addition of MDMB enhanced the Li ion transference ability and charging-discharging performance under high rate. It can also improve the cyclability of battery by forming boron-containing durable interface.

Chapter 3 investigates the enhancement of LIBs by incorporating a boron-containing additive, EGMB, to improve the cathode-electrolyte interphase (CEI) in NMC-based cathodes. LIBs have become essential in portable electronics and electric vehicles, yet face challenges under extreme conditions, including high voltage, fast charge-discharge rates, and temperature fluctuations. Traditional electrolytes often fail to maintain stable interfaces with cathodes under these conditions, leading to performance deterioration through side reactions, metal dissolution, and structural breakdown. EGMB, a cyclic boric ester synthesized via a solvent-free method, was introduced into the electrolyte at low concentrations. The study demonstrates that EGMB enhances the CEI through the formation of a B- and F-rich layer, which stabilizes the cathode, minimizes side reactions, and improves Li-ion migration. Specifically, the research shows that EGMB-containing electrolytes enable higher capacity retention and cycling stability, reducing degradation under ultrahigh voltage, extreme charging conditions, and wide temperature ranges.

In this thesis, the role of boron-containing components in improving the electrolyte systems of lithium-ion batteries (LIBs) with NMC cathodes is systematically explored. The research addresses critical challenges in LIB technology, including interfacial instability, low

lithium-ion conductivity, and capacity degradation under different conditions. Mesityldimethoxyborane (MDMB) was shown to enhance lithium-ion transport and high-rate performance by forming a robust boron-rich cathode-electrolyte interphase (CEI). Ethylene glycol mesityl borane (EGMB) demonstrated multifunctional benefits, stabilizing the CEI while mitigating degradation under high voltage and extreme temperature conditions. TFELiMB, a boron-containing lithium salt, further advanced performance by reducing interfacial resistance and improving capacity retention under extreme cycling rates. Together, these findings establish boron-based materials as effective tools for enhancing battery stability and durability. This thesis contributes valuable insights for designing advanced electrolytes to support the development of high-performance, next-generation LIBs.

Reference

(1) Pezeshki, Z. Classification, modeling, and requirements for separators in rechargeable batteries. *Rechargeable Batteries: History, Progress, and Applications* **2020**, 265-314.

(2) Huggins, R., & Huggins, R. A. Primary, non-rechargeable batteries. *Energy storage: Fundamentals, materials and applications* **2016**, 291-307.

(3) Aljamali, N. M., Mohsein, H. F., & Wannas, F. A. Review on Engineering Designs for Batteries **2021**.

(4) Costandi, S., Mekhail, N., Azer, G., Mehanny, D. S., Hanna, D., Salma, Y., ... & Saweris, Y. Longevity and utilization cost of rechargeable and non-rechargeable spinal cord stimulation implants: a comparative study. *Pain Practice* **2020**, *20* (8), 937-945.

(5) Wei, C. L., Huang, M. F., Sun, Y., Cheng, A., & Yen, C. W. A method for fully utilizing the residual energy in used batteries. In *2016 IEEE International Conference on Industrial Technology (ICIT)* **2016** (pp. 230-233). IEEE.

(6) Olabi, A. G., Abbas, Q., Shinde, P. A., & Abdelkareem, M. A. Rechargeable batteries: Technological advancement, challenges, current and emerging applications. *Energy* **2023**, *266*, 126408.

(7) Xu, C., Chen, Y., Shi, S., Li, J., Kang, F., & Su, D. Secondary batteries with multivalent ions for energy storage. *Scientific Reports* **2015**, *5* (1), 14120.

(8) Chen, R., Luo, R., Huang, Y., Wu, F., & Li, L. Advanced high energy density secondary batteries with multi-electron reaction materials. *Advanced Science* **2016**, *3*(10), 1600051.

(9) Fichtner, M., Edström, K., Ayerbe, E., Berecibar, M., Bhowmik, A., Castelli, I. E., ... & Weil, M. Rechargeable batteries of the future—the state of the art from a BATTERY 2030+ perspective. *Adv. Ener. Mater.* **2022**, *12*(17), 2102904.

(10) Fu, W., Turcheniuk, K., Naumov, O., Mysyk, R., Wang, F., Liu, M., ... & Yushin, G. Materials and technologies for multifunctional, flexible or integrated supercapacitors and batteries. *Materials Today* **2021**, *48*, 176-197.

(11) Chen, R., Luo, R., Huang, Y., Wu, F., & Li, L. Advanced high energy density secondary batteries with multi-electron reaction materials. *Advanced Science* **2016**, *3*(10), 1600051.

(12) May, G. J., Davidson, A., & Monahov, B. Lead batteries for utility energy storage: A review. *J. energy storage* **2018**, *15*, 145-157.

(13) Sikiru, S., Dele-Afolabi, T. T., Ghotbi, M. Y., & Rehman, Z. U. Recent advancements in technology projection on electric double layer effect in battery recycling for energy storage. *J. Power Sources* **2024**, *596*, 234056.

(14) Ramanan, A. Nobel Prize in Chemistry 2019. *Resonance* **2019**, *24*(12), 1381-1395.

(15) Manfo, T. A. A Comprehensive Analysis of Material Revolution to Evolution in Lithium-ion Battery Technology. *Turk. J. Mater. Vol* **2023**, *8*(1), 1-13.

(16) Amici, J., Asinari, P., Ayerbe, E., Barboux, P., Bayle-Guillemaud, P., Behm, R. J., ... & Edström, K. A roadmap for transforming research to invent the batteries of the future designed within the european large scale research initiative battery 2030+. *Adv. Ener. Mater.* **2022**, *12*(17), 2102785.

(17) Pomerantseva, E., Bonaccorso, F., Feng, X., Cui, Y., & Gogotsi, Y. Energy storage: The future enabled by nanomaterials. *Science* **2019**, *366*(6468), eaan8285.

(18) Placke, T., Kloepsch, R., Dühnen, S., & Winter, M. Lithium ion, lithium metal, and alternative rechargeable battery technologies: the odyssey for high energy density. *Journal of Solid State Electrochemistry* **2017**, *21*, 1939-1964.

(19) Weiss, M., Ruess, R., Kasnatscheew, J., Levartovsky, Y., Levy, N. R., Minnmann, P., ... & Janek, J. Fast charging of lithium-ion batteries: a review of materials aspects. *Adv. Ener. Mater.* **2021**, *11*(33), 2101126.

(20) Ciez, R. E., & Whitacre, J. F. Examining different recycling processes for lithium-ion batteries. *Nature Sustainability* **2019**, *2*(2), 148-156.

(21) Roy, J. J., Rarotra, S., Krikstolaityte, V., Zhuoran, K. W., Cindy, Y. D. I., Tan, X. Y., ... & Srinivasan, M. Green recycling methods to treat lithium-ion batteries E-waste: a circular approach to sustainability. *Adv. Mater.* **2022**, *34*(25), 2103346.

(22) Ma, S., Jiang, M., Tao, P., Song, C., Wu, J., Wang, J., ... & Shang, W. Temperature effect and thermal impact in lithium-ion batteries: A review. *Progress in Natural Science: Materials International* **2018**, *28*(6), 653-666.

(23) Bandhauer, T. M., Garimella, S., & Fuller, T. F. A critical review of thermal issues in lithium-ion batteries. *J. Electrochem. Soc.* **2011**, *158*(3), R1.

(24) Wang, C. Y., Zhang, G., Ge, S., Xu, T., Ji, Y., Yang, X. G., & Leng, Y. Lithium-ion battery structure that self-heats at low temperatures. *Nature* **2016**, *529*(7587), 515-518.

(25) Fan, E., Li, L., Wang, Z., Lin, J., Huang, Y., Yao, Y., ... & Wu, F. Sustainable recycling technology for Li-ion batteries and beyond: challenges and future prospects. *Chemical Reviews* **2020**, *120*(14), 7020-7063.

(26) Wen, J., Zhao, D., & Zhang, C. An overview of electricity powered vehicles: Lithium-ion battery energy storage density and energy conversion efficiency. *Renewable Energy* **2020**, *162*, 1629-1648.

(27) Xu, J., Cai, X., Cai, S., Shao, Y., Hu, C., Lu, S., & Ding, S. High-energy lithium-ion batteries: recent progress and a promising future in applications. *Energy & Environmental Materials* **2023**, *6*(5), e12450.

(28) Wang, L., Chen, B., Ma, J., Cui, G., & Chen, L. Reviving lithium cobalt oxide-based lithium secondary batteries-toward a higher energy density. *Chemical Society Reviews* **2018**, *47*(17), 6505-6602.

(29) Chakraborty, P., Parker, R., Hoque, T., Cruz, J., Du, L., Wang, S., & Bhunia, S. Addressing the range anxiety of battery electric vehicles with charging en route. *Scientific Reports* **2022**, *12*(1), 5588.

(30) Okubo, M., Ko, S., Dwibedi, D., & Yamada, A. (2021). Designing positive electrodes with high energy density for lithium-ion batteries. *J. Mater. Chem. A* **2021**, *9*(12), 7407-7421.

(31) Xiang, J., Wei, Y., Zhong, Y., Yang, Y., Cheng, H., Yuan, L., ... & Huang, Y. Building practical high-voltage cathode materials for lithium-ion batteries. *Advanced Materials* **2022**, *34*(52), 2200912.

(32) Cavers, H., Molaiyan, P., Abdollahifar, M., Lassi, U., & Kwade, A. Perspectives on improving the safety and sustainability of high voltage lithium-ion batteries through the electrolyte and separator region. *Adv. Ener. Mater.* **2022**, *12*(23), 2200147.

(33) Streipert, B., Stolz, L., Homann, G., Janßen, P., Cekic-Laskovic, I., Winter, M., & Kasnatscheew, J. Conventional Electrolyte and Inactive Electrode Materials in Lithium-Ion Batteries: Determining Cumulative Impact of Oxidative Decomposition at High Voltage. *ChemSusChem* **2020**, *13*(19), 5301-5307.

(34) Chen, S., Wen, K., Fan, J., Bando, Y., & Golberg, D. Progress and future prospects of high-voltage and high-safety electrolytes in advanced lithium batteries: from liquid to solid electrolytes. *J. Mater. Chem. A* **2018**, *6*(25), 11631-11663.

(35) Xiang, J., Wei, Y., Zhong, Y., Yang, Y., Cheng, H., Yuan, L., ... & Huang, Y. Building practical high-voltage cathode materials for lithium-ion batteries. *Adv. Mater.* **2022**, *34*(52), 2200912.

(36) Wassiliadis, N., Schneider, J., Frank, A., Wildfeuer, L., Lin, X., Jossen, A., & Lienkamp, M. Review of fast charging strategies for lithium-ion battery systems and their applicability for battery electric vehicles. *J. energy*

storage **2021**, *44*, 103306.

(37) Collin, R., Miao, Y., Yokochi, A., Enjeti, P., & Von Jouanne, A. Advanced electric vehicle fast-charging technologies. *Energies* **2019**, *12*(10), 1839.

(38) Li, G. Regulating mass transport behavior for high-performance lithium metal batteries and fast-charging lithium-ion batteries. *Adv. Ener. Mater.* **2021**, *11*(7), 2002891.

(39) Li, G.; Liao, Y.; Li, Z.; Xu, N.; Lu, Y.; Lan, G.; Sun, G.; Li, W. Constructing a Low-Impedance Interface on a High-Voltage $LiNi_{0.8}Co_{0.1}Mn_{0.1}O_2$ Cathode with 2,4,6-Triphenyl Boroxine as a Film-Forming Electrolyte Additive for Li-Ion Batteries. *ACS Appl. Mater. Interfaces* **2020**, *12* (33), 37013–37026. https://doi.org/10.1021/acsami.0c05623.

(40) Li, N., Chen, Z., Ren, W., Li, F., & Cheng, H. M. Flexible graphene-based lithium ion batteries with ultrafast charge and discharge rates. *Proceedings of the National Academy of Sciences* **2012**, *109*(43), 17360-17365.

(41) Deshpande, A., Kariyawasam, L., Dutta, P., & Banerjee, S. Enhancement of lithium ion mobility in ionic liquid electrolytes in presence of additives. *The J. Phys. Chem. C* **2013**, *117*(48), 25343-25351.

(42) Forsyth, M., Porcarelli, L., Wang, X., Goujon, N., & Mecerreyes, D. Innovative electrolytes based on ionic liquids and polymers for next-generation solid-state batteries. *Accounts of Chemical Research* **2019**, *52*(3), 686-694.

(43) Giffin, G. A. The role of concentration in electrolyte solutions for non-aqueous lithium-based batteries. *Nat. Comm.* **2022**, *13*(1), 5250.

(44) Yamada, Y., Wang, J., Ko, S., Watanabe, E., & Yamada, A. (2019). Advances and issues in developing salt-concentrated battery electrolytes. *Nat. Ener.* **2019**, *4*(4), 269-280.

(45) Wassiliadis, N., Schneider, J., Frank, A., Wildfeuer, L., Lin, X., Jossen, A., & Lienkamp, M. Review of fast charging strategies for lithium-ion battery systems and their applicability for battery electric vehicles. *J. energy storage* **2021**, *44*, 103306.

(46) Lyu, P., Liu, X., Qu, J., Zhao, J., Huo, Y., Qu, Z., & Rao, Z. Recent advances of thermal safety of lithium ion battery for energy storage. *Energy Storage Materials* **2020**, *31*, 195-220.

(47) Raijmakers, L. H. J., Danilov, D. L., Eichel, R. A., & Notten, P. H. L. A review on various temperature-indication methods for Li-ion batteries. *Applied Energy* **2019**, *240*, 918-945.

(48) Worku, B. E., Zheng, S., & Wang, B. Review of low-temperature lithium-ion battery progress: new battery system design imperative. *International Journal of Energy Research* **2022**, *46*(11), 14609-14626.

(49) Feng, Y., Zhou, L., Ma, H., Wu, Z., Zhao, Q., Li, H., ... & Chen, J. Challenges and advances in wide-temperature rechargeable lithium batteries. *Energy & Environmental Science* **2022**, *15* (5), 1711-1759.

(50) Lin, X., Salari, M., Arava, L. M. R., Ajayan, P. M., & Grinstaff, M. W. High temperature electrical energy storage: advances, challenges, and frontiers. *Chemical Society Reviews* **2016**, *45* (21), 5848-5887.

(51) Hou, J., Yang, M., Wang, D., & Zhang, J. Fundamentals and challenges of lithium ion batteries at temperatures between− 40 and 60° C. *Adv. Ener. Mater.* **2020**, *10*(18), 1904152.

(52) Zhao, S., Guo, Z., Yan, K., Wan, S., He, F., Sun, B., & Wang, G. Towards high-energy-density lithium-ion batteries: Strategies for developing high-capacity lithium-rich cathode materials. *Energy Storage Materials* **2021**, *34*, 716-734.

(53) Julien, C. M., Mauger, A., Zaghib, K., & Groult, H. Comparative issues of cathode materials for Li-ion batteries. *Inorganics* **2014**, *2*(1), 132-154.

(54) Li, J., Armstrong, B. L., Daniel, C., Kiggans, J., & Wood III, D. L. Optimization of multicomponent aqueous

suspensions of lithium iron phosphate ($LiFePO_4$) nanoparticles and carbon black for lithium-ion battery cathodes. *Journal of Colloid and Interface Science* **2013**, *405*, 118-124.

(55) Toh, W. D., Xu, B., Jia, J., Chin, C. S., Chiew, J., & Gao, Z. Lithium iron phosphate (LiFePO4) battery power system for deepwater emergency operation. *Energy Procedia* **2017**, *143*, 348-353.

(56) Benedek, R., & Thackeray, M. M. Simulation of the surface structure of lithium manganese oxide spinel. *Physical Review B—Condensed Matter and Materials Physics* **2011**, *83* (19), 195439.

(57) Huang, Y., Dong, Y., Li, S., Lee, J., Wang, C., Zhu, Z., ... & Li, J. Lithium manganese spinel cathodes for lithium-ion batteries. *Adv. Ener. Mater.* **2021**, *11* (2), 2000997.

(58) Zawrah, M. F., El Fadaly, E. A., Khattab, R. M., Aly, M. H., & El Shafei, H. Synthesis and characterization of nano Mn_3O_4 and $LiMn_2O_4$ spinel from manganese ore and pure materials. *Ceramics International* **2020**, *46*(11), 17514-17522.

(59) Lyu, Y., Wu, X., Wang, K., Feng, Z., Cheng, T., Liu, Y., ... & Guo, B. An overview on the advances of $LiCoO_2$ cathodes for lithium-ion batteries. *Adv. Ener. Mater.* **2021**, *11* (2), 2000982.

(60) Zhang, J. C., Liu, Z. D., Zeng, C. H., Luo, J. W., Deng, Y. D., Cui, X. Y., & Chen, Y. N. High-voltage $LiCoO_2$ cathodes for high-energy-density lithium-ion battery. *Rare Metals* **2022**, *41*(12), 3946-3956.

(61) Saaid, F. I., Kasim, M. F., Winie, T., Elong, K. A., Azahidi, A., Basri, N. D., ... & Rusop, M. Ni-rich lithium nickel manganese cobalt oxide cathode materials: A review on the synthesis methods and their electrochemical performances. *Heliyon* **2023**.

(62) Vakhrusheva, D. M., & Xu, J. Model-driven Manufacturing of High-Energy-Density Batteries: A Review. *Batteries & Supercaps*, e202400539.

(63) Teichert, P., Eshetu, G. G., Jahnke, H., & Figgemeier, E. Degradation and aging routes of Ni-rich cathode based Li-ion batteries. *Batteries* **2020**, *6*(1), 8.

(64) Johnston, B. I. J. *High energy density positive insertion electrodes for next generation lithium-ion batteries* **2021** (Doctoral dissertation, University of Sheffield).

(65) Wentker, M., Greenwood, M., & Leker, J. *A bottom-up approach to lithium-ion battery cost modeling with a focus on cathode active materials. Energies* **2019** *12: 504*.

(66) Teichert, P., Eshetu, G. G., Jahnke, H., & Figgemeier, E. Degradation and aging routes of Ni-rich cathode based Li-ion batteries. *Batteries* **2020**, *6* (1), 8.

(67) Cabana, J., Kwon, B. J., & Hu, L. Mechanisms of degradation and strategies for the stabilization of cathode–electrolyte interfaces in Li-ion batteries. *Accounts of Chemical Research* **2018**, *51* (2), 299-308.

(68) Xu, K. Electrolytes and interphases in Li-ion batteries and beyond. *Chemical Reviews* **2014**, *114* (23), 11503-11618.

(69) Yang, H., & Wu, N. Ionic conductivity and ion transport mechanisms of solid-state lithium-ion battery electrolytes: A review. *Energy Science & Engineering* **2022**, *10* (5), 1643-1671.

(70) Cabana, J., Kwon, B. J., & Hu, L. Mechanisms of degradation and strategies for the stabilization of cathode–electrolyte interfaces in Li-ion batteries. *Accounts of Chemical Research* **2018**, *51* (2), 299-308.

(71) Lee, S., & Park, S. S. Thermodynamic and dynamic properties in binary mixtures of propylene carbonate with dimethyl carbonate and ethylene carbonate. *J. Molecular Liquids* **2012**, *175*, 97-102.

(72) Foss, C. E. L., Svensson, A. M., Gullbrekken, Ø., Sunde, S., & Vullum-Bruer, F. Temperature effects on performance of graphite anodes in carbonate based electrolytes for lithium ion batteries. *J. energy storage* **2018**,

17, 395-402.

(73) Hayamizu, K. Temperature dependence of self-diffusion coefficients of ions and solvents in ethylene carbonate, propylene carbonate, and diethyl carbonate single solutions and ethylene carbonate+ diethyl carbonate binary solutions of LiPF6 studied by NMR. *J. Chemical & Engineering Data* **2012**, *57* (7), 2012-2017.

(74) Susarla, N., & Ahmed, S. Estimating Cost and Energy Demand in Producing Lithium Hexafluorophosphate for Li-Ion Battery Electrolyte. *Industrial & Engineering Chemistry Research* **2019**, *58* (9), 3754-3766.

(75) Li, Z., Wang, L., Huang, X., & He, X. Lithium Bis (Trifluoromethanesulfonyl) Imide (LiTFSI): A Prominent Lithium Salt in Lithium-Ion Battery Electrolytes–Fundamentals, Progress, and Future Perspectives. *Adv. Func. Mater.* **2024**, 2408319.

(76) Yang, G., Li, Y., Liu, S., Zhang, S., Wang, Z., & Chen, L. LiFSI to improve lithium deposition in carbonate electrolyte. *Energy Storage Materials* **2019**, *23*, 350-357.

(77) Nguyen, C. C., & Lucht, B. L. Comparative study of fluoroethylene carbonate and vinylene carbonate for silicon anodes in lithium ion batteries. *J. Electrochem. Soc.* **2014**, *161*(12), A1933.

(78) Grugeon, S., Jankowski, P., Cailleu, D., Forestier, C., Sannier, L., Armand, M., ... & Laruelle, S. Towards a better understanding of vinylene carbonate derived SEI-layers by synthesis of reduction compounds. *J. Power Sources* **2019**, *427*, 77-84.

(79) Chang, C. C., Hsu, S. H., Jung, Y. F., & Yang, C. H. Vinylene carbonate and vinylene trithiocarbonate as electrolyte additives for lithium ion battery. *J. Power Sources* **2011**, *196*(22), 9605-9611.

(80) Shin, H., Park, J., Sastry, A. M., & Lu, W. Effects of fluoroethylene carbonate (FEC) on anode and cathode interfaces at elevated temperatures. *J. Electrochem. Soc.* **2015**, *162*(9), A1683.

(81) Lee, Y., Lee, J., Kim, H., Kang, K., & Choi, N. S. Highly stable linear carbonate-containing electrolytes with fluoroethylene carbonate for high-performance cathodes in sodium-ion batteries. *J. Power Sources* **2016**, *320*, 49-58.

(82) Nguyen, C. C., & Lucht, B. L. Comparative study of fluoroethylene carbonate and vinylene carbonate for silicon anodes in lithium ion batteries. *J. Electrochem. Soc.* **2014**, *161*(12), A1933.

(83) Pieczonka, N. P., Yang, L., Balogh, M. P., Powell, B. R., Chemelewski, K., Manthiram, A., ... & Kim, J. H. Impact of lithium bis (oxalate) borate electrolyte additive on the performance of high-voltage spinel/graphite Li-ion batteries. *J. Phys. Chem. C* **2013**, *117* (44), 22603-22612.

(84) Choi, N. S., Han, J. G., Ha, S. Y., Park, I., & Back, C. K. Recent advances in the electrolytes for interfacial stability of high-voltage cathodes in lithium-ion batteries. *Rsc Advances* **2015**, *5*(4), 2732-2748.

(85) Dalavi, S., Xu, M., Knight, B., & Lucht, B. L. Effect of added LiBOB on high voltage ($LiNi_{0.5}Mn_{1.5}O_4$) spinel cathodes. *Electrochemical and Solid-State Letters* **2011**, *15*(2), A28.

(86) Wu, Y., Liu, X., Wang, L., Feng, X., Ren, D., Li, Y., ... & Ouyang, M. Development of cathode-electrolyte-interphase for safer lithium batteries. *Energy Storage Materials* **2021**, *37*, 77-86.

(87) Sungjemmenla, SK, V., Soni, C. B., Kumar, V., & Seh, Z. W. Understanding the cathode–electrolyte interphase in lithium-ion batteries. *Energy Technology* **2022**, *10*(9), 2200421.

(88) Liang, L., Zhang, W., Zhao, F., Denis, D. K., Zaman, F. U., Hou, L., & Yuan, C. Surface/interface structure degradation of Ni-rich layered oxide cathodes toward lithium-ion batteries: fundamental mechanisms and remedying strategies. *Adv. Mater. Interfaces* **2020**, *7*(3), 1901749.

(89) Xu, J. CEI and SEI Formation in Li-Ion Batteries. In *Corrosion and Degradation in Fuel Cells, Supercapacitors*

and Batteries **2024** (pp. 307-324). Cham: Springer Nature Switzerland.

(90) Zhang, H., Liu, H., Piper, L. F., Whittingham, M. S., & Zhou, G. Oxygen loss in layered oxide cathodes for Li-ion batteries: mechanisms, effects, and mitigation. *Chemical Reviews* **2022**, *122*(6), 5641-5681.

(91) Mu, P., Zhang, H., Jiang, H., Dong, T., Zhang, S., Wang, C., ... & Cui, G. Bioinspired antiaging binder additive addressing the challenge of chemical degradation of electrolyte at cathode/electrolyte interphase. *J. Am. Chem. Soc.* **2021**, *143*(43), 18041-18051.

(92) Hu, X., Li, Y., Liu, J., Wang, Z., Bai, Y., & Ma, J. Constructing LiF/Li_2CO_3-rich heterostructured electrode electrolyte interphases by electrolyte additive for 4.5 V well-cycled lithium metal batteries. *Science Bulletin* **2023**, *68*(12), 1295-1305.

(93) Cabana, J., Kwon, B. J., & Hu, L. Mechanisms of degradation and strategies for the stabilization of cathode–electrolyte interfaces in Li-ion batteries. *Accounts of Chemical Research* **2018**, *51* (2), 299-308.

(94) Du, H., Wang, Y., Kang, Y., Zhao, Y., Tian, Y., Wang, X., ... & Li, B. Side Reactions/Changes in Lithium-Ion Batteries: Mechanisms and Strategies for Creating Safer and Better Batteries. *Advanced Materials* **2024**, 2401482.

(95) Qi, M., Wang, L., Huang, X., Ma, M., & He, X. Surface Engineering of Cathode Materials: Enhancing the High Performance of Lithium-Ion Batteries. *Small* **2024**, 2402443.

(96) Malik, I., Kumar, A., Lohan, R., & Deopa, N. Coating Technologies for the Surface Modification of Energy Storage Materials. In *Materials for Boosting Energy Storage. Volume 3: Advances in Sustainable Energy Technologies* **2024** (pp. 123-141). American Chemical Society.

(97) Kwon, N. H., Conder, J., Srout, M., & Fromm, K. M. Surface modifications of positive-electrode materials for lithium ion batteries. *CHIMIA International Journal for Chemistry* **2019**, *73*, 880.

(98) Ma, L., Tan, J., Wang, Y., Liu, Z., Yang, Y., Gray, T., ... & Shen, J. Boron-Based High-Performance Lithium Batteries: Recent Progress, Challenges, and Perspectives. *Adv. Ener. Mater.* **2023**, *13* (25), 2300042.

(99) Yamada, A., Iwane, N., Harada, Y., Nishimura, S. I., Koyama, Y., & Tanaka, I. Lithium iron borates as high-capacity battery electrodes. *Adv. Mater.* **2010**, *32* (22), 3583-3587

(100) Ma, C., Feng, Y., Xing, F., Zhou, L., Yang, Y., Xia, Q., ... & Wei, W. A borate decorated anion-immobilized solid polymer electrolyte for dendrite-free, long-life Li metal batteries. *J. Am. Chem. Soc.* **2019**, *7*(34), 19970-19976.

(101) Yue, H., Yang, Y., Xiao, Y., Dong, Z., Cheng, S., Yin, Y., ... & Yang, S. Boron additive passivated carbonate electrolytes for stable cycling of 5 V lithium–metal batteries. *J. Am. Chem. Soc.* **2019**, *7*(2), 594-602.

(102) Luo, W., Zhou, L., Fu, K., Yang, Z., Wan, J., Manno, M., ... & Hu, L. A thermally conductive separator for stable Li metal anodes. *Nano letters J. Am. Chem. Soc.* **2015**, *15*(9), 6149-6154.

(103) Pradhan, A., Badam, R., Miyairi, R., Takamori, N., & Matsumi, N. (2023). Extreme fast charging capability in graphite anode via a lithium borate type biobased polymer as aqueous polyelectrolyte binder. *ACS Mater. Lett.* **2023**, *5*(2), 413-420.

Chapter 2 A Boron-Containing Ternary Electrolyte for Excellent Ion Transference and Stabilization of LiNMC Cathode in Lithium-ion Battery

2.1 Introduction

Since the commercialization of lithium-ion batteries (LIBs) in 1991, these energy storage devices have undergone a transformative evolution, revolutionized electronic applications, and generated a growing demand for high-energy-density rechargeable battery technologies. Originally, being employed in portable devices, LIBs have pushed the boundaries to electric vehicles and electric vertical take-off and landing[1–4]. This demand for such applications necessitates the development of high energy density cathode electrodes and exceptional stability for prolonged cycling. In pursuit of this objective, numerous efforts for developments and/or improvements of cathode materials specifically tailored for high-density cathode LIBs have been made, as extensively documented in literature[5]. A better and more convenient focus involves investigating electrolyte systems that are well-suited for high energy density batteries. Traditional electrolytes based on alkyl carbonate solvents are susceptible to degradation at a voltage above 4.3 V vs. Li^+/Li[6]. Addressing this challenge becomes paramount for ensuring high-energy-density lithium-ion batteries with sustained performance and reliability in diverse applications.

Among various high-energy-density lithium transition-metal oxides, $Li[Ni_xCo_yMn_z]O_2$ (LiNMC) have received considerable attention and been extensively studied. LiNMC has garnered interest due to its high discharge capacity, better rate capability and structural stability[7], while a moderate rise in cutoff voltage limit led to specific discharge capacity at the expense of capacity fading[8,9]. The root cause is linked to enhanced surface reactivity between the delithiated unstable cathode and the electrolyte, giving rise to high interfacial impedance. Moreover, the poor electrochemical performance is associated with the polarization effect, decomposition of electrolyte solution and gradual decaying of cobalt into electrolytes or structural alterations in the cathode material[10]. In-depth investigations into the effect of electrode surface and performance based on electrolyte composition have led to an

understanding that the oxydation of the solvent on the cathode surface before the intercalation process results in the formation of a surface film known as the cathode electrolyte interphase (CEI). The CEI's composition reflects the stability of electrode by forming compact and passivating layers that isolate the electrolyte solution from active component of electrode[1,11]. In addition, CEI acts as a protective barrier, permitting Li^+ migration while keeping the solvent molecules out. One approach to improve the cathode life cycle is changing the surface chemistry of cathode to avoid undesired surface reactions and protect the integrity of bulk material.

Some surface modification methods are AlF_3[9] or ZrO_2[12] surface coatings, lattice doping[13,14], electrolyte additives and reactive gas treatments[15,16] to improve the rate capability, capacity retention and interface stability. The different methods based on forming a buffer layer between the electrolyte and highly reactive oxygen species in the cathode require an additional step or tedious process for synthesis and fabrication.

An effective way to protect the surface of electrode would be using a functional solvent. The properties of functional solvent will render unique properties that stabilise the cell containing high energy density cathode for extended cycles. Some solvents that are reported to be better solvents than commercially available solvents (ethylene carbonate (EC), diethyl carbonate (DEC), dimethyl carbonate (DMC) etc.) are fluorinated solvents[17], sulfones[18] and dinitriles[19]. But the above functional solvents need high cost, produce gas in Li cells and increase impedance[20–22]. Incorporating multiple solvents into the electrolyte has proven to be effective in enhancing the performance of LIBs. Conversely, introducing boron compounds as electrolyte additives has demonstrated a notable reduction in electrode-electrolyte interface resistance. Furthermore, boron favours anion coordination in electrolytes, which offers enhanced ionic conductivity and transference number, as reported by McBreen et al. Polymer electrolytes containing boron showed significant cation transport selectivity by interacting with

the anion group of the lithium salt[23–26]. Alkylborane-based molten salt resulted in high lithium transport due to alkylborane Lewis acidity, however, its ionic conductivity is 10^{-5} S cm^{-1} at 51 ℃[27]. Looking into the benefits of solvent-based electrolyte and boron-based organic compounds in Li^+ transference and ionic conductivity, a multi-solvent electrolyte will be well suited for high-energy-density LIBs.

This study's primary objective is to prepare a multi-solvent matrix containing boron-based organic molecules and carbonate solvents. By adding low polarity boron compound, multi-solvent matrix can increase lithium transference number by breaking strong dipole-dipole interaction between solvent sheath and lithium ion, subsequently forming favorable coordination with the anion species of the salt [28]. In addition, the enhanced Li^+ mobility will enhance battery performance, through lower overpotential and better discharge capacity under high rate. Moreover, the boron can eliminate F^- formed on the surface by coordinating with the boron atom before HF reacts with lithiated transition metal oxides to cause the leaching of transition metals from the electrode into the electrolyte. Hence, a ternary solution containing mesityldimethoxyborane (MDMB), EC and DEC were used to incorporate the benefits of carbonate solvent (good dissociation of lithium salt, low viscosity[29]) and boron-based organic molecule (F^- elimination, anion trapping and boron-containing CEI). This ternary MDMB-containing electrolytes exhibit good compatibility with LiNMC and enhance battery performance of cathodic half-cells. Besides, oxidating boron-based solvent on the electrode surface will form boron-rich CEI, facilitating Li^+ diffusion in the electrode by developing Li^+ diffusion sites[30].

2.2 Experimental

2.2.1 Materials and synthesis

Magnesium turnings were purchased from NACALAI TESQUE, INC. Crystal iodine, THF, trimethoxy borane and diethyl ether super dehydrated were purchased from FUJIFILM Wako Pure Chemical Corporation. 2-Bromomesitylene was purchased from Sigma-Aldrich Co. LLC. Ethylene carbonate (EC)/Diethylene carbonate (DEC) electrolyte with volume ratio of 50:50 was purchased from KISHIDA CHEMICAL Co., Ltd. LiTFSI was purchased from KANTO CHEMICAL CO., INC. The $LiNi_{0.33}Mn_{0.33}Co_{0.33}O_2$ electrode was purchased from Piotrek Co., Ltd.

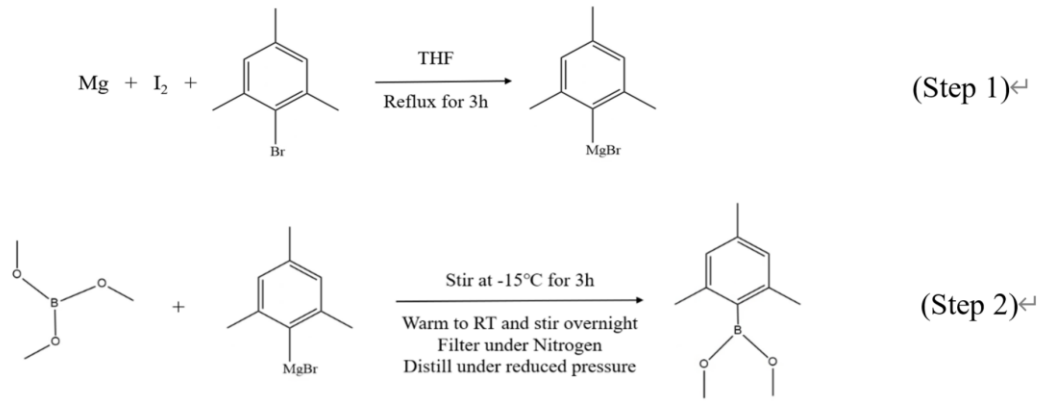

Figure 1. Schematic illustration of the synthesis of MDMB.

The modified synthetic method of MDMB has been reported in previous work of Matsumi, N. et al[31]. Synthesis of MDMB is presented in **Figure 1**. A solution of 2-bromomesitylene in THF was added dropwise to magnesium turnings and crystal iodine. The reaction mixture was refluxed for 3h under nitrogen and then the resulting solution was added into an ether solution of trimethoxyborane at -15 °C. After it was stirred overnight and warmed to room temperature,

it was filtered, concentrated, and distilled under a reduced pressure to give mesityldimethoxyborane (MDMB). All the steps were completed under nitrogen atmosphere.

2.2.2 Cell preparation

Three electrolytes were prepared with different ratios of MDMB into EC/DEC solvent. As volume ratio of EC : DEC : MDMB is equal to 1:1:0, this solvent is further named as 110. In the same way, the solvents with volume ratio of EC : DEC : MDMB=1:1:1 and 1:1:2 are named as 111 and 112 for short. Finally, the LiTFSI salt was dissolved into these three solvents to prepare 1.0 M LiTFSI electrolyte. Three kinds of cells were fabricated to measure various electrochemical properties as shown in **Figure 2 and Table 1**, including:

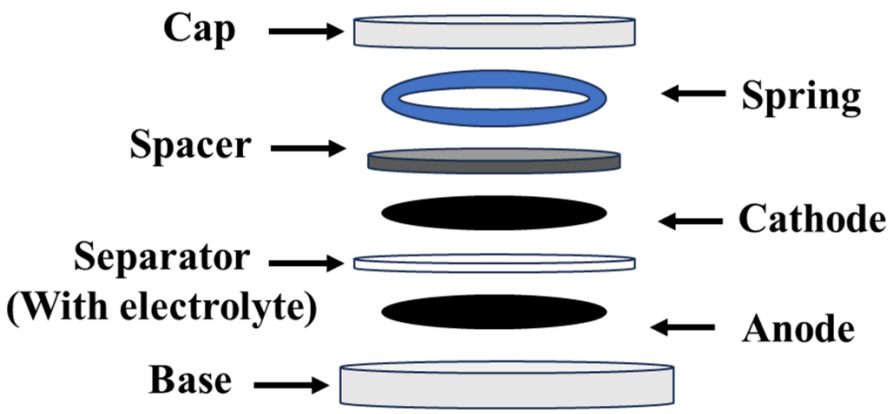

Figure 2. Coin cell fabrication setup.

(1) Lithium symmetric cell: Lithium foil was punched into 13 mm diameter circular discs. Then Li||electrolyte(separator)||Li symmetric cell was fabricated for lithium-ion transference number and lithium plating measurements.

(2) Stainless steel symmetric cell: two discs of spacer in CR-2025 coin were used as cathode and anode in stainless steel symmetric cell to measure the ionic conductivity through coin cell.

(3) Cathodic half-cell: The $LiNi_{0.33}Mn_{0.33}Co_{0.33}O_2$ sheet was punched into circular discs of 13 mm diameter, then dried at 80 ℃ overnight to remove the water moisture attached to the surface of cathodic electrode. Then the dried $LiNi_{0.33}Mn_{0.33}Co_{0.33}O_2$ was used as cathode in CR-2025 coin-cell with lithium disc as counter electrode to fabricate cathodic half-cell using 70 μL of electrolyte. All these cells were fabricated in the argon-filled glove box.

Table 1. Setups for various coin cells and corresponding measurements.

Cell name	Anode	Cathode	Measurements
Lithium symmetric cell	Li disc	Li disc	Li^+ transference number, lithium plating
Stainless steel symmetric cell	Stainless steel spacer	Stainless steel spacer	Ionic conductivity
Cathodic half-cell	Li disc	NMC111 disc	DEIS, charge-discharge, rate study, CV, activation energy
Full battery	Graphite disc	NMC111 disc	Rate study, long cycle

2.2.3 Electrochemical studies

A Biologic VSP electrochemical workstation equipped with a frequency response analyzer (FRA) was utilized for electrochemical characterizations. Lithium-ion transference number was determined with Li||Li symmetric cells by electrochemical impedance spectroscopy (EIS) and chronoamperometry (CA)[32,33]. After the initial EIS (frequency range: 0.1 Hz to 1 MHz), a 30 mV constant voltage was applied. At the same time, the current fluctuation was monitored by CA technique until a stable current was achieved. Then the EIS of steady-off cell was measured and recorded. Lithium plating was measured with 0.5 $mA \cdot cm^{-2}$ current density and 1.5 $mAh \cdot cm^{-2}$ at 25 ℃ with Li||Li symmetric cells. Stainless steel symmetric cells were applied for ionic conductivities by EIS technique with a temperature range from 30 ℃ to 60 ℃. The thickness of separator was used as the height of electrolyte for ionic conductivity calculation.

The following measurements were carried out on $LiNi_{0.33}Mn_{0.33}Co_{0.33}O_2$ cathodic half-cell. Dynamic electrochemical impedance spectroscopy (DEIS) studies were conducted through EIS technique at different working potential in range of 2.8V to 4.2V. In the floating test, the battery was firstly charged to a certain voltage, then kept for 10h under this voltage and was monitored its current during this process. Cyclic voltammetry (CV) was performed between 2.8 V and 4.2 V vs Li/Li^+ at 0.1 mV s^{-1} and 0.2 mV s^{-1}. The charge and discharge tests were carried out by Electrofield ABE through a battery cycler at 25 °C under different rates and modes.

2.2.4 Post-morphology studies

The morphology and composition of the samples were determined by field emission scanning electron microscopy (FESEM, Hitachi S-4500 instrument at 1.0 kV), and X-ray photoelectron spectroscopy (XPS) measurements were conducted on Fisons instruments S-

probe TM 2803.

2.2.5 Computational calculations

Material studio was applied to calculate the interaction energy of electrolytes. To calculate the interaction energy of different electrolyte modes, corresponding forcite and charge of each molecule and ion were set first. After setting the forcite for all solution compositions, amorphous cell mode was applied to build the solution cells. The temperature of cells was constant at 298 K, and 'Ultra-fine' was selected as the convergence accuracy. E_{total} was calculated based on the amorphous cell including all electrolyte compounds — DEC, EC, MDMB, $TFSI^-$, and Li^+. This system maintained electrical neutrality. E_{Li+} was calculated based on the amorphous cell including only Li^+. $E_{rest\ electrolyte\ component}$ was calculated based on the amorphous cell including DEC, EC, MDMB and $TFSI^-$. The following formula calculated the interaction energy:

$$E_{int} = E_{total} - E_{Li+} - E_{rest\ electrolyte\ component}$$

Correct forcite and charge of each molecule and ion are set. In the forcite calculation mode, 'energy' task, and 'COMPASS III' forcefield were used. In forcite preparation options, choose 'Forcefield assigned' for charges and calculation was done. Then the charges given by this calculation were checked. By this method, the Netcharge of MDMB, EC, DEC, lithium ion, $TFSI^-$ are $-2.32e^{-10}$, $-5.21e^{-8}$, $-4.47e^{-8}$, 1.00, and -1.00, respectively.

After setting the forcite for all compositions of the solution, the amorphous cell mode, construction task, COMPASS III forcefield, 'use current' were used for charges to build the solution cell. The mole amount of each composition was calculated by the mass weight divided by molecular weight. The ratio used for each cell building is listed below:

110: DEC: EC: Li: TFSI= 48: 64: 10: 10, lengths (Å):27.6*27.6*27.6

111: DEC: EC: MDMB: Li: TFSI= 31: 42: 19: 10: 10, lengths (Å):27.6*27.6*27.6

112: DEC: EC: MDMB: Li: TFSI= 23: 31: 28: 10: 10, lengths (Å):27.6*27.6*27.6

After the solution amorphous cell mode was built, it included all the components DEC, EC, MDMB, Li, $TFSI^-$, here it was named as mode 1. In order to calculate the interaction energy between the Li ion and its sheath (other components in the solution), another two cells were also built to calculate their total energy.

Mode 2: Amorphous cell included DEC, EC, MDMB, $TFSI^-$, without Li. It was built by deleting all lithium ion in mode 1.

Mode 3: Amorphous cell only had Li. It was built by selecting 10 whole lithium ions and copied them into a new cell. The positions of Li ions kept same with the mode 1.

In the Dmol3, the systems were calculated with COMPASSIII (version 1.2) as forcefield, Ewald as summation method, Use current as charges, 2 A as buffer width. For van der waals terms, the settings were ‘atom based’ for summation method, ‘cubic spline’ for truncation method, ‘12.5 A’ for cutoff distance, ‘1 A’ for spline width, ‘2 A’ for buffer width.

The color codes for the atoms in the molecules studied are gray for carbon, pink for borane, purple for lithium, blue for nitrogen, yellow for sulfur, cyan for fluorine, red for oxygen and white for hydrogen.

2.3 Result and discussion

2.3.1 Characterization of MDMB

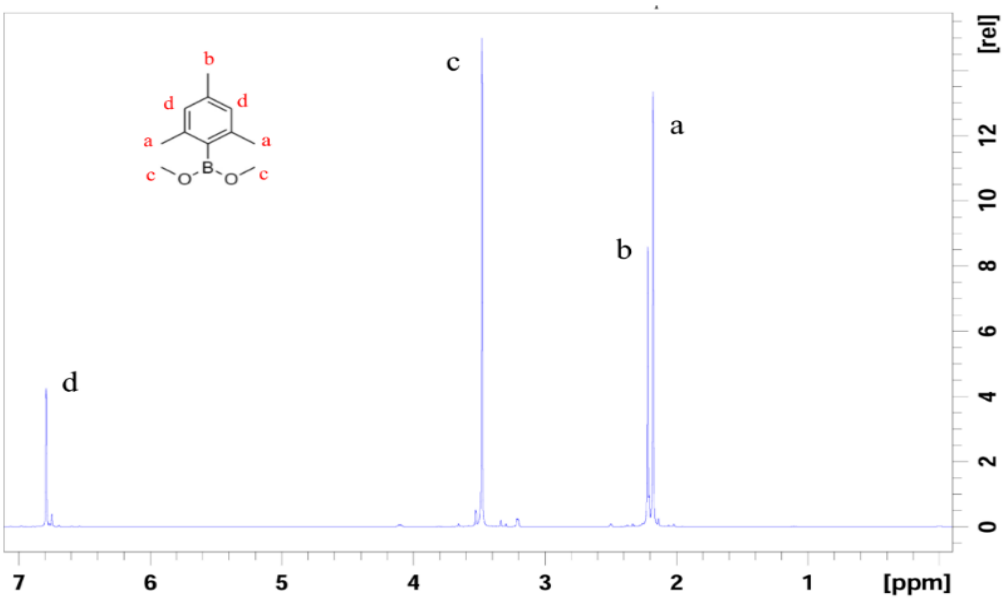

Figure 3. ^{1}H-NMR spectrum of MDMB in $CDCl_3$.

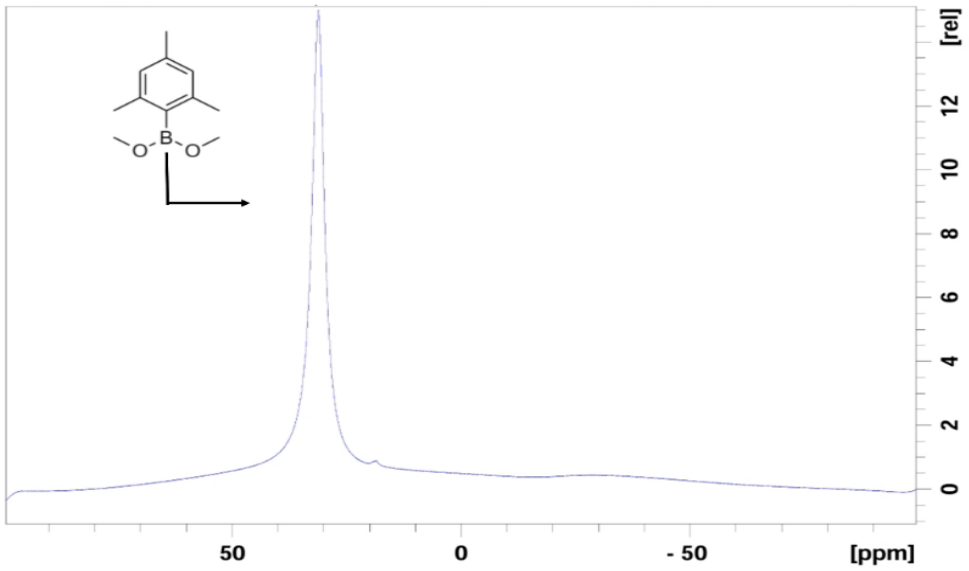

Figure 4. ^{11}B-NMR spectrum of MDMB in $CDCl_3$.

Figure 3 shows ^{1}H-NMR (400 MHz) spectrum of MDMB with peaks at 2.17 ppm ($-CH_3$, s, 3H), 2.21 ppm ($-CH_3$, s, 6H), 3.47 ppm ($-OCH_3$, s, 6H) and 6.79 ppm (C_6H_2, s, 2H), which

confirmed the structure of MDMB. **Figure 4** shows ^{11}B-NMR spectrum of MDMB with a peak at 30.90 ppm. This single peak at 30.9 ppm referring to the incorporation of boron as a boric ester in ^{11}B-NMR, which confirmed the presence of a single pure environment of boron. The ^{1}H-, ^{11}B-NMR spectra were consistent with the result reported by Matsumi, N. et al[31].

2.3.2 Comparative studies of ionic conductivity, transference number, and energy of solution systems, plating and stripping test of 110, 111 and 112 electrolytes

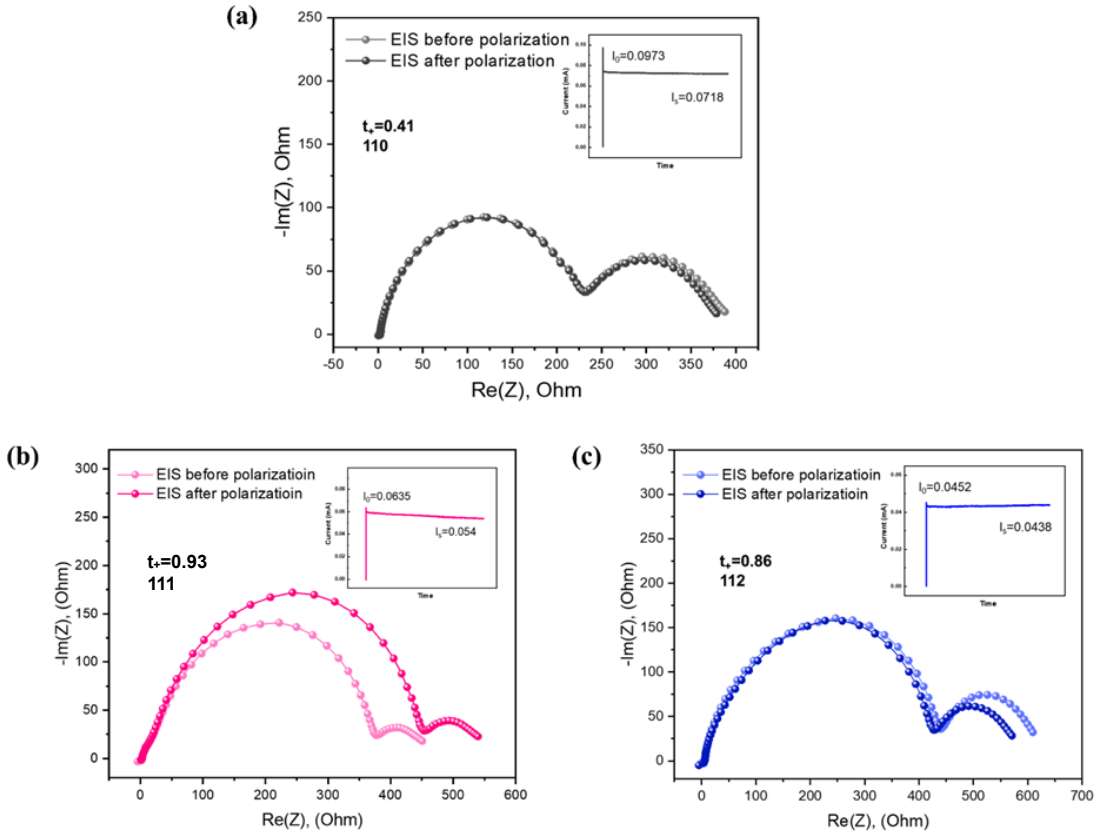

Figure 5. Impedance spectra of Li symmetric cell with (a) electrolyte 110, (b) electrolyte 111, and (c) electrolyte 112 before and after polarization. The inset shows current during the polarization process under 30 mV.

The lithium transference numbers were determined by potentiostastic polarization method, which was devised by Bruce and Vincet. The current during DC polarization under 30 mV, and impedance spectra before and after polarization of lithium symmetric cell with various electrolytes are shown in **Figure 5**. The EIS before polarization, after polarization and stabilized current of electrolytes 110, 111 and 112 were presented in Figure 5a, 5b, and 5c respectively. The lithium transference number was calculated based on the formula referring to Bruce and Vincent method:

$$t_{Li^+} = \frac{I_{ss}(\Delta V - I_0 R_0)}{I_0(\Delta V - I_{ss} R_{ss})}$$

ΔV represents the potential applied during the measurement. The terms I_{ss} and I_0 refer to the steady-state current and the initial current, respectively, which are observed from the CA profile. These currents provide information about the cell's behavior in response to a step change in voltage, where I_0 is the current at the moment the potential is first applied, and I_{ss} is the current once the system was stabilized at the new applied potential.

The resistances R_0 and R_{ss} represent the interfacial resistance before and after the CA measurement, respectively. R_0 is the initial interfacial resistance at the beginning of the measurement, reflecting the resistance of the electrode-electrolyte interface before any significant charge or discharge has occurred. R_{ss} refers to the steady-state interfacial resistance, which is the resistance after the system has reached equilibrium, typically once the electrochemical reactions were stabilized and the current has settled.

The value of lithium transference number of each electrolyte was presented in **Figure 6a**. Lithium-ion transference number for electrolyte 111 was 0.93, more than twice that of 110 (0.41). As an equimolar amount of LiTFSI was added into electrolyte, the high lithium-ion mobility presented by 111 and 112 is attributed to the addition of MDMB. In 111 and 112, the

high t_{Li^+} indicates that the dominant charge transfer in electrolyte is due to Li^+ conduction. This is mainly due to two reasons: the weaker interaction between Li^+ and solvation sheath[28], and the decreased anion mobility caused by efficient anion trapping[34].

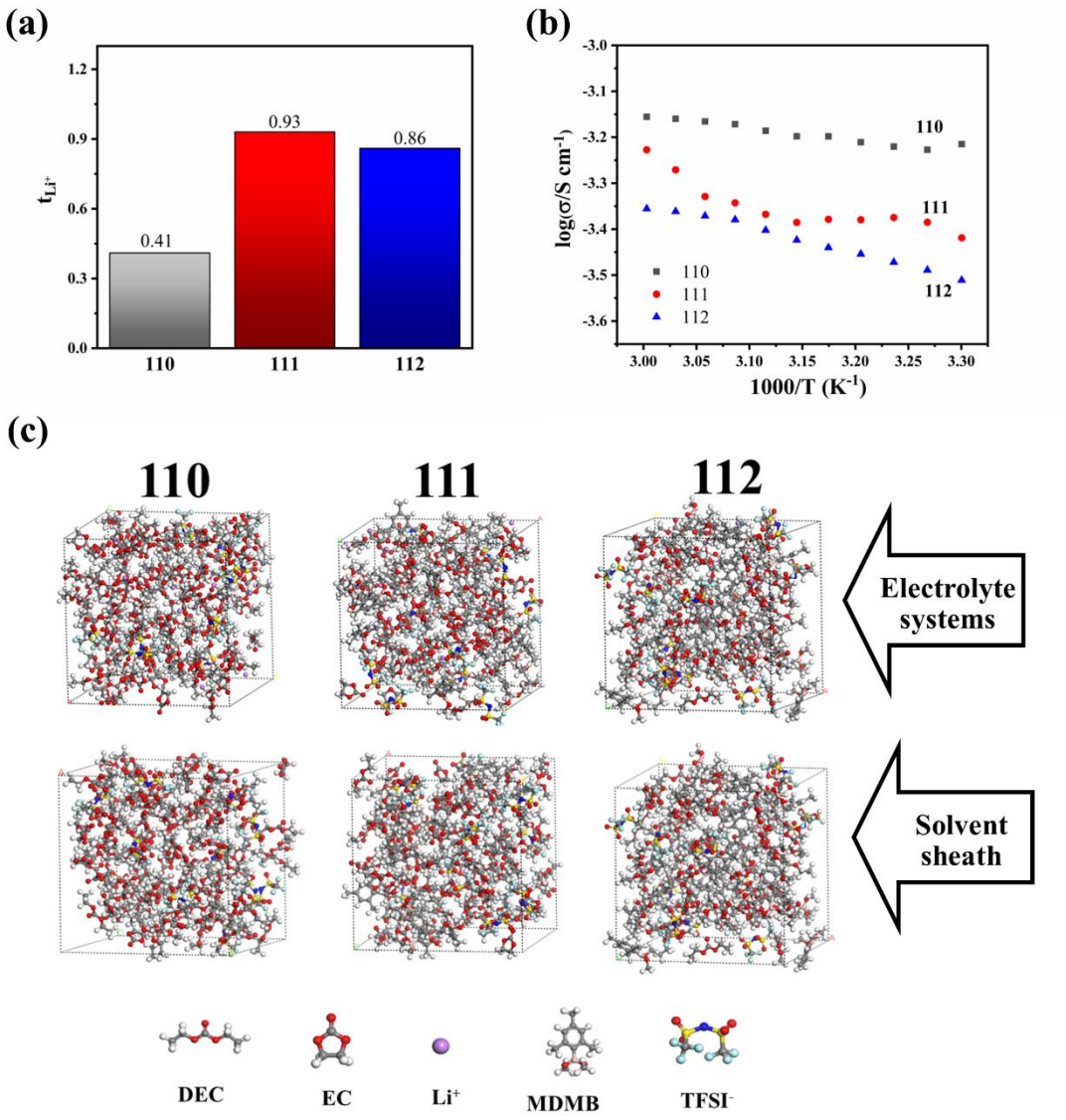

Figure 6. (a) Transference number of electrolyte 110, 111 and 112. (b) Ionic conductivity measurements at 30-60 ℃ temperature range. (c) Models of electrolyte (with lithium ions) and solvent sheath (without lithium ions) at 298 K.

Ionic conductivity of electrolytes was also studied to understand the conduction of cations and anions. In **Figure 6b**, it is shown that the ionic conductivity in 110 is higher than in 111 and 112. High lithium transference numbers of 111 and 112 demonstrated the strongly

decreased anionic mobility in 111 and 112 with MDMB addition. Ionic conductivity of these electrolytes at 51°C is $6.7*10^{-4}$ S cm^{-1}, $4.5*10^{-4}$ S cm^{-1}, and $4.2*10^{-4}$ S cm^{-1} for 110, 111 and 112, respectively.

To demonstrate the interaction energy of Li-solvent sheath and anion trapping in the electrolyte, solution systems were constructed and calculated by Material Studio software, as shown in **Figure 6c**. Calculation results of electrolyte systems shows that the E_{int} of Li^+-solvent sheath for 110 (-156.67 KJ/mol) is higher than 111(-147.97 KJ/mol) and 112 (-149.97 KJ/mol), consistent with the result of t_{Li+} (0.93 for 111 and 0.86 for 112). As 111 has the highest t_{Li+} value, its E_{int} is the lowest among the three electrolyte systems. Addition of MDMB into the electrolyte weakened the binding energy between Li^+ and solvent sheath, contributing to excellent lithium-ion mobility. Moreover, the decreased transference ability of anion is also demonstrated by the calculation of solvent sheath energy. Energy of the solvent sheath including EC, DEC, MDMB and $TFSI^-$ is -3111.72 kcal/mol, -3531.47 kcal/mol, and -3186.75 kcal/mol for 110, 111 and 112, respectively. Lower energy indicates the solvent sheath to be more stable, which means the bonding between the components of solvent sheath is stronger. The strengthened trapping for anion led to mobility diminishment, similarly as ionic conductivity results presented[34]. This is possibly due to the electron withdrawing boron center in MDMB interacting with the lone pair electron of oxygen and nitrogen in EC, DEC and $TFSI^-$. As this interaction is formed, it could not only impede anions movement, but also weaken the coordination power of oxygen and nitrogen atoms towards lithium ion which increases lithium transference ability.

The stability of MDMB-containing electrolyte was further demonstrated by the plating and stripping test of lithium symmetric cells with various electrolytes in **Figure 7**. The results demonstrated the superior stability of MDMB-containing electrolytes during lithium plating

and stripping cycles. Both 111 and 112 exhibited enhanced cyclability, as evidenced by reduced polarization compared to the cell using 110 electrolyte. This suggests that the inclusion of MDMB improves the reversibility of lithium deposition and dissolution processes, which is critical for minimizing dendrite formation and enhancing cycle life.

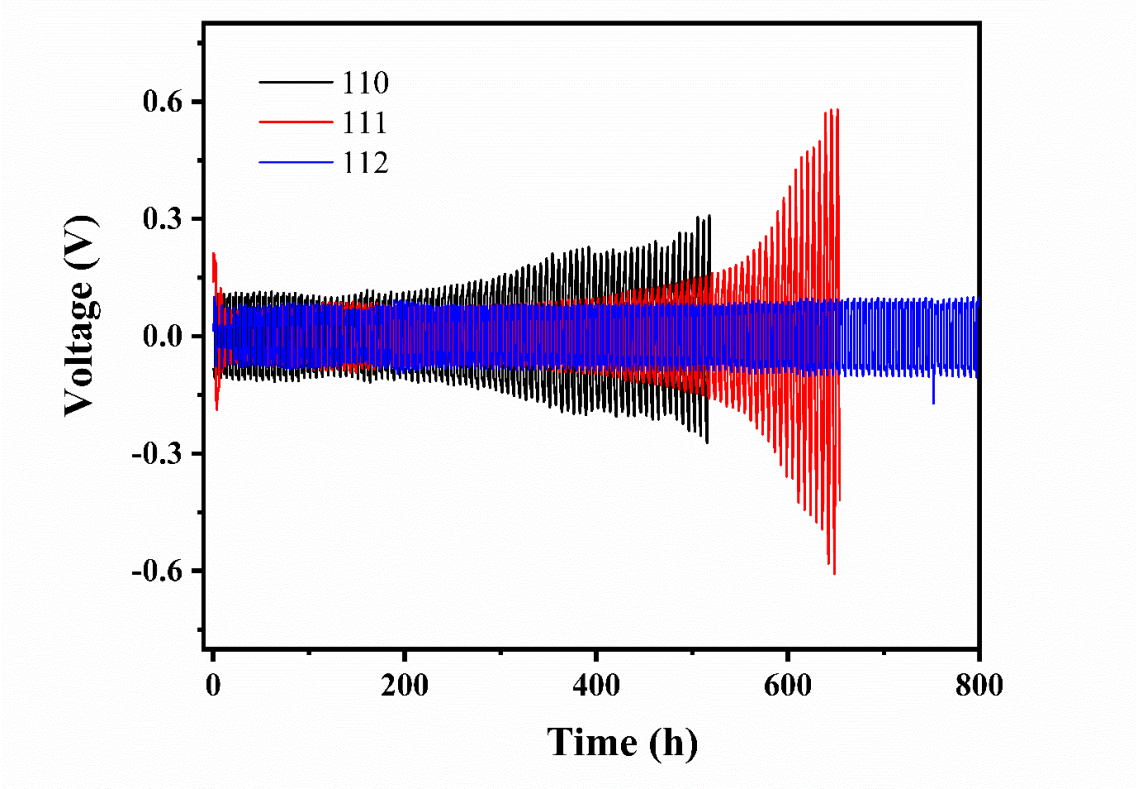

Figure 7. Lithium plating and stripping test with lithium symmetric cells with various electrolytes at 0.5 mAcm^{-2} and 1.5 mAh cm^{-2}.

In the case of 110, the relatively poor performance in plating and stripping tests results from the electrolyte's inability to form a stable, protective solvation sheath around lithium ions, which can lead to uneven lithium deposition and dendrite growth. In contrast, the MDMB-containing electrolytes (111 and 112) facilitate more uniform lithium deposition and stripping by reducing the formation of lithium dendrites, thereby mitigating polarization and enhancing overall electrochemical performance. Tthese results underscore the positive impact of MDMB-containing electrolytes in improving the cycling stability and safety of lithium-ion batteries by facilitating more efficient and stable lithium plating and stripping processes.

2.3.3 Electrochemical performance of 110, 111 and 112 in the cathodic half-cell and full cells

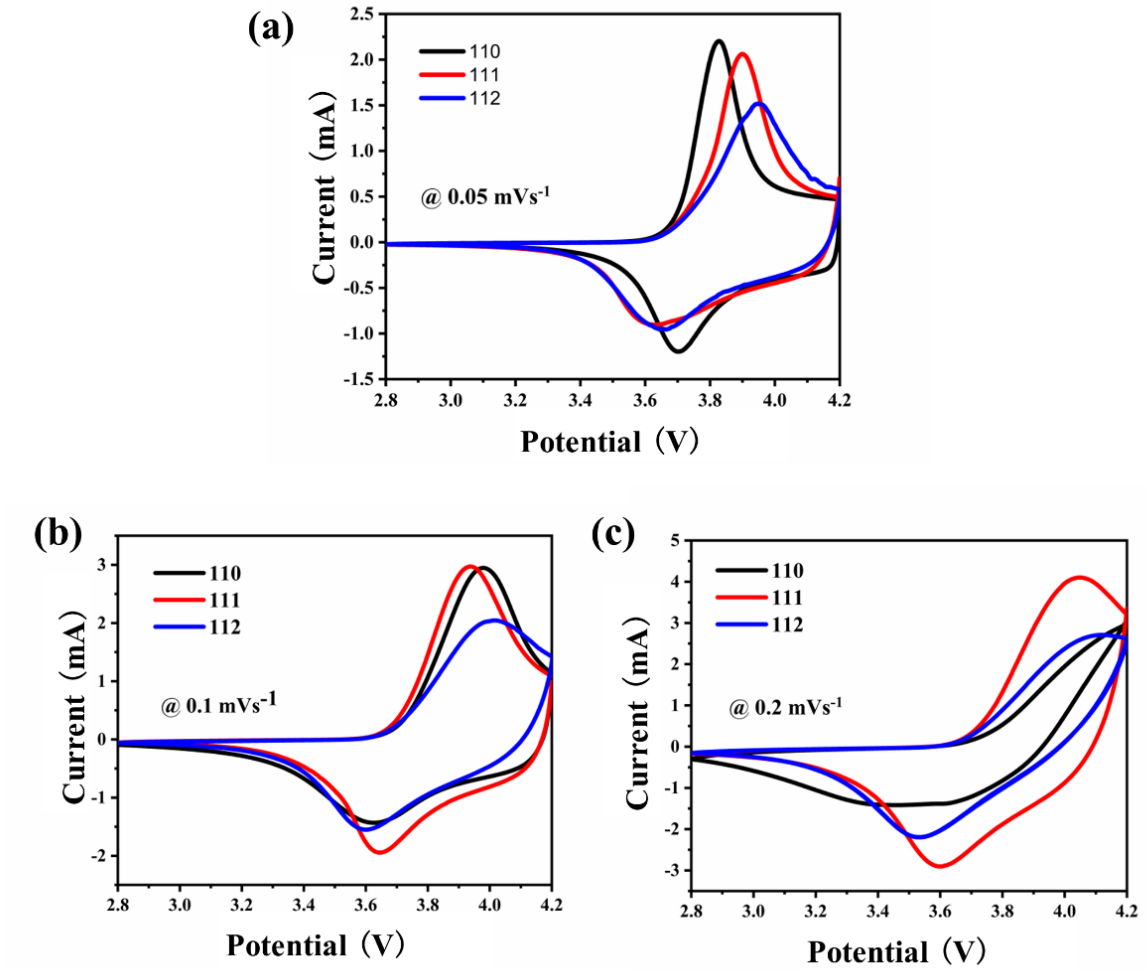

Figure 8. CV studies of cathodic half-cells between 2.8 V to 4.2 V with electrolyte 110, 111 and 112 at (a) 0.05 mVs^{-1}, (b) 0.1 mVs^{-1}, and (c) 0.2 mVs^{-1}

As the lithium mobility of 110, 111 and 112 bulk electrolytes had a huge difference, it further influenced the performances of cells. In the cathodic half-cell fabricated with $LiNi_{0.33}Mn_{0.33}Co_{0.33}O_2$, 110, 111 and 112 were studied by cyclic voltammetry technique under 0.05 mV s^{-1}, 0.1 mV s^{-1} and 0.2 mV s^{-1} scan rate. The CV result at 0.05 mV s^{-1} was studied and presented in **Figure 8a**, and position of oxidation peaks was listed in **Table 2** to further understand the overpotential. The overpotential obtained from oxidation peaks at 0.05 mV s^{-1}

to 0.1 mV s^{-1} was 0.15 V, 0.04 V and 0.07 V for 110-, 111- and 112- based cells respectively. The high overpotential signifies more energy would be consumed for the oxidation reaction to occur with 110 electrolyte at increased scan rate compared with 111 and 112 which own lower overpotential. In **Figure 8b**, the oxidation peaks were 3.98 V for 110, 3.94 V for 111 and 4.02 V for 112 at 0.1 mV s^{-1}. The differences between them were small. However, in **Figure 8c**, as the scan rate increased to 0.2 mV s^{-1}, it could be observed that the oxidation potential for 110 would be over 4.2 V. It shifted hugely from the position presented at 0.1 mV s^{-1}. In contrast, the oxidation potential for 111 and 112 at 0.2 mVs^{-1} was 4.040 V and 4.105 V respectively. The oxidation potential of 110 based cells was much higher than 111 and 112, which meant 110 had a higher overpotential. This result is consistent with lithium-ion transference ability. A low t_{Li^+} worsens concentration polarization during charging and discharging, especially at high rates, increasing not only the overpotential but also intensifying side reactions. Considering t_{Li^+} of 111 and 112 is markedly increased through ternary electrolyte method, it accounts for the small overpotential obtained under high rate.

Table 2. Positions of oxidation peak in CV at different scan rates with various electrolyte.

Electrolyte / Scan rate	110	111	112
0.05 mVs^{-1}	3.83 V	3.90 V	3.95 V
0.1 mVs^{-1}	3.98 V	3.94 V	4.02 V
0.2 mVs^{-1}	> 4.2 V	4.04 V	4.11 V

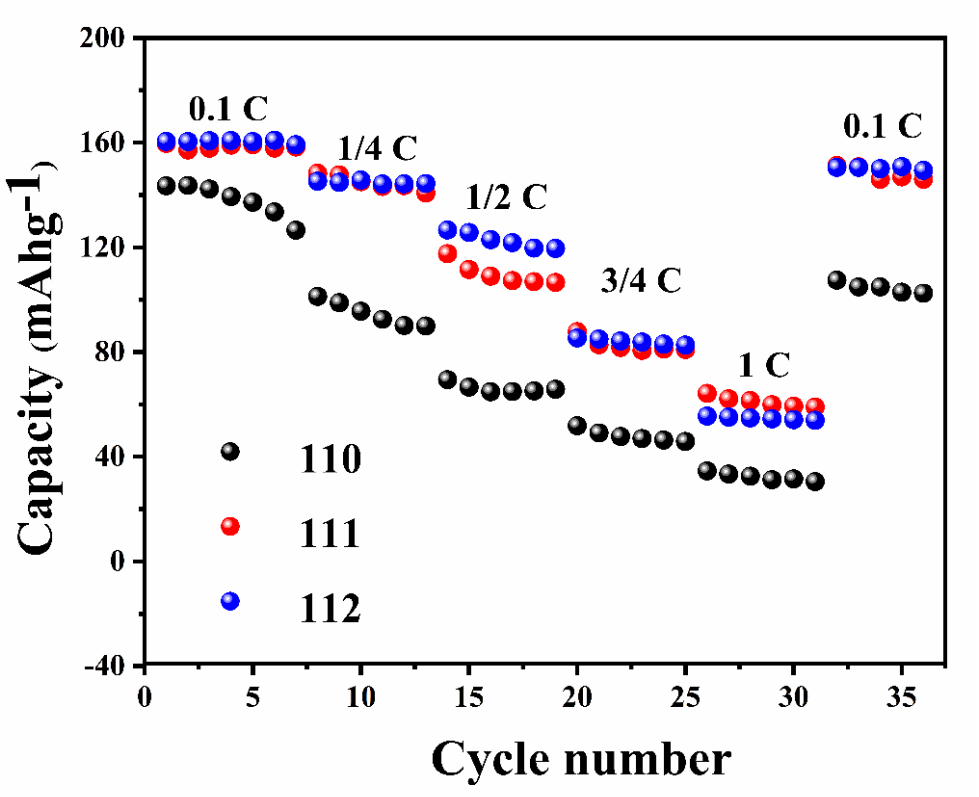

Figure 9. Rate capability of cathodic half-cells with electrolyte 110, 111 and 112.

In addition, charging and discharging ability of cathodic half-cells with electrolyte 110, 111 and 112 under different rates was also studied to learn the impact of MDMB on the electrolyte. As presented in **Figure 9**, batteries using MDMB containing electrolytes-111 and 112 exhibited better capacity than 110 as the rate increased. At a 1C rate, the discharge capacities of the electrolytes were 34.6 mAh/g, 64.2 mAh/g, and 55.5 mAh/g for 110, 111, and 112, respectively. These results indicate that the addition of MDMB to the electrolyte significantly improved the mobility of lithium cations, especially under high-rate conditions, which aligns with the higher lithium-ion transference number observed for electrolytes 111 and 112. This enhanced Li^+ mobility at elevated current rates is a critical factor for improving the overall performance of the battery, as it facilitates faster charge and discharge cycles with minimal polarization. Furthermore, after subjecting the cells to high-rate charge-discharge cycles, the cathodic half-cells using electrolytes 111 and 112 demonstrated excellent capacity recovery when the rate was reduced back to 0.1C. Specifically, the cells with 111 and 112

electrolytes recovered to 151.2 mAh/g (94.7% retention of the initial capacity) and 150.6 mAh/g (93.8% retention), respectively, indicating that the MDMB-containing electrolytes help maintain high reversibility and minimize capacity fade even under demanding conditions. In contrast, the cell with the 110 electrolyte showed a much lower recovery, reaching only 102.4 mAh/g (71% retention), highlighting the superior cycling stability and rate performance of MDMB-based electrolytes. This superior recovery in cells with 111 and 112 electrolytes suggests that the MDMB additive not only enhances high-rate performance but also contributes to better structural stability of the electrodes, reducing irreversible capacity loss and ensuring more consistent long-term cycling behavior. The improved electrochemical stability and performance under high-rate conditions make these MDMB-containing electrolytes highly advantageous for high-performance, long-lasting lithium-ion batteries.

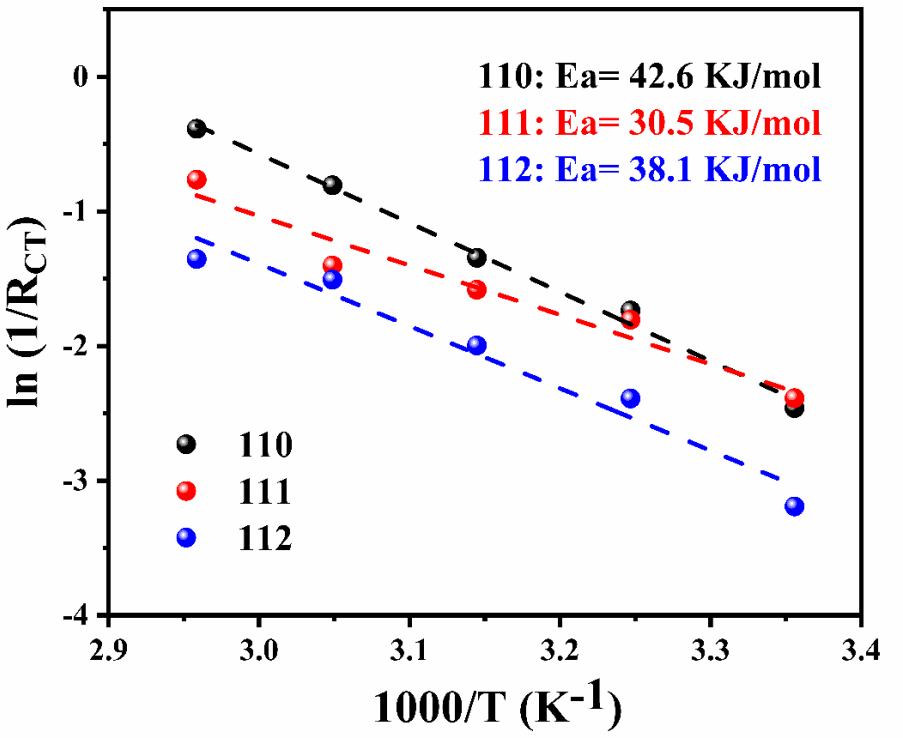

Figure 10. Comparison of E_a values of different electrolyte systems.

Activation energy for charge transference process was calculated through the slope of Arrhenius plot in cathodic half-cell at 4.2 V under different temperatures, as shown in **Figure**

10. The E_a value obtained by linear fitting of impendence for 110, 111 and 112 was 42.6 kJ/mol, 30.5 kJ/mol, 38.1 kJ/mol. This corroborated that an easier desolvation process on cathode surface and Li^+ intercalation into electrode was realized by MDMB- containing electrolyte. The activation energy of the electrolyte mixture 111 was found to be the lowest among the three tested electrolytes. This indicates that the optimal solvent composition, consisting of a 1:1:1 ratio of ethylene carbonate EC, DEC, and MDMB, effectively forms a stable solvation sheath around the lithium ions. This solvation sheath facilitates improved ionic conductivity by reducing the energy barrier for lithium-ion migration, thereby enhancing the overall electrochemical performance. These results suggest that this specific solvent ratio is particularly conducive to promoting efficient lithium-ion transport in the electrolyte, which is consistent with the previous result.

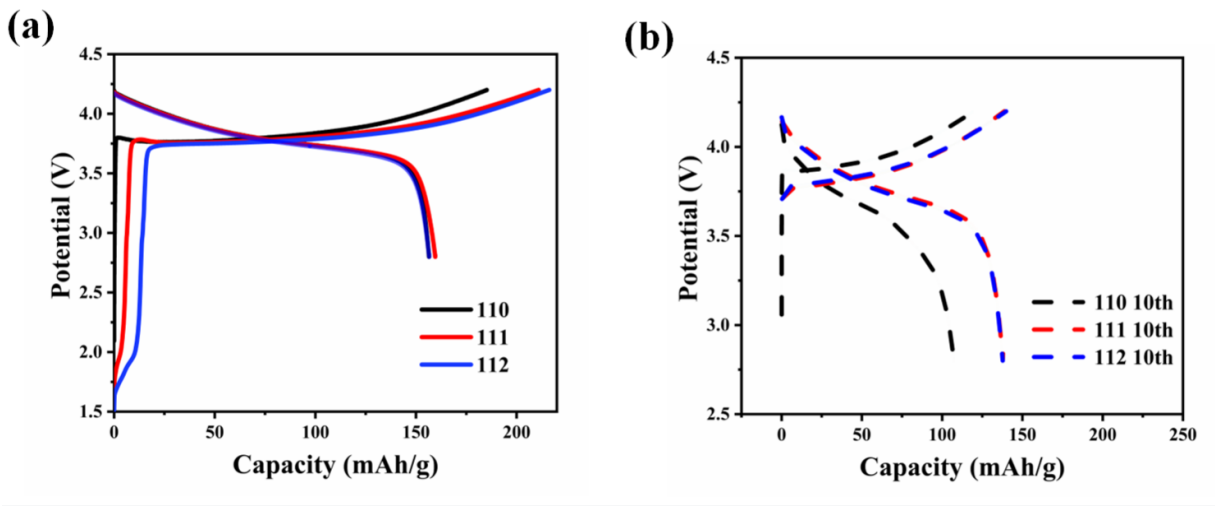

Figure 11. Charge/discharge profile of cathodic half-cells between 2.8 V to 4.2 V at 0.1 C for initial cycle and (b) 10th cycle with different electrolytes.

In addition, MDMB-containing electrolytes demonstrated improved stability in electrochemical performance. As shown in Figure 11a, the charge and discharge profiles of the initial cycle reveal that both 111 and 112 exhibited higher charging capacities, likely due to the decomposition of MDMB and its participation in the formation of the CEI. During the charging

process (from 2.8 V to 3.8 V), electrolytes 111 and 112 delivered higher capacities compared to 110, with 112 showing approximately double the capacity of 111. However, the discharge capacities of all three electrolytes were relatively similar in the initial cycle. This suggests that the additional charging capacity observed in 111 and 112 corresponds to an irreversible reaction. Furthermore, the capacity difference between 111 and 112 implies that MDMB decomposes to form the CEI, and that varying the ratio of MDMB in the electrolyte results in differences in the composition of the CEI.

After 10 cycles, discharge capacity of cell with 110 electrolyte decayed seriously compared to 111 and 112, as shown in **Figure 11b**. The discharge capacities after 10th cycle of cells with various electrolyte are 107.29 mAh/g, 137.91 mAh/g and 137.69 mAh/g for 110, 111 and 112. The capacity retention of 110 is 68.6%, much lower than 111 (86.5%), and 112 (87.9%). Although the addition of MDMB into conventional electrolyte could not terminate the decay happened inside cathodic half-cell, it significantly reduces the degree of attenuation and extends cells' service life. The electrochemical floating test was performed under 3.9V, 4.0V, 4.1V and 4.2V for 10h in succession.

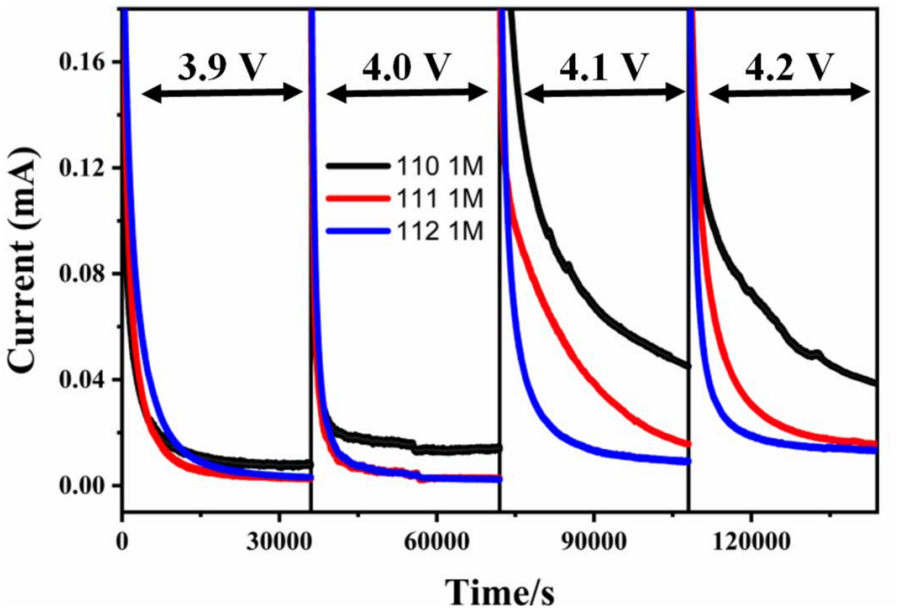

Figure 12. Electrochemical floating test of $LiNi_{0.33}Mn_{0.33}Co_{0.33}O_2$||Li cathodic half-cells under

various potential with 110, 111 and 112 electrolytes.

As shown in **Figure 12**, the $LiNi_{0.33}Mn_{0.33}Co_{0.33}O_2$||Li cathodic half-cells were charged to the potential and kept under this potential for 10 hours to monitor the current leakage situation. Three electrolytes exhibited similar current leakage curves. However, boron-containing electrolytes always had lower leakage currents under different voltages. This result further proved that MDMB improved the oxidation stability of electrolytes. The addition of MDMB could passivate surface of cathodic electrode and reduce decomposition of electrolyte[35]. It was worth mentioning that under 4.2V, the leakage current of 110 was more than twice that of 111 and 112 (0.0386 mA for 110, 0.0156 mA for 111, and 0.0132 mA for 112). It suggested that the side reactions like electrolyte decomposing, cathodic material dissolution, and aluminum corrosion happened in cell with traditional carbonate electrolyte, were considerably hindered by MDMB addition.

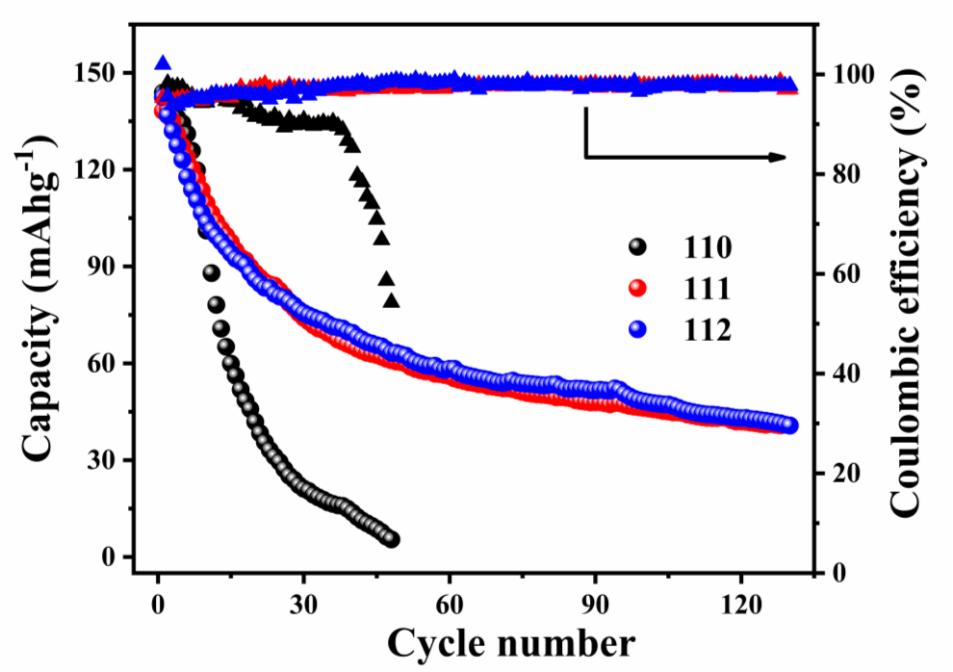

Figure 13. Discharge capacities and coulombic efficiencies of cathodic half-cells with different electrolytes at 1C in CCCV mode.

On the basis of excellent stability of boron-containing electrolytes, the constant current constant voltage (CCCV) cycling mode was employed to evaluate the durability of cells with

various electrolytes. Cells using MDMB-containing electrolytes exhibited significantly longer lifetimes compared to the blank electrolyte. The cells were cycled at a 1C constant current to 4.2 V, followed by charging under constant voltage at 4.2 V. For the cell with the 110 electrolyte, both coulombic efficiency and capacity experienced substantial degradation. After 48 cycles, its capacity had dropped to 5.4 mAh/g, while its coulombic efficiency plummeted to 54.3%, as shown in **Figure 13**. In contrast, cells with 111 and 112 electrolytes demonstrated superior durability, retaining 40.8 mAh/g with a coulombic efficiency of 97.02% for 111, and 40.7 mAh/g with a coulombic efficiency of 97.75% for 112 after 130 cycles. Compared to the extremely poor cyclability of the 110-based cell, the boron-containing electrolytes enabled cells to cycle for 130 cycles while maintaining a capacity retention of approximately 40 mAh/g. These results suggest that the incorporation of MDMB significantly enhances the durability of NMC, improving both capacity retention and coulombic efficiency over extended cycling.

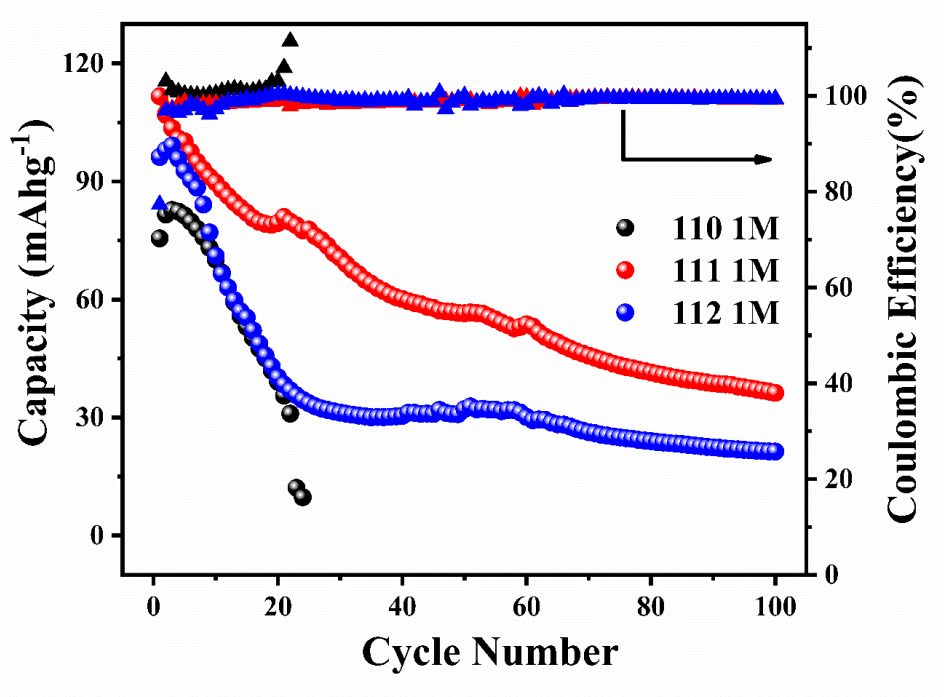

Figure 14. Discharge capacities and coulombic efficiencies of cathodic half-cells with different electrolytes at 1C in CC mode.

The charging and discharging results under 1C constant current (CC) mode are shown in

Figure 14. The durability of the cathodic half-cell was significantly enhanced by MDMB-containing electrolytes. The cell with the conventional electrolyte (110) exhibited a discharge capacity of 9.74 mAh/g and a coulombic efficiency of 111.40% at the 24th cycle, indicating substantial dissolution of $LiNi_{0.33}Mn_{0.33}Co_{0.33}O_2$ into the electrolyte at the cathode surface. In contrast, cells with electrolytes 111 and 112 effectively mitigated the dissolution of $LiNi_{0.33}Mn_{0.33}Co_{0.33}O_2$, maintaining a coulombic efficiency of approximately 99% over 100 cycles. These results highlight the superior protective effect of MDMB-containing electrolytes in preventing cathode material degradation and improving the long-term cycling stability of cathodic half-cells.

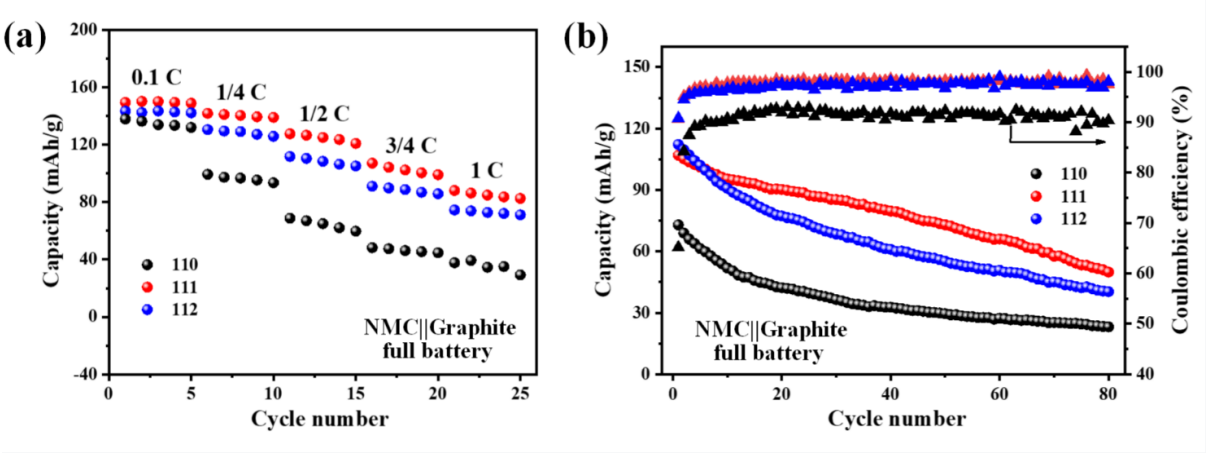

Figure 15. (a) Rate capability for $LiNi_{0.33}Mn_{0.33}Co_{0.33}O_2$||graphite full battery from 0.1 C to 1C, and (b) long cycling of $LiNi_{0.33}Mn_{0.33}Co_{0.33}O_2$||graphite full battery under 0.5 C.

The rate capability of full batteries using graphite as the anode is shown in **Figure 15a**. Consistent with the results obtained from the cathodic half-cell testing, the full cell with the 110 electrolyte demonstrated significantly lower capacities compared to those with 111 and 112 electrolytes, particularly under high-rate conditions. Specifically, at a 1C rate, the full cell with the 110 electrolyte delivered a capacity of only 37.7 mAh/g, which is notably lower than the capacities achieved with the 111 and 112 electrolytes, which were 88.0 mAh/g and 74.5 mAh/g, respectively.

These results clearly indicate that the incorporation of MDMB into the electrolyte (in electrolytes 111 and 112) significantly enhances the rate performance of the full cell. The superior performance of the MDMB-containing electrolytes can be attributed to improved lithium-ion mobility and charge transfer kinetics, particularly under high-current conditions. The presence of MDMB likely facilitates more efficient ionic conduction within the electrolyte, as well as stabilizing the CEI on the cathode, which in turn improves the overall efficiency and capacity retention during high-rate cycling.

The long-term cyclability of full batteries at a 0.5C rate is shown in **Figure 15b**. Notably, the full cell using the 110 electrolyte maintained a coulombic efficiency of approximately 91%. In contrast, cells with 111 and 112 electrolytes demonstrated significantly higher coulombic efficiencies of around 97%, indicating a substantial reduction in side reactions and enhanced electrochemical stability. This improvement suggests that the MDMB-containing electrolytes help minimize parasitic processes, such as electrolyte decomposition and the formation of unwanted by-products, leading to better overall efficiency.

Moreover, the capacity of full batteries with 111 and 112 electrolytes remained consistently higher throughout the cycling process, with minimal capacity fade over time. This suggests that the incorporation of MDMB into the electrolyte not only improves the electrochemical stability but also enhances capacity retention. The enhanced stability can be attributed to the formation of a more robust solid electrolyte interphase (SEI) and the reduction of interfacial resistance, which prevent degradation of the electrode material and maintain efficient lithium-ion transport during repeated cycling. As a result, the performance of the full battery with MDMB-containing electrolytes is significantly improved, making them more suitable for long-term, high-efficiency operation in practical applications.

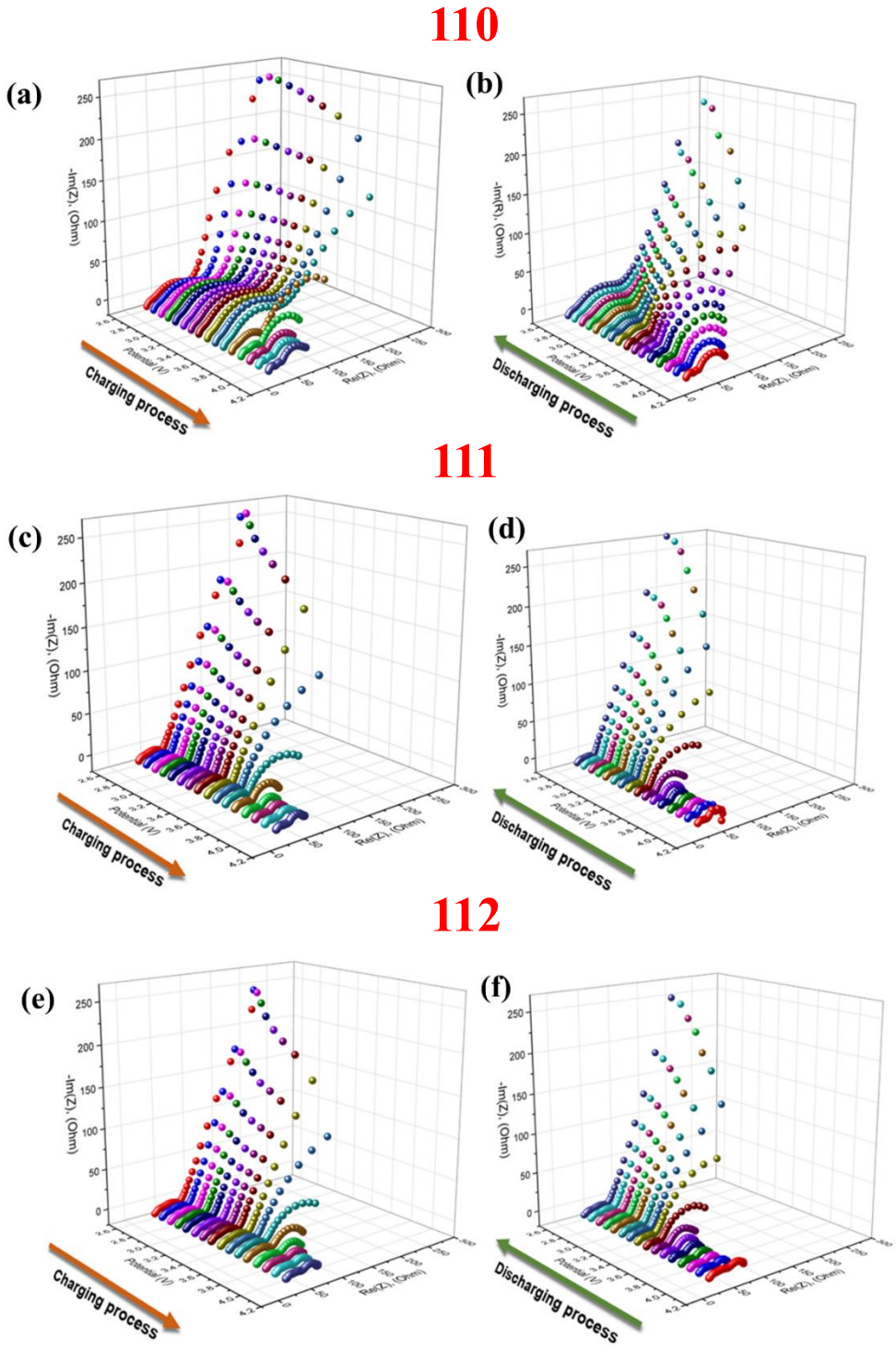

Figure 16. 3D DEIS Nyquist profiles for (a) charging and (b) discharging process under 2.8V–4.2V of cycled cathodic half-cell with 110 electrolyte; (c) charging and (d) discharging for 111 electrolyte; and (e) charging and (f) discharging for 112 electrolyte.

Dynamic electrochemical impedance spectroscopy (DEIS) is a powerful technique used to investigate the impedance characteristics of battery systems over a broad frequency range,

capturing information about different electrochemical processes, including charge transfer resistance, CEI layer resistance, and the impedance associated with bulk ionic conductivity. By analyzing the Nyquist plots, which display the real versus imaginary components of the impedance at different frequencies, one can assess the overall electrochemical performance of the battery, particularly the internal resistance dynamics during cycling. It was employed to evaluate the changes in resistance during the charging and discharging processes, providing insights into the internal electrochemical dynamics of the cells. DEIS measurements were performed on cycled cathodic half-cells within a potential range of 2.8 V to 4.2 V, covering frequencies from 0.01 Hz to 1.0 MHz, as shown in **Figure 16**.

In the high-frequency region, the impedance typically reflects the resistance of the electrolyte and the resistance to lithium-ion transport. At intermediate frequencies, the impedance is associated with the charge transfer resistance at the electrode-electrolyte interface, including the formation and stability of the CEI. Finally, at low frequencies, the impedance data are influenced by processes related to lithium-ion diffusion and the overall battery state of charge, which provides insight into the long-term stability of the electrochemical system.

The impedance spectra for cells with MDMB-containing electrolytes (111 and 112) exhibit lower overall resistance compared to those with the 110 electrolyte, indicating improved lithium-ion conductivity and more efficient charge transfer processes. This is consistent with the improved performance observed in the cycling tests, where the cells with 111 and 112 electrolytes demonstrated better capacity retention and lower polarization during charging and discharging cycles.

Moreover, the reduced impedance observed over multiple cycles in cells with MDMB-containing electrolytes suggests that these systems offer superior long-term stability, with minimal increase in resistance due to the protection provided by the CEI layer. This is in contrast to the cells with 110 electrolyte, which showed higher impedance growth, likely due

to the degradation of the CEI and increased internal resistance as a result of electrolyte decomposition or poor lithium-ion solvation.

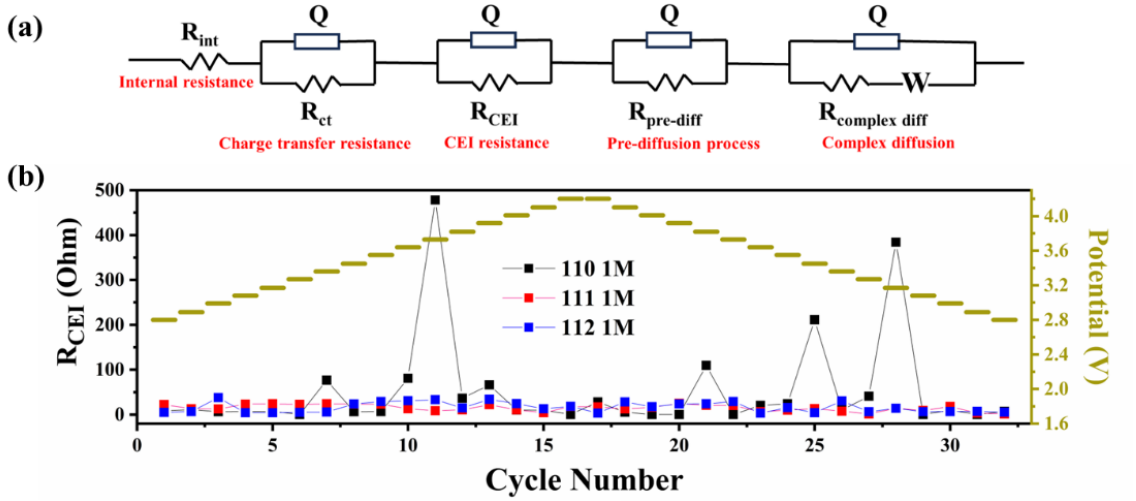

Figure 17. (a) Equivalent circuit used for DEIS fitting. (b) R_{CEI} under different voltages.

In **Figure 17a**, the circuit used for plot fitting was $R_{int}L(QR_{ct})(QR_{CEI})(QR_{pre\text{-}diff})(Q(R_{complex\ diffusion}W))$ to obtain component impedance values inside cathodic half-cell[30]. Resistances in the circuit stand for internal resistance, charge transfer resistance, CEI resistance, pre-diffusion resistance, and complex diffusion resistance respectively. W symbolises Warburg diffusion coefficient, and Q symbolized constant phase element[36]. The data obtained by fitted through this mode are presented in Table 3-8, which show the respective DEIS fitted parameters for cells with various electrolytes during charging and discharging process.

In **Figure 17b**, R_{CEI} under different potentials in charging and discharging process was presented. The plots reveal that the CEI formed by boron-containing electrolyte-111 and 112 was more stable than that of 110. The larger difference in R_{CEI} in 110 electrolyte system was possibly attributed to the decomposing and recompositing of CEI. In boron-containing electrolyte systems, R_{CEI} in 111 was in range of 1.43 Ω-25.08 Ω, and R_{CEI} in 112 was in range of 3.55 Ω-38.02 Ω. The low value of R_{CEI} indicated that a thin, robust, and highly ion conductive CEI formed on the surface of LiNMC, which also resulted in decreased activation energy.

Table 3. DEIS data obtained by Nyquist plot fitting in charging process with 110.

V (V)	R_{int} (Ω)	R_{ct} (Ω)	R_{CEI} (Ω)	$R_{pre\text{-}diff}$ (Ω)	$R_{com\text{-}diff}$ (Ω)	W ($\Omega s^{-1/2}$)	chi2
2.8	3.273	72.84	8.441	0.6069	2.54E+03	2.16E+07	5.41E-05
2.89	3.726	32.27	10.94	74.79	1.49E+03	1.28E-02	6.07E-04
2.99	2.89	67.85	6.339	1.17E+06	1564	2.66E+05	7.89E-05
3.08	2.793	67.27	6.956	187.1	817.4	1.57E-03	6.06E-05
3.17	3.304	109	7.411	3.79E+04	1.00E-02	1.19E-10	1.61E-04
3.27	3.164	112.3	0.3796	6.284	1.00E-02	1.05E-13	2.78E-04
3.36	2.762	6.619	76.65	500.7	2.28E+03	3.18E+02	6.15E-05
3.45	2.675	346.6	6.393	79.66	7.86E+03	1.40E-02	6.38E-05
3.55	2.936	112.9	6.903	0.3822	4.79E+00	2.45E-13	1.94E-04
3.64	2.583	2.04E+07	80.95	6.229	5.50E+02	4.68E+07	6.86E-05
3.73	2.815	29.3	478	81.76	3.99E+00	8.34E-01	5.37E-05
3.82	3.056	12.79	36.28	168.6	1.00E-02	1.24E-06	2.32E-04
3.92	2.896	10.14	66.29	21.19	5.09E-01	1.24E-01	3.50E-05
4.01	3.081	39.19	10.22	0.4731	1.65E+01	1.16E-01	3.97E-05
4.1	3.201	32.8	9.783	0.4622	1.42E+01	1.21E-01	3.30E-05
4.2	3.04	9.464	0.445	13.07	3.34E+01	1.16E-01	4.06E-05

Table 4. DEIS data obtained by Nyquist plot fitting in discharging process with 110.

V (V)	R_{int} (Ω)	R_{ct} (Ω)	R_{CEI} (Ω)	$R_{pre\text{-}diff}$ (Ω)	$R_{com\text{-}diff}$ (Ω)	W ($\Omega s^{-1/2}$)	chi2
4.2	2.867	5.229	28.51	8.884	8.48E-03	1.53E-04	8.46E-05
4.1	2.913	40.32	5.287	9.915	0.03949	1.66E-05	8.44E-05
4.01	2.876	9.683	0.4514	10.51	70.03	2.77E-01	2.22E-05
3.92	2.878	11.55	0.4403	10.06	89.83	3.93E-01	2.90E-05
3.82	2.846	10.17	109.8	0.4519	1.30E+01	1.85E+02	3.64E-05
3.73	2.793	15.92	0.4713	132	10.15	2.85E+00	3.48E-05
3.64	2.945	10.07	20.72	0.4123	167.6	4.52E+07	3.27E-04
3.55	2.644	0.6781	23.95	220.6	11.12	2.27E+01	7.24E-05
3.45	2.59	4.509	211.5	266.3	15.03	4.45E-01	1.14E-04
3.36	2.496	5.382	10.32	333.6	35.81	2.04E+08	8.66E-05
3.27	2.779	0.4478	41.1	11.92	466.1	3.61E+03	1.16E-04
3.17	2.764	0.4481	384.1	12.19	4.75E+01	1.80E-02	1.41E-04
3.08	2.773	57.88	0.4481	11.18	1265	4.49E+08	9.34E-05
2.99	2.754	69.04	10.05	0.5031	2112	1399	1.56E-04
2.8	2.093	65.91	7.31	3.06E+07	1.51E-01	8.21E-12	2.01E-05
2.89	2.751	9.86E+00	0.52	74.37	7122	5.72E-02	9.78E-05

Table 5. DEIS data obtained by Nyquist plot fitting in charging process with 111.

V (V)	R_{int} (Ω)	R_{ct} (Ω)	R_{CEI} (Ω)	$R_{pre\text{-}diff}$ (Ω)	$R_{complex\text{-}diff}$ (Ω)	W ($\Omega s^{-1/2}$)	chi2
2.8V	8.724	57.84	22.48	12.77	5.81E+02	5.92E-03	2.01E-05
2.89V	8.623	9.68E+09	13.11	20.32	6913	6.95E-15	5.61E-05
2.99V	8.714	23.73	12.57	42.2	776	0.001733	2.07E-05
3.08V	8.716	57.27	23.27	12.69	856.9	2.07E-03	1.80E-05
3.17V	8.705	7.459	24.26	12.21	1.78E+04	3.43E-12	2.48E-05
3.27V	8.704	66.15	23.12	12.55	644.3	2.18E-03	1.61E-05
3.36V	8.75	1636	24.02	12.26	103.5	0.008454	2.70E-05
3.45V	8.553	11.27	23.41	0.4221	1874	5.62E-02	2.38E-05
3.55V	8.553	11.27	23.41	0.4221	1874	5.62E-02	2.38E-05
3.64V	8.71	375.1	12.83	21.45	0.01	3.02E-06	4.65E-05
3.73V	0.302	8.837	8.906	23.47	93.41	1.32E-01	7.70E-06
3.82V	7.737	32.76	10.6	8.606	5.92E+05	4.31E-02	4.84E-05
3.92V	8.096	0.01	22.11	3.18	21.8	3.24E-01	1.76E-05
4.01V	5.322	0.83	10.7	24.62	9.18	6.94E+13	8.75E-05
4.1V	8.157	20.33	4.23	16.32	6.395	1.90E+05	2.07E-05
4.2V	7.744	2.781	17.9	21.11	2.54E+05	1.80E-05	1.29E-05

Table 6. DEIS data obtained by Nyquist plot fitting in charging process with 111.

V (V)	R_{int} (Ω)	R_{ct} (Ω)	R_{CEI} (Ω)	$R_{pre\text{-}diff}$ (Ω)	$R_{complex\text{-}diff}$ (Ω)	W ($\Omega s^{-1/2}$)	chi2
4.2V	8.12	11.22	17.25	3.058	1.07E+01	6.27E+00	1.70E-03
4.1V	6.164	0.2095	12.52	6.705	3.03E+13	1.45E-08	5.82E-04
4.01V	7.926	3.15	16.62	11.62	1138	1.91E-02	3.53E-05
3.92V	0.05846	7.502	25.08	15.86	447.5	2.72E-14	3.41E-05
3.82V	7.91	2.79	20.57	12.66	5.44E-02	6.20E-01	1.73E-05
3.73V	7.008	1.02E+15	20.39	9.437	0.01	3.95E+06	5.54E-05
3.64V	4.487	6.812	6.52	9.91	52.34	3.37E+00	5.44E-05
3.55V	8.225	99.84	9.91	2.787	8.083	1.23E-01	5.78E-05
3.45V	8.345	1.567	13.52	265.5	7.886	3.73E+05	7.05E-05
3.36V	7.918	3.878	7.49	13.96	560.8	1.91E-01	5.05E-05
3.27V	8.335	9.787	1.44	14.75	969.5	6.53E+05	5.55E-05
3.17V	7.598	11.19	14.30	1.888	1.59E+03	1.15E+00	7.52E-05
3.08V	7.788	18.19	9.12	2.154	95.92	2.11E-03	3.98E-05
2.99V	7.534	8.922	18.16	2.712	135.6	0.001553	4.42E-05
2.8V	8.145	10.62	1.63	17.07	3.39E+02	8.37E-04	4.45E-05
2.89V	7.745	8.48E+00	3.33	18	202.7	1.23E-03	4.70E-05

Table 7. DEIS data obtained by Nyquist plot fitting in charging process with 112.

V (V)	R_{int} (Ω)	R_{ct} (Ω)	R_{CEI} (Ω)	$R_{pre\text{-}diff}$ (Ω)	$R_{complex\text{-}diff}$ (Ω)	W ($\Omega s^{-1/2}$)	chi2
2.8V	19.11	34.04	4.912	13.76	3.13E+03	2.23E+05	9.97E-05
2.89V	6.242	6.491	6.769	35.8	7.02E+00	1.91E-14	5.73E-05
2.99V	0.01	12.64	38.02	6.16	499.4	1.00E-20	9.84E-05
3.08V	7.044	5.664	4.167	4114	2.60E+09	2.47E-17	1.02E-04
3.17V	7.038	6.047	4.024	40.93	1.07E+13	9.09E+01	1.32E-04
3.27V	0.2014	1967	4.756	10.65	1.31E+08	1.71E+04	1.42E-04
3.36V	5.072	7.56E+02	5.618	49.64	4.41E+10	3.42E+05	2.16E-04
3.45V	10.83	20.36	23.75	0.7126	1.66E+05	1.24E-09	6.06E-05
3.55V	10.7	13.71	28.96	0.4351	2.92E+03	2.68E+01	2.30E-04
3.64V	3.959	8.348	31.01	10.39	3.92E+02	3.22E-01	8.45E-06
3.73V	0.02552	14.62	33.28	6.517	1.15E+02	5.89E-01	1.26E-05
3.82V	0.05138	5.163	15.04	32.53	5.27E+01	4.18E-01	2.09E-05
3.92V	9.417	39.99	34.12	1.292	1.00E-02	1.00E-20	2.01E-04
4.01V	0.03796	10.3	24.33	36.72	6.38E+11	3.13E+02	2.80E-04
4.1V	0.01399	26.86	12.9	3.756	1.81E+01	3.20E-01	4.26E-05
4.2V	3.217	23.4	18.37	9.442	3.63E+00	3.27E-01	3.10E-05

Table 8. DEIS data obtained by Nyquist plot fitting in charging process with 112.

V (V)	R_{int} (Ω)	R_{ct} (Ω)	R_{CEI} (Ω)	$R_{pre\text{-}diff}$ (Ω)	$R_{complex\text{-}diff}$ (Ω)	W ($\Omega s^{-1/2}$)	chi2
4.2V	7.973	17.65	3.555	32.24	2.46E+00	2.40E-01	8.12E-05
4.1V	1.144	8.381	28.32	19.06	122.2	4.09E-10	3.39E-04
4.01V	9.743	26.06	17.69	2.171	9.391	9.93E-04	1.43E-04
3.92V	7.882	21.94	23.67	2.246	5.752	7.01E-13	1.44E-04
3.82V	9.964	25.32	23.96	24.98	1.00E-02	2.20E-11	1.38E-04
3.73V	9.717	25.6	29.04	2.624	1.00E+16	3.13E-05	1.21E-04
3.64V	8.052	19.65	3.579	3.884	47.44	1.18E+13	3.62E-05
3.55V	0.9231	3.857	15.66	94.37	17.65	6.45E+01	3.24E-05
3.45V	0.01241	26.38	4.071	12.93	218.7	1.23E-01	3.78E-05
3.36V	7.461	5.29	30.53	4.631	526.7	8.60E+06	1.36E-04
3.27V	0.07414	14.5	6.518	26.74	1414	2.37E+06	6.71E-05
3.17V	0.1681	7.319	14.19	27.29	2.98E+03	1.29E+05	2.50E-05
3.08V	0.05732	15.86	6.373	28.48	5354	3.41E+05	4.48E-05
2.99V	0.06574	15.13	6.872	29.42	1.49E+04	9.77E+05	3.09E-05
2.8V	0.5559	15	5.477	33.41	1.03E+06	3.23E-15	6.07E-05
2.89V	0.01	1.48E+01	7.12	30.72	0.4162	3.61E-16	4.57E-05

2.3.4 Post-morphology studies

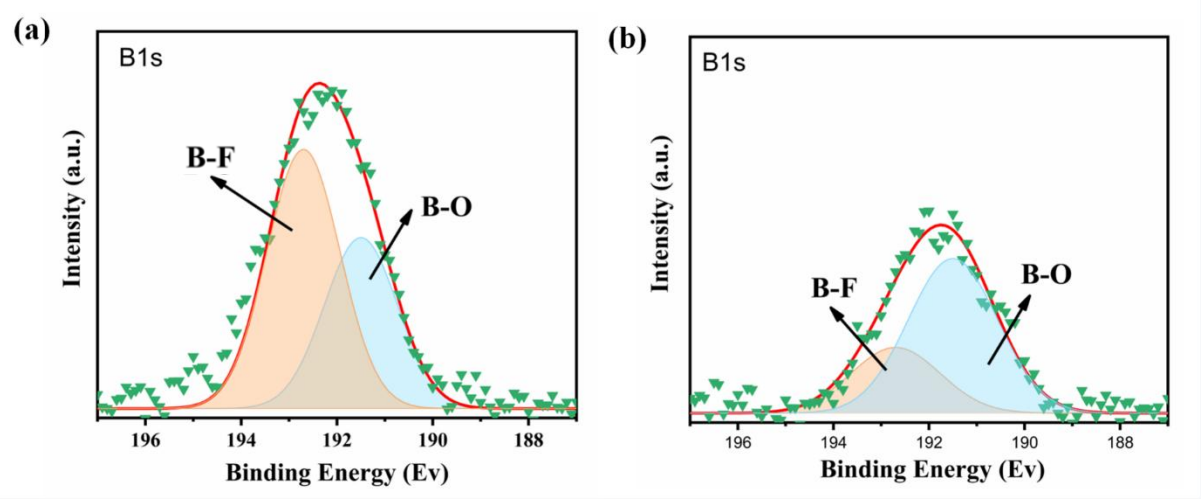

Figure 18. XPS spectra of B 1s for (a) 111 and (b) 112 based cells.

In **Figure 18a** and **18b**, apparent B 1s peaks were observed in both 111 and 112 electrolyte systems. It was reconfirmed that MDMB induced the construction of robust CEI on $LiNi_{0.33}Mn_{0.33}Co_{0.33}O_2$. The peaks centered at a binding energy of 192.5 eV corresponded to B-O[37], and the peaks centered at 194.0 eV were attributed to B-F[38]. Based on previous reports[38-41], B-O bonds in CEI could enhance the charge transfer process in the interface of LiNMC and reduce the interfacial impedance, consistent with the R_{CEI} analyzed in DEIS measurement. Moreover, as HF could interact with LiNMC, resulting in the leaching and desolvation of transition metals from the electrode into the electrolyte, the B-F bond formation allows it to remove F^- produced on the surface by coordinating with the boron atom.

XPS analysis was conducted over a binding energy range of 0–800 eV to examine the elemental composition, including F, O, N, C, B, S, and Li, and to quantify the boron content within CEI. As presented in **Figure 19-21** and detailed in **Table 9-11**, the boron content in the CEI was determined to be 1.51% and 0.91% for the cathodic surfaces with the 111 and 112 electrolytes, respectively. A decrease in the concentrations of S, N, and F, which was derived from the LiTFSI salt, was observed within the CEI, indicating that the incorporation of MDMB interacted with the TFSI anion and reduced its decomposition.

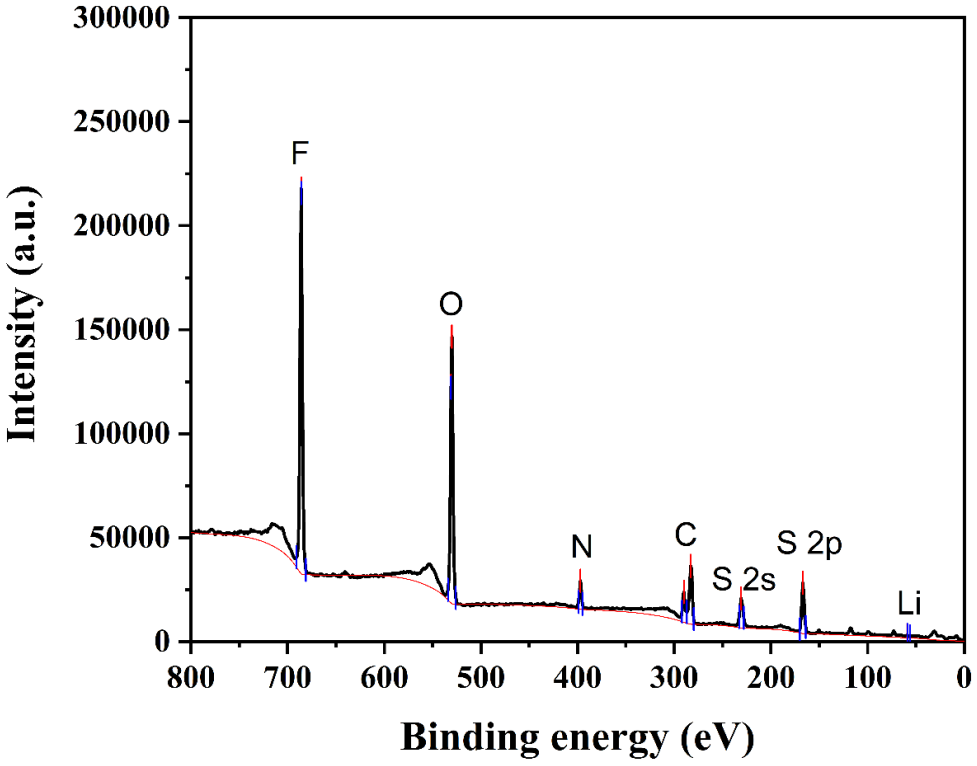

Figure 19. XPS survey spectrum of F, O, N. C, S, Li elements on NMC111 after cycled with electrolyte 110.

Table 9. Components of elements in CEI after cycled with electrolyte 110.

Element	ASF	Peak area	Percentage in CEI
Li	0.025	3103.53293	5.83%
S	0.57	76608.97888	6.32%
C	0.296	200465.7999	31.83%
N	0.477	34086.84015	3.36%
O	0.711	391515.634	25.88%
F	1	569886.0524	26.78%

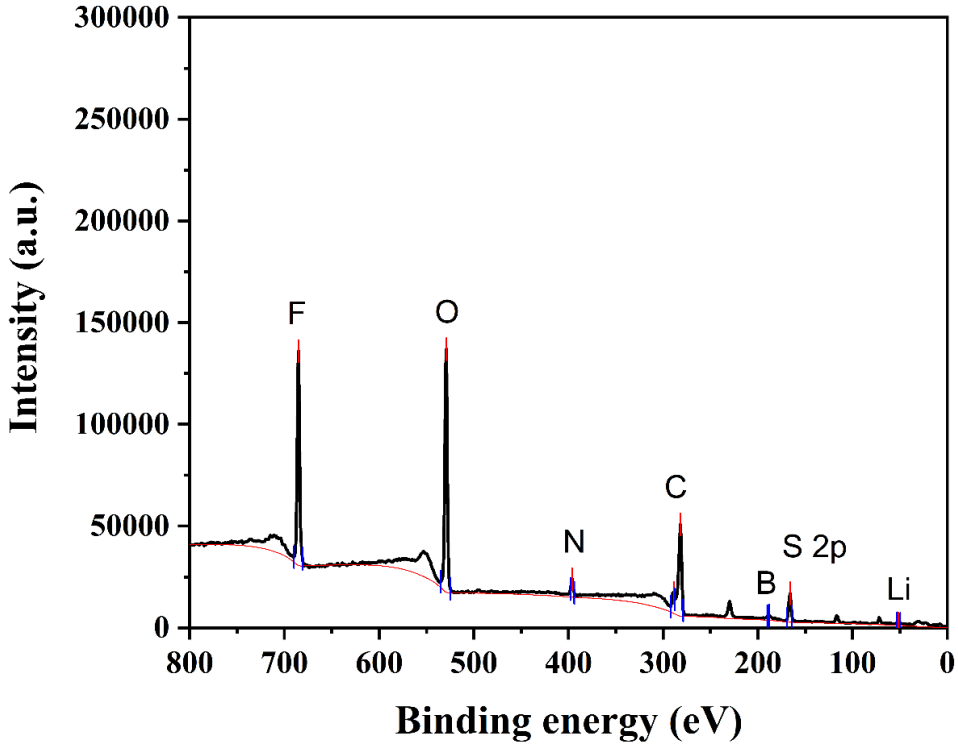

Figure 20. XPS survey spectrum of F, O, N. C, B, S, Li elements on NMC111 after cycled with electrolyte 111.

Table 10. Components of elements in CEI after cycled with electrolyte 111.

Element	ASF	Peak area	Percentage in CEI
Li	0.025	2675.3929	5.70%
S	0.57	42077.91889	3.93%
B	0.159	4498.3058	1.51%
C	0.296	216,159.82	38.91%
N	0.477	24288.56112	2.71%
O	0.711	387021.2672	29.00%
F	1	342455.9241	18.24%

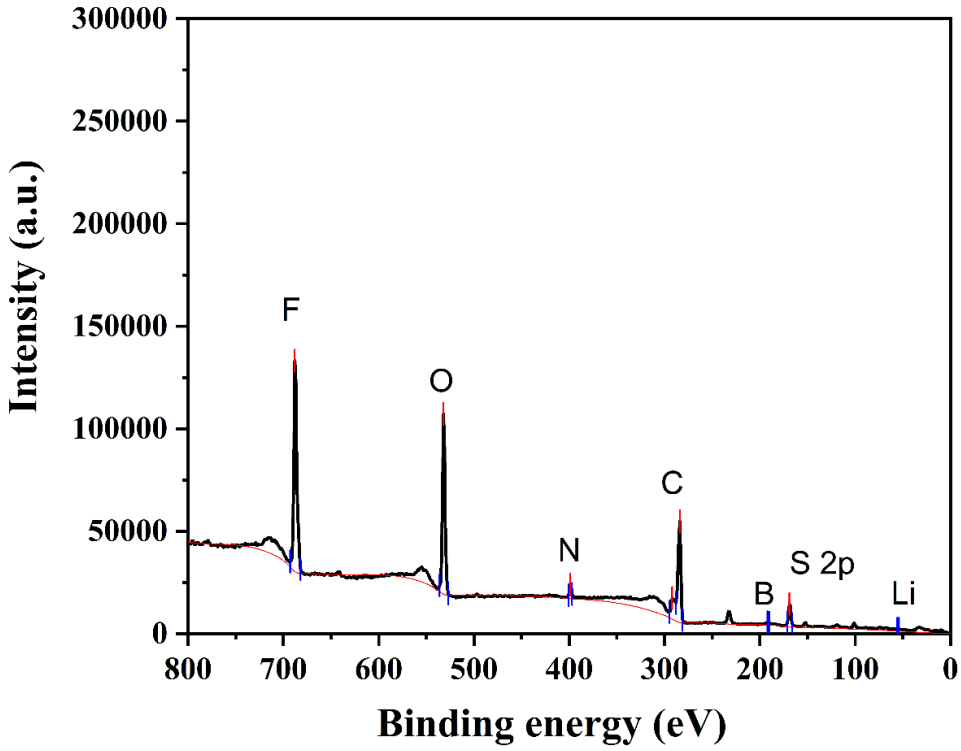

Figure 20. XPS survey spectrum of F, O, N. C, B, S, Li elements on NMC111 after cycled with electrolyte 112.

Table 11. Components of elements in CEI after cycled with electrolyte 112.

Element	ASF	Peak area	Percentage in CEI
Li	0.025	2150.72593	4.85%
S	0.57	33275.70862	3.29%
B	0.159	2556.4163	0.91%
C	0.296	231,670.04	44.14%
N	0.477	17953.77807	2.12%
O	0.711	284448.0207	22.56%
F	1	392361.2572	22.13%

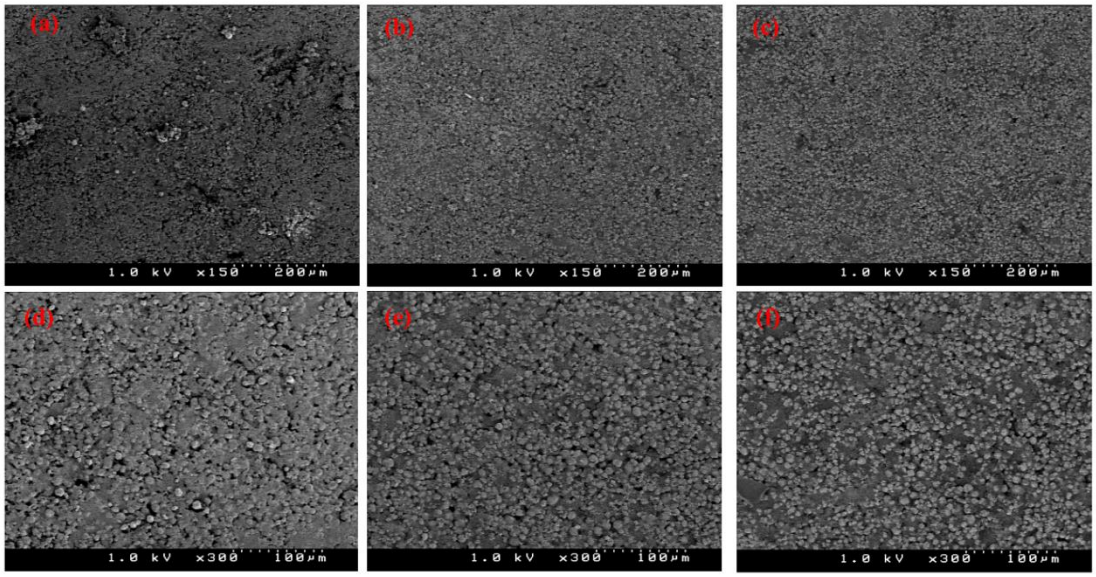

Figure 21. FESEM images under different scales of cathode after long cycling measurements. (a) and (d) for cathode cycled with 110 electrolyte; (b) and (e) for 111 electrolyte; (c) and (f) for 112 electrolyte.

LiNMC surface morphology after cycling in various electrolyte was studied using FESEM. **Figure 21** exhibited surface of $LiNi_{0.33}Mn_{0.33}Co_{0.33}O_2$ after cycling with different electrolyte systems. The leaching of transition metals from the electrode into the electrolyte happened on the surface of $LiNi_{0.33}Mn_{0.33}Co_{0.33}O_2$ electrode with traditional electrolyte. The surfaces of $LiNi_{0.33}Mn_{0.33}Co_{0.33}O_2$ electrodes cycled with MDMB as electrolyte component were smoother and more uniform. In Figure 19a and 19d, shape of the transition metal particles cycled with electrolyte 110 becomes blurred, compared with 111 (Figure 19b, 19e) and 112 (Figure 19c, 19f). It was attributed to the cathode dissolution phenomena. As surface of cathode was broken seriously, its surface area and thickness decreased simultaneously, leading to the fast capacity decay that appeared in cycling process. In MDMB containing systems, tangible damaged area was not observed. Moreover, shape of particles was clear and obvious. It validated the excellent protection of cathode underwent by MDMB and robust B-rich CEI formed on cathodic surface.

2.4 Conclusion

Herein, ternary electrolyte systems with MDMB as a component were prepared to apply into cathodic half-cell fabricated with $LiNi_{0.33}Mn_{0.33}Co_{0.33}O_2$. Three electrolyte systems 110, 111 and 112, with different volume ratios of MDMB added into traditional carbonate electrolyte (1.0M LiTFSI in 50%EC-50%DEC) were studied in this work. By adding boron compound, a stable solvent sheath was formed with $TFSI^-$ anion and the interaction energy between Li-ion and solvent sheath was reduced. As a result, the lithium-ion transference ability in boron-containing electrolyte systems was markedly increased to 0.93 for 111 and 0.86 for 112, more than twice of 110. In addition, ionic conductivity of 111 and 112 decreased owing to strong anion trapping effect. The intensification of lithium-ion mobility by ternary electrolyte was also demonstrated by E_a value of cathodic half-cells. As Li^+ mobility was enhanced, overpotential obtained under high scan rate decreased in CV measurement. Discharge capacity of 111 based cells and 112 based cells under 1C was 64.2 mAh/g, and 55.5 mAh/g respectively, higher than 34.6 mAh/g of 110 based cells. Moreover, this boron-containing ternary electrolyte enabled better durability and stability of cathodes by forming robust B-rich CEI on cathode surface. 111 and 112 electrolyte systems exhibited much lower leakage current than 110 especially under high voltage of 4.2 V. Cathodic half-cell with 111 and 112 electrolytes maintained discharge capacity of ~ 40 mAh/g for 130 cycles and high coulombic efficiency of ~ 97% at 1C CCCV mode. It was beneficial for B-O formed in CEI by MDMB to increase the ionic conductivity of interface, which is responsible to the low activation energy and low R_{CEI}. Moreover, the robust B-rich CEI also prevented leaching and desolvation of transition metal particles on cathodic surface. Although the performance of conventional carbonate electrolyte was poor, this boron-containing ternary electrolyte realized significant enhancement. This methodology could be applied to further optimize electrolyte system for improvement of LiNMC based cells.

Reference

(1) Patra, A.; Matsumi, N. Charge–Discharge Behavior of Lithium-Ion Batteries Using a Polymer Electrolyte Bearing High-Density Functional Groups. *ACS Appl. Ener. Mater.* **2023**, *6* (23), 11973–11982. https://doi.org/10.1021/acsaem.3c02137.

(2) Mishra, S. N.; Punyasloka, S.; Mantripragada, B. S.; Pradhan, A.; Matsumi, N. Enabling Ultrafast Charging in Graphite Anodes Using BIAN-Based Conjugated Polymer/Lithium Polyacrylate as a Binder. *ACS Appl. Ener. Mater.* **2023**, *6* (23), 11954–11962. https://doi.org/10.1021/acsaem.3c02129.

(3) Joshi, P.; Vedarajan, R.; Matsumi, N. A Crystalline Low Molecular Weight Cyclic Organoboron Compound for Efficient Solid State Lithium Ion Transport. *Chem. Commun.* **2015**, *51* (81), 15035–15038. https://doi.org/10.1039/c5cc04753f.

(4) Jayakumar, T. P.; Badam, R.; Matsumi, N. Allylimidazolium-Based Poly(Ionic Liquid) Anodic Binder for Lithium-Ion Batteries with Enhanced Cyclability. *ACS Appl. Ener. Mater.* **2020**, *3* (4), 3337–3346. https://doi.org/10.1021/acsaem.9b02376

(5) Lavi, O.; Luski, S.; Shpigel, N.; Menachem, C.; Pomerantz, Z.; Elias, Y.; Aurbach, D. Electrolyte Solutions for Rechargeable Li-Ion Batteries Based on Fluorinated Solvents. *ACS Appl. Ener. Mater.* **2020**, *3* (8), 7485–7499. https://doi.org/10.1021/acsaem.0c00898.

(6) Kanamura, K.; Kawai, Y.; Yonezawa, S.; Takehara, Z. I. Effect of Morphology of Polyaniline on Its Discharge Characteristics in Nonaqueous Electrolyte. *J. Electrochem. Soc.* **1995**, *142* (9), 2894. https://doi.org/10.1149/1.2048661.

(7) Myung, S.-T.; Izumi, K.; Komaba, S.; Sun, Y.-K.; Yashiro, H.; Kumagai, N. Role of Alumina Coating on Li−Ni−Co−Mn−O Particles as Positive Electrode Material for Lithium-Ion Batteries. *Chem. Mater.* **2005**, *17* (14), 3695–3704. https://doi.org/10.1021/cm050566s.

(8) Shaju, K. M.; Subba Rao, G. V.; Chowdari, B. V. R. Performance of Layered $Li(Ni_{1/3}Co_{1/3}Mn_{1/3})O_2$ as Cathode for Li-Ion Batteries. *Electrochim. Acta* **2002**, *48* (2), 145–151. https://doi.org/10.1016/S0013-4686(02)00593-5.

(9) Sun, Y.-K.; Cho, S.-W.; Lee, S.-W.; Yoon, C. S.; Amine, K. AlF_3-Coating to Improve High Voltage Cycling Performance of $Li[Ni_{1/3}Co_{1/3}Mn_{1/3}]O_2$ Cathode Materials for Lithium Secondary Batteries. *J. Electrochem. Soc.* **2007**, *154* (3), A168. https://doi.org/10.1149/1.2422890.

(10) Amatucci, G. G.; Tarascon, J. M.; Klein, L. C. Cobalt Dissolution in $LiCoO_2$-Based Non-Aqueous Rechargeable Batteries. *Solid State Ioics.* **1996**, *83* (1–2), 167–173. https://doi.org/10.1016/0167-2738(95)00231-6.

(11) Markevich, E.; Salitra, G.; Aurbach, D. Fluoroethylene Carbonate as an Important Component for the Formation of an Effective Solid Electrolyte Interphase on Anodes and Cathodes for Advanced Li-Ion Batteries. *ACS Ener. Lett.* **2017**, pp 1337–1345. https://doi.org/10.1021/acsenergylett.7b00163.

(12) Hu, S. K.; Cheng, G. H.; Cheng, M. Y.; Hwang, B. J.; Santhanam, R. Cycle Life Improvement of ZrO2-Coated Spherical $LiNi_{1/3}Co_{1/3}Mn_{1/3}O_2$ Cathode Material for Lithium Ion Batteries. *J. Power Sources* **2009**, *188* (2), 564–569. https://doi.org/10.1016/J.JPOWSOUR.2008.11.113.

(13) Nayak, P. K.; Grinblat, J.; Levi, M.; Levi, E.; Kim, S.; Choi, J. W.; Aurbach, D. Al Doping for Mitigating the Capacity Fading and Voltage Decay of Layered Li and Mn-Rich Cathodes for Li-Ion Batteries. *Adv. Energy Mater.* **2016**, *6* (8). https://doi.org/10.1002/aenm.201502398.

(14) Nayak, P. K.; Grinblat, J.; Levi, E.; Levi, M.; Markovsky, B.; Aurbach, D. Understanding the Influence of Mg Doping for the Stabilization of Capacity and Higher Discharge Voltage of Li- and Mn-Rich Cathodes for Li-Ion Batteries. *Phys. Chem. Chem. Phys.* **2017**, *19* (8), 6142–6152. https://doi.org/10.1039/c6cp07383b.

(15) Erickson, E. M.; Sclar, H.; Schipper, F.; Liu, J.; Tian, R.; Ghanty, C.; Burstein, L.; Leifer, N.; Grinblat, J.; Talianker, M.; Shin, J. Y.; Lampert, J. K.; Markovsky, B.; Frenkel, A. I.; Aurbach, D. High-Temperature Treatment of Li-Rich Cathode Materials with Ammonia: Improved Capacity and Mean Voltage Stability during Cycling. *Adv. Energy Mater.* **2017**, *7* (18). https://doi.org/10.1002/aenm.201700708.

(16) Zhang, H. Z.; Qiao, Q. Q.; Li, G. R.; Ye, S. H.; Gao, X. P. Surface Nitridation of Li-Rich Layered $Li(Li_{0.17}Ni_{0.25}Mn_{0.58})O_2$ Oxide as Cathode Material for Lithium-Ion Battery. *J. Mater. Chem.* **2012**, *22* (26), 13104–13109. https://doi.org/10.1039/c2jm30989k.

(17) Zhang, Z.; Hu, L.; Wu, H.; Weng, W.; Koh, M.; Redfern, P. C.; Curtiss, L. A.; Amine, K. Fluorinated Electrolytes for 5 v Lithium-Ion Battery Chemistry. *Energy Environ. Sci.* **2013**, *6* (6), 1806–1810. https://doi.org/10.1039/c3ee24414h.

(18) Xia, J.; Self, J.; Ma, L.; Dahn, J. R. Sulfolane-Based Electrolyte for High Voltage $Li(Ni_{0.42}Mn_{0.42}Co_{0.16})O_2$ (NMC442)/Graphite Pouch Cells. *J. Electrochem. Soc.* **2015**, *162* (8), A1424–A1431. https://doi.org/10.1149/2.0121508jes.

(19) Duncan, H.; Salem, N.; Abu-Lebdeh, Y. Electrolyte Formulations Based on Dinitrile Solvents for High Voltage Li-Ion Batteries. *J. Electrochem. Soc.* **2013**, *160* (6), A838–A848. https://doi.org/10.1149/2.088306jes.

(20) Xu, K. Electrolytes and Interphases in Li-Ion Batteries and Beyond. *Chem. Rev.* **2014**, *114* (23), 11503–11618 https://doi.org/10.1021/cr500003w.

(21) Xia, J.; Nie, M.; Burns, J. C.; Xiao, A.; Lamanna, W. M.; Dahn, J. R. Fluorinated Electrolyte for 4.5 V $Li(Ni_{0.4}Mn_{0.4}Co_{0.2})O_2$/Graphite Li-Ion Cells. *J. Power Sources* **2016**, *307*, 340–350. https://doi.org/10.1016/J.JPOWSOUR.2015.12.132.

(22) Lim, J. J. N.; Lim, G. J. H.; Cai, Y.; Chua, R.; Guo, Y.; Yan, Y.; Srinivasan, M. Electrolyte Designs for Safer Lithium-Ion and Lithium-Metal Batteries. *J. Mater. Chem. A* **2023**, *11*, 22688–22717. https://doi.org/10.1039/d3ta02916f.

(23) Matsumi, N.; Mizumo, T.; Ohno, H. Single Ion Conductive Characteristics of Poly(Organoboron Halide)-Imidazole Complex. *Polym. Bull.* **2004**, *51*, 389–394. https://doi.org/10.1007/~00289-004-0229-5.

(24) Matsumi, N.; Sugai, K.; Ohno, H. Ion Conductive Characteristics of Alkylborane Type and Boric Ester Type Polymer Electrolytes Derived from Mesithylborane. *Macromolecules* **2003**, *36* (7), 2321–2326. https://doi.org/10.1021/ma021734u.

(25) Matsumi, N.; Sugai, K.; Ohno, H. Selective Ion Transport in Organoboron Polymer Electrolytes Bearing a Mesitylboron Unit. *Macromolecules* **2002**, *35* (15), 5731–5733. https://doi.org/10.1021/ma0121666.

(26) Matsumi, N.; Sugai, K.; Miyake, M.; Ohno, H. Polymerized Ionic Liquids via Hydroboration Polymerization as Single Ion Conductive Polymer Electrolytes. *Macromolecules* **2006**, *39* (20), 6924–6927. https://doi.org/10.1021/ma060472j.

(27) Matsumi, N.; Miyake, M.; Ohno, H. Molten Salts Bearing Anion Receptor. *Chem. Commun.* **2004**, 2852–2853. https://doi.org/10.1039/b408839e.

(28) Vedarajan, R.; Matsui, K.; Tamaru, E.; Dhankhar, J.; Takekawa, T.; Matsumi, N. Ionic Liquid/Boric Ester Binary Electrolytes with Unusually High Lithium Transference Number. *Electrochem. Commun.* **2017**, *81*, 132–135.

https://doi.org/10.1016/J.ELECOM.2017.06.019.

(29) Peng, Y.; Nishikawa, K.; Kanamura, K. Effects of Carbonate Solvents and Lithium Salts in High-Concentration Electrolytes on Lithium Anode. *J. Electrochem. Soc.* **2022**, *169* (6), 060548. https://doi.org/10.1149/1945-7111/ac797a.

(30) Pradhan, A.; Badam, R.; Miyairi, R.; Takamori, N.; Matsumi, N. Extreme Fast Charging Capability in Graphite Anode via a Lithium Borate Type Biobased Polymer as Aqueous Polyelectrolyte Binder. *ACS Mater. Lett.* **2023**, *5* (2), 413–420. https://doi.org/10.1021/acsmaterialslett.2c00999.

(31) Matsumi, N.; Chujo, Y. Synthesis of Novel Organoboron Polymers by Haloboration Polymerization of Bisallene Compounds. *Polym. Bull*. **1997**, *39*, 295–302. https://doi.org/10.1007/s002890050151.

(32) Grewal, M. S.; Kisu, K.; Orimo, S. I.; Yabu, H. Increasing the Ionic Conductivity and Lithium-Ion Transport of Photo-Cross-Linked Polymer with Hexagonal Arranged Porous Film Hybrids. i*science* **2022**, *25* (9), 104910. https://doi.org/10.1016/j.isci.2022.104910.

(33) Rosenbach, D.; Krimalowski, A.; Erabhoina, H.; Thelakkat, M. Solid Polymer Electrolytes from Polyesters with Diester Sidechains for Lithium Metal Batteries. *J. Mater. Chem. A* **2022**, *10* (16), 8932–8947. https://doi.org/10.1039/D2TA00800A.

(34) Zhou, P.; Zhang, X.; Xiang, Y.; Liu, K. Strategies to Enhance Li^+ Transference Number in Liquid Electrolytes for Better Lithium Batteries. *Nano Res.* **2023**, *16* (6), 8055–8071. https://doi.org/10.1007/s12274-022-4833-1.

(35) Li, Y.; Veith, G. M.; Browning, K. L.; Chen, J.; Hensley, D. K.; Paranthaman, M. P.; Dai, S.; Sun, X.-G. Lithium Malonatoborate Additives Enabled Stable Cycling of 5 V Lithium Metal and Lithium Ion Batteries. *Nano Energy* **2017**, *40*, 9–19. https://doi.org/10.1016/j.nanoen.2017.07.051.

(36) Shi, Q.; Heng, S.; Qu, Q.; Gao, T.; Liu, W.; Hang, L.; Zheng, H. Constructing an Elastic Solid Electrolyte Interphase on Graphite: A Novel Strategy Suppressing Lithium Inventory Loss in Lithium-Ion Batteries. *J. Mater. Chem. A* **2017**, *5* (22), 10885–10894. https://doi.org/10.1039/C7TA02706K.

(37) Wang, P.; Cui, X.; Zhao, D.; Yan, D.; Ding, H.; Dong, H.; Wang, J.; Wu, S.; Li, S. Effects of Soluble Products Decomposed from Chelato-Borate Additives on Formation of Solid Electrolyte Interface Layers. *J. Power Sources* **2022**, *535*, 231451. https://doi.org/10.1016/j.jpowsour.2022.231451.

(38) Li, G.; Li, Z.; Cai, Q.; Yan, C.; Xing, L.; Li, W. Construction of Low-Impedance and High-Passivated Interphase for Nickel-Rich Cathode by Low-Cost Boron-Containing Electrolyte Additive. *ChemSusChem* **2022**, *15* (11), e202200543. https://doi.org/10.1002/cssc.202200543.

(39) Sun, H. H.; Dolocan, A.; Weeks, J. A.; Rodriguez, R.; Heller, A.; Mullins, C. B. In Situ Formation of a Multicomponent Inorganic-Rich SEI Layer Provides a Fast Charging and High Specific Energy Li-Metal Battery. *J. Mater. Chem. A* **2019**, *7* (30), 17782–17789.

(40) Li, G.; Liao, Y.; Li, Z.; Xu, N.; Lu, Y.; Lan, G.; Sun, G.; Li, W. Constructing a Low-Impedance Interface on a High-Voltage $LiNi_{0.8}Co_{0.1}Mn_{0.1}O_2$ Cathode with 2,4,6-Triphenyl Boroxine as a Film-Forming Electrolyte Additive for Li-Ion Batteries. *ACS Appl. Mater. Interfaces* **2020**, *12* (33), 37013–37026. https://doi.org/10.1021/acsami.0c05623.

(41) Li, J.; Liao, Y.; Fan, W.; Li, Z.; Li, G.; Zhang, Q.; Xing, L.; Xu, M.; Li, W. Significance of Electrolyte Additive Molecule Structure in Constructing Robust Interphases on High-Voltage Cathodes. *ACS Appl. Ener. Mater.* **2020**, *3* (3), 3049–3058. https://doi.org/10.1021/acsaem.0c00168.

Chapter 3 Functionalized Boron-Containing Additive for Enhanced Cycling Performance of Various NMC-Based Cathode in Lithium-ion Batteries Under Extreme Operating Conditions

3.1 Introduction

As lithium-ion batteries became the irreplaceable power resource for portable electronic devices and electric vehicles, various requests are about to arrive, such as high energy density[1–3], wide temperature range[4,5] and fast charging-discharging[6–8]. To meet various requirements, scientists reform and renew each component of battery system, such as cathode, electrolyte and anode. For the cathode-active materials (CAMs), $LiNi_xCo_yMn_{1-x-y}O_2$ (LiNMC) as a kind of ternary layered oxide exhibits the most common high energy density and offers a better cyclability compared to spinel cathodes like $LiMn_2O_4$ and polyanionic cathodes[9]. Among various LiNMC, there are two typical materials. The nickel-rich CAM, $LiNi_{0.8}Co_{0.1}Mn_{0.1}O_2$ (NMC811), presents high operational voltage and high energy density due to ample active redox reaction of Ni ($Ni^{2+} \leftrightarrow Ni^{4+}$). Whereas the $LiNi_{0.33}Co_{0.33}Mn_{0.33}O_2$ (NMC111) are more developed as they adopt all benefits of the transition metals (Mn for long cycle life and Co for good rate capability) into the cathodic active material. Although LiNMC has many merits among numerous CAMs, it still faces challenges from deterioration of highly active surface-particle cracking, transition metal (TM) dissolution and surface reconstruction[10]. These issues arise because the conventional carbonate electrolyte fails to provide a stable and robust interphase between electrolyte and cathodic surface[11].

To mitigate the severe degradation of LiNMC materials, modification of the cathode surface is essential. Optimizing the electrolyte offers a simpler and more cost-effective approach to passivate the cathode surface compared to coating or doping techniques[12]. Among diverse electrolyte modification methods, incorporating a potent additive into the electrolyte is more feasible in practical production than altering the primary components of the electrolyte. Organoboron molecules are capable of promoting film formation and widely used in interphase modification on both anode and cathode surface[13]. Besides, boron compound could remove the HF produced by lithium salts ($LiPF_6$, $LiBF_4$ and LiTFSI) during cycling by forming complex

with boron molecule thus inhibiting interphase and CAM corrosion, thereby mitigating the serious dissolution of TM[14]. Despite the boron-containing additives providing cathode with a strengthen interface, unfortunately it is not strong enough to overcome every extreme conditions. For example, lithium bis(oxalate)borate (LiBOB) is impressive on multiplicity and cyclability enhancement as a classic boron-containing additive, however LiBOB-interphase decomposed under ultrahigh voltage condition (>4.7 V) and caused a rapid decay of specific capacity and coulombic efficiency[16]. Therefore, identifying a robust additive to enhance the battery's performance under extreme conditions is essential.

Considering the widespread use of batteries, it becomes inevitable for batteries to encounter each of the aforementioned extreme conditions at some stage throughout their service life. It is meaningful and necessary to find an efficient way to enable batteries to operate normally under every extreme conditions. In this study, the electrochemical performance of cells under ultrahigh voltage, extreme fast charging-discharging, and wide temperature conditions was enhanced by incorporating a strategically chosen additive to mitigate undesirable reactions and stabilize the interfacial structure of NMC-type cathodic materials. Ethylene glycol-mesitylborane adduct (EGMB), a cyclic boric ester, was incorporated into the conventional carbonate electrolyte at a low concentration of 2 mg/mL (0.16 wt%) as the additive. EGMB is air-stable and synthesized via a solvent-free one-pot method. The cyclic boric ester in EGMB interacts with the transition metal oxides in the cathode active material, facilitating film formation. Upon decomposition, EGMB forms a B- and F-rich cathode-electrolyte interphase (CEI) with excellent mechanical strength.

EGMB improves the interphase properties of NMC electrodes through three primary functions: (i) It forms a boron-rich organic film at cathode surface before other electrolyte components, optimizing the interfacial compositions and enhancing the mechanical stability of the organic layer, thereby improving NMC/CEI/electrolyte compatibility; (ii) It enhances Li-

ion migration through the interphase layer by establishing a low impedance CEI with excellent stability; and (iii) It reduces the release of reactive lattice oxygen from the electrode surface, thereby decreasing HF formation and its detrimental effect on transition metal dissolution by forming complexes with the boron moiety. This work offers new insights into the selection of functional additives with self-optimizing interfacial characteristics, leading to long cycling life and enhanced safety performance in NMC-based batteries.

3.2 Experimental

3.2.1 Materials

Mesitylboronic acid (TCI, 98%) and excess of ethylene glycol dehydrated (Wako, 99.5%), were added to a Schlaker reaction tube (Sigma-Aldrich). The lithium hexafluorophosphate solution in ethylene carbonate and diethyl carbonate (1.0 M $LiPF_6$ in EC/DEC = 50/50 (v/v)) was purchased from Sigma-Aldrich Co., Ltd. The $LiNi_{0.33}Mn_{0.33}Co_{0.33}O_2$ (NMC111) and $LiNi_{0.8}Mn_{0.1}Co_{0.1}O_2$ (NMC811) electrode were purchased from Piotrek Co., Ltd.

3.2.2 Synthesis

Ethylene glycol-mesitylborane adduct (EGMB)[15] was synthesized using solvent free one pot synthesis in vacuum-sealed tubes. After executing a freeze-thaw cycle, the mixture was stirred at 60 °C for 24 hours. Following the reaction, the reaction product was extracted into hexane. The hexane was subsequently removed, and the EGMB was dried under vacuum overnight. The excess of ethylene glycol can again be reused after vacuum evaporation of hexane. The resulting product had a yield of 92%.

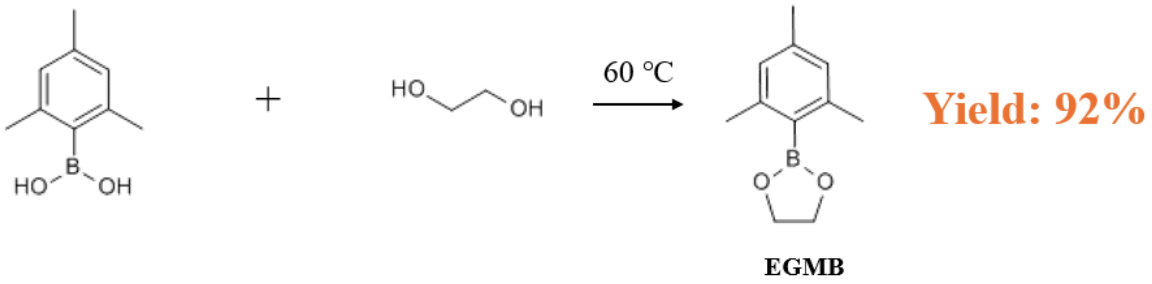

Figure 1. Schematic illustration of the synthesis of EGMB.

3.2.3 Cell preparation

The lithium hexafluorophosphate solution in ethylene carbonate and diethyl carbonate (1.0 M $LiPF_6$ in EC/DEC = 50/50 (v/v)) was used as control system in the following experiment.

2 mg/ml EGMB-containing electrolyte was obtained via adding EGMB into the commercial electrolyte. To fabricate the cathode electrodes, the cathode sheets were punched into 13 mm diameter discs and subsequently dried at 80°C overnight to eliminate any surface moisture. The dried cathode materials were then used to assemble the cathodic half-cells in CR-2025 coin cells. In each coin cell, 70 μL of electrolyte was added. All cell assembly procedures were carried out in an argon-filled glove box to ensure an oxygen- and moisture-free environment.

3.2.4 Electrochemical studies

The experiment to obtain lithium transference numbers was conducted using a Biologic VSP electrochemical workstation, which was equipped with a frequency response analyzer (FRA). The lithium-ion transference number was determined using Li||Li symmetric cells, employing both electrochemical impedance spectroscopy (EIS) and chronoamperometry (CA) techniques. The experimental procedure began with an initial EIS measurement, covering a frequency range from 0.1 Hz to 1 MHz. Following this, a constant voltage of 30 mV was applied to the cells, and the current fluctuations were monitored using the CA technique. The current was allowed to stabilize, after which a final EIS measurement was conducted on the steady-state cell, and the data were recorded for analysis.

Dynamic electrochemical impedance spectroscopy (DEIS) measurements were performed using the EIS technique at various operating potentials within the range of 2.8 V to 4.2 V. These studies aimed to analyze the impedance characteristics of the system across different voltage conditions, providing valuable information about the electrochemical processes and interfacial dynamics occurring at the cathode during operation. In the floating test, the battery was initially charged to a specific voltage (4.6 V, 4.8 V, 5.0 V) and then held at this voltage for 10 hours. During this period, the current was continuously monitored to observe any variations, providing insights into the battery's behavior under a constant voltage condition. Cyclic voltammetry (CV) was conducted in the potential range of 2.8 V to 4.2 V for Li||NMC111 cells

and 2.5 V-4.8 V for Li||NMC811 cells at scan rates of 0.1 mV s^{-1}. The charge and discharge tests were carried out by Electrofield ABE through a battery cycler under different rates, temperatures, and voltage ranges with NMC111 or NMC811.

3.2.5 Post-morphology studies

The cycled cell was carefully disassembled, and the cathode and separator were extracted for further analysis. To remove the diethyl carbonate (DEC) solvent, the solvent-saturated separator was placed under vacuum overnight, allowing for the removal of DEC and the formation of solid ethylene carbonate (EC) crystals, which contained dissolved transition metals. The cathode was then washed three times with DEC solution to eliminate any residual electrolyte, followed by vacuum drying overnight to prepare the sample for investigation of the interphase structure and composition. The morphology and elemental composition of surface were examined using a Hitachi TM3030Plus scanning electron microscope (SEM) at 1.0 kV in combination with energy dispersive X-ray spectroscopy (EDS).

Additionally, X-ray photoelectron spectroscopy (XPS) measurements were performed using a Fisons Instruments S-probe™ 2803 system. These techniques provided detailed information on the surface structure, elemental composition, and chemical states of the materials under investigation.

3.3 Result and discussion

3.3.1 Characterization

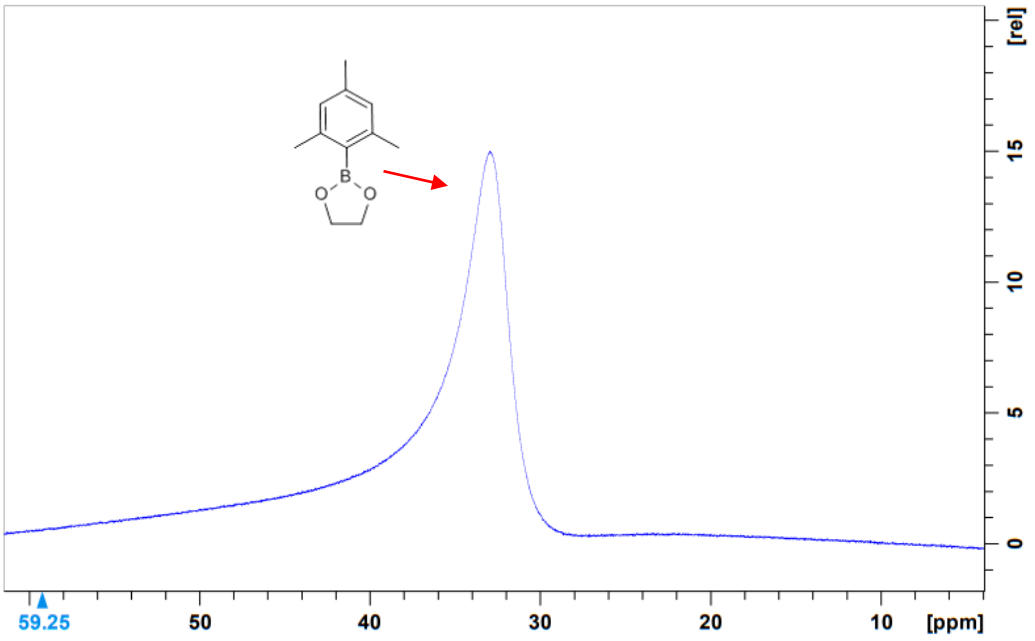

Figure 2. ^{11}B-NMR of EGMB in DMSO-d_6.

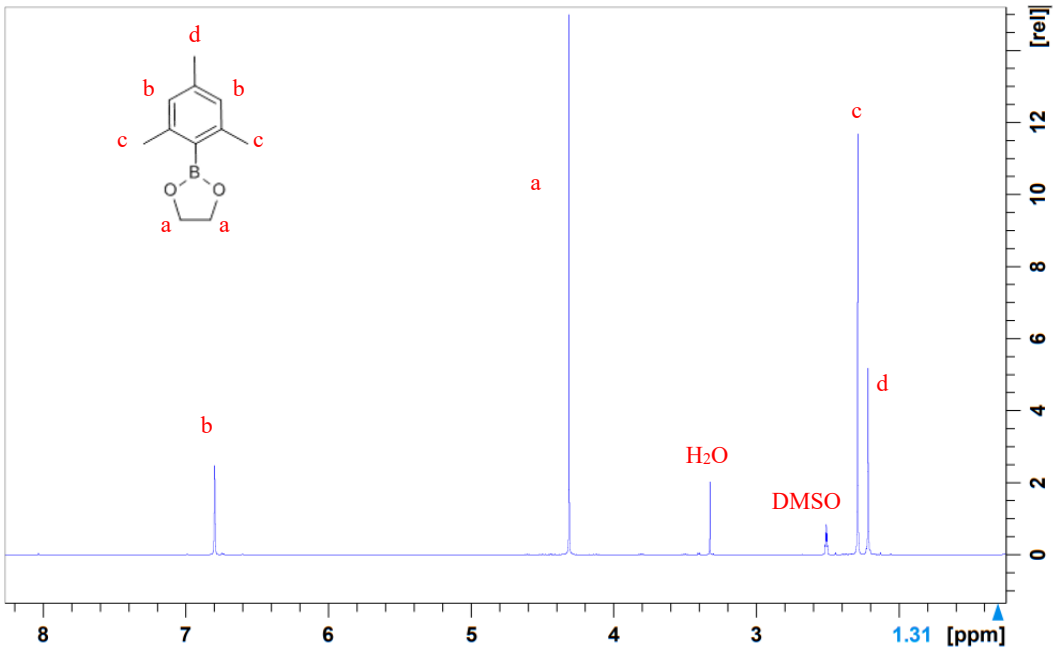

Figure 3. ^{1}H-NMR of EGMB in DMSO-d_6.

The synthesized low molecular weight cyclic organoboron electrolyte, EGMB, was characterized using ^{1}H and ^{11}B NMR spectroscopy in DMSO-d_6 at 400 MHz. In the ^{11}B NMR

spectrum, a distinct peak at 32.1 ppm, attributed to the boron in the boric ester functional group, confirmed the presence of a single, pure boron. The ^{1}H NMR spectrum further supported the structure of EGMB, with the following resonances observed: δ 6.80 ppm (aromatic protons of the phenyl ring), δ 4.32 ppm (–CH_2– protons of the ethylene glycol moiety), and δ 2.27–2.20 ppm (–CH_3 protons of the mesityl group). The ^{1}H NMR spectrum aligns with the results in previous work[15]: ^{1}H NMR (400 MHz, DMSO-d_6): δ 6.79–6.72 (phenyl ring protons), δ 4.30 (–CH_2– groups of ethylene glycol), δ 2.27–2.08 (–CH_3 protons of the mesityl group).

3.3.2 Basic electrochemical studies

Based on prior research, the formation of both the solid electrolyte interphase (SEI) and the cathode electrolyte interphase (CEI) is governed by the competitive interfacial chemical reactions between various solvent components and the anions of lithium salts in the electrolyte. The composition of these interphases is dictated by the oxidation or reduction behavior of the solvent molecules, which can be predicted using computational calculations of the highest occupied molecular orbital (HOMO) and lowest unoccupied molecular orbitals (LUMO)[17]. In previous researches, conventional additives such as vinylene carbonate (VC) and fluoroethylene carbonate (FEC) are designed to enhance cell stability and longevity[18]. They primarily target SEI modification and those additives exhibit relatively low lowest unoccupied molecular orbitals (LUMO). However, their low HOMO levels limit their ability to establish a stable CEI prior to other electrolyte components like ethylene carbonate (EC) and diethyl carbonate (DEC), thereby restricting their effectiveness in CEI formation. Therefore, the development of additives with low HOMO levels which could facilitate the formation of a robust CEI became a significant study. Previous studies by Yue *et al.* and Li *et al.* have utilized tris(pentafluorophenyl)borane (TPFPB)[19] with a HOMO level of -7.89 eV, and phenyl boric

acid (PBA)[20] with a HOMO level of -7.12 eV, which were shown to oxidize on the cathodic surface and improved the performance of lithium metal batteries. In this study, our additive EGMB exhibits a relatively higher HOMO energy of -5.75 eV as shown in **Figure 4a**, indicating its potential to form an initial film layer on the cathode prior to other components. This early deposition could play a critical role in shaping the formation and development of the CEI from the beginning.

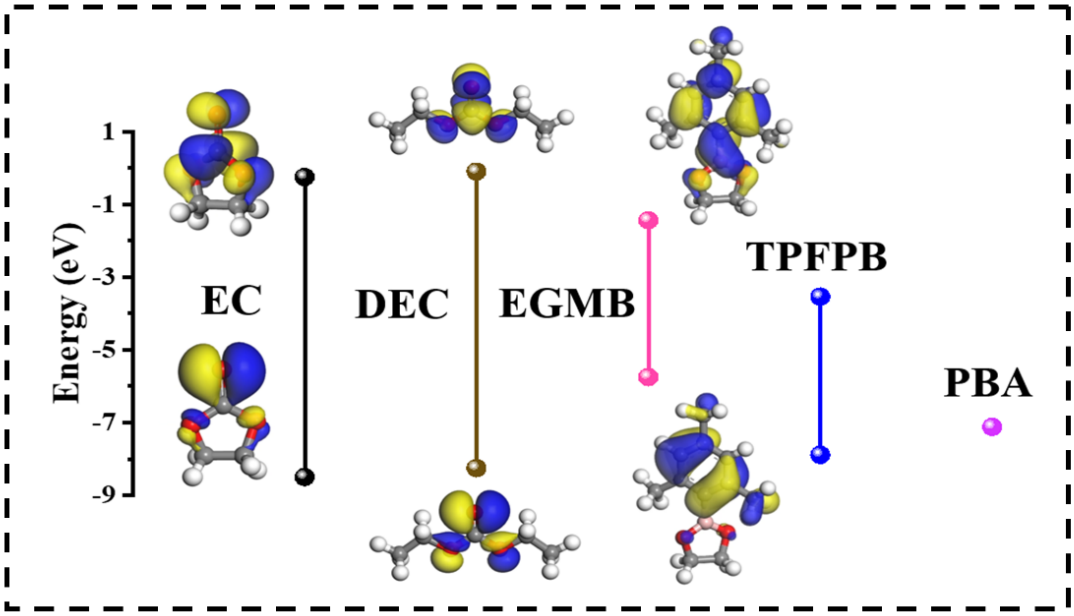

Figure 4. Calculated HOMO and LUMO energy levels of EC, DEC, EGMB, TPFB, and PBA.

To investigate the impact of EGMB additive on NMC cathodes, $LiNi_{0.8}Co_{0.1}Mn_{0.1}O_2$ (NMC811) and $LiNi_{0.33}Co_{0.33}Mn_{0.33}O_2$ (NMC111) were chosen and investigated. A slight amount of EGMB (2 mg/ml, 0.16 wt% of electrolyte) was introduced into the commercial electrolyte (1.0 M $LiPF_6$ in a solution of 50% EC: 50% DEC, volume ratio). The modified electrolyte was then used in both Li||NMC811 and Li||NMC111 cathodic half-cells and compared with the commercial electrolyte to evaluate the impact of the EGMB additive.

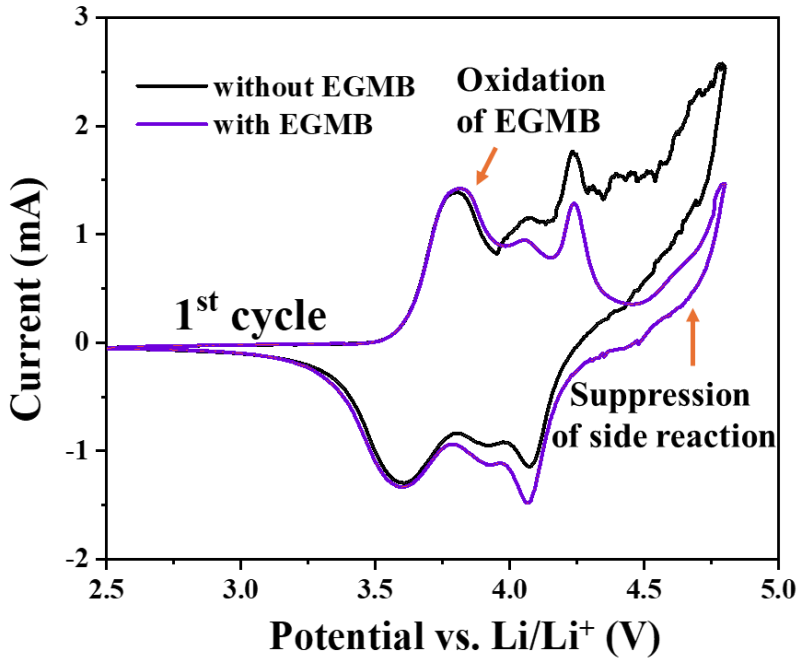

Figure 5. CV curves of Li||NMC811 cells at the potential range between 2.5 to 4.8 V with a scan rate of 0.1 mV s^{-1} in control system and 2 mg/ml EGMB containing electrolyte.

Cyclic voltammetry (CV) was conducted at a scan rate of 0.1 mV s^{-1} on NMC811 and NMC111 in cathodic half-cells to investigate the oxidation behavior of EGMB. In the initial cycle of the CV test for the Li||NMC811 cell with the potential range of 2.5 V to 4.8 V, the oxidation of EGMB is found at 3.74 V, as depicted in **Figure 5**. Notably, despite only partial formation of the CEI during the initial cycle, the reversibility of $Ni^{2+} \leftrightarrow Ni^{4+}$ and $Co^{3+} \leftrightarrow Co^{4+}$ redox couples are markedly enhanced. Furthermore, the presence of EGMB markedly reduces side oxidation reactions occurring above 4.4 V.

Interestingly, this potential matched with one significant side reaction occurring above 4.4 V vs. Li/Li^+ on the surface of NMC811, involving the release of lattice oxygen[21-23]. NMC811 as a kind of nickel-rich cathodic material, possess lower potential for gas release (~4.4 V) compared to NMC111 (~4.6 V), highlighting a crucial consideration for its use under high-voltage conditions[24]. The release of reactive lattice oxygen from NMC811 surface can further cause reaction with EC in the electrolyte, producing CO, CO_2, H_2O and protic species[25]. The

evolved H_2O and protic species subsequently lead to the decomposition of $LiPF_6$ to generate HF, OPF_3, PO_2F^{2-}.[26-28] These byproducts accelerate the degradation of the cathodic active materials and contribute to capacity loss in the cell.

The addition of EGMB introduces a substantial amount of boron in sp^2 hybridization with available unoccupied p-orbitals. The electron-deficient property of boron allows it to act as an electron acceptor[29], supporting to stabilize the oxygen on the surface of the electrode during the CEI formation process. This stabilization reduces the release of oxygen and subsequently mitigates the chain of side reactions. Therefore, the oxidation current above 4.4 V for Li||MNC811 with EGMB-containing electrolyte is much lower than that with commercial electrolyte in CV studies.

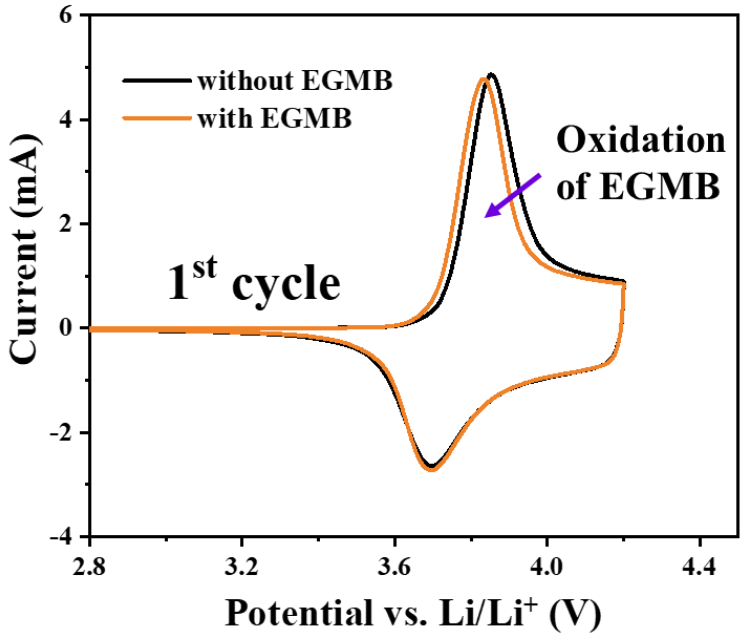

Figure 6. CV curves of Li||NMC111 cells at the potential range between 2.5 to 4.2 V with a scan rate of 0.1 mV s^{-1} in control system and 2 mg/ml EGMB containing electrolyte.

The CV of Li||NMC111 was conducted with a potential range from 2.8 V to 4.2 V at 0.1 mV s^{-1}, as shown in **Figure 6**. In EGMB-containing electrolyte, there is an earlier responsive current appeared at 3.62 V in comparison with control system, suggesting the oxidation of

EGMB in Li||NMC111 cells. Furthermore, the cyclability of cathodic half-cells with NMC811 and NMC111 was evaluated under a voltage range of 2.8–4.2 V at 1C rate to assess the advantages of EGMB for cathode materials under ordinary conditions.

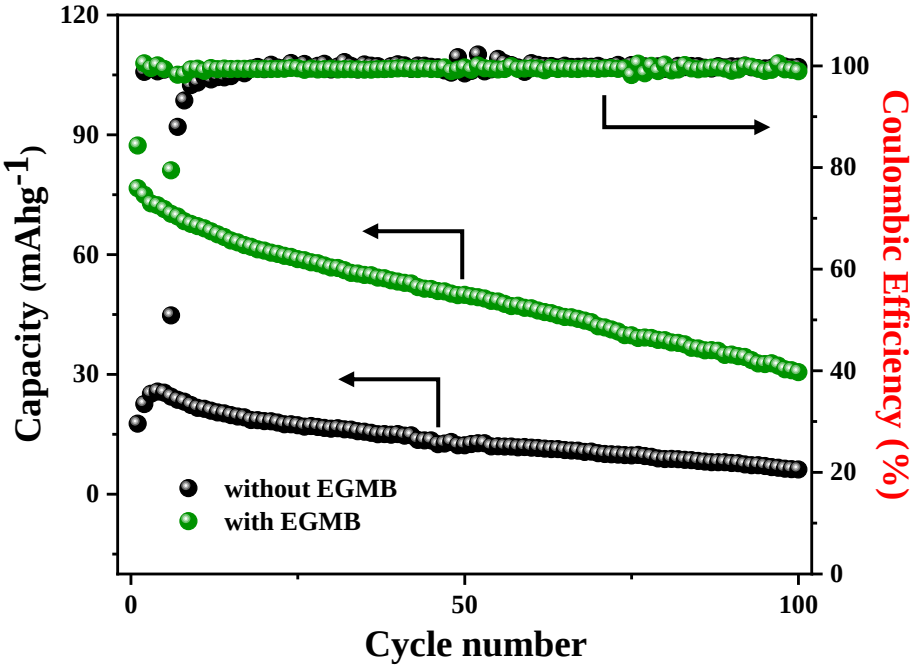

Figure 7. Cycling performance of Li||NMC811 with commercial electrolyte and EGMB-containing electrolyte from 2.8 V to 4.2 V at 1C rate.

As shown in **Figure 7**, the use of the EGMB electrolyte in Li||NMC811 cells significantly enhances capacity, with a fourfold increase, reaching 76.63 mAh/g in the initial cycle, compared to just 17.63 mAh/g with conventional electrolytes. This substantial improvement is attributed to the unique properties of EGMB, which, when integrated into the electrolyte, facilitates a higher discharge capacity under 1C high-rate conditions, with voltage range from 2.8 V to 4.2 V. The observed performance enhancement can be linked to the formation of a robust B-O bond in CEI, which boosts ionic conductivity and stabilizes the electrode-electrolyte interface. In contrast, the CEI formed with conventional electrolytes exhibits poorer lithium-ion conductivity, leading to higher energy barriers for lithium-ion transport. This results in reduced discharge capacity and diminished cycling stability.

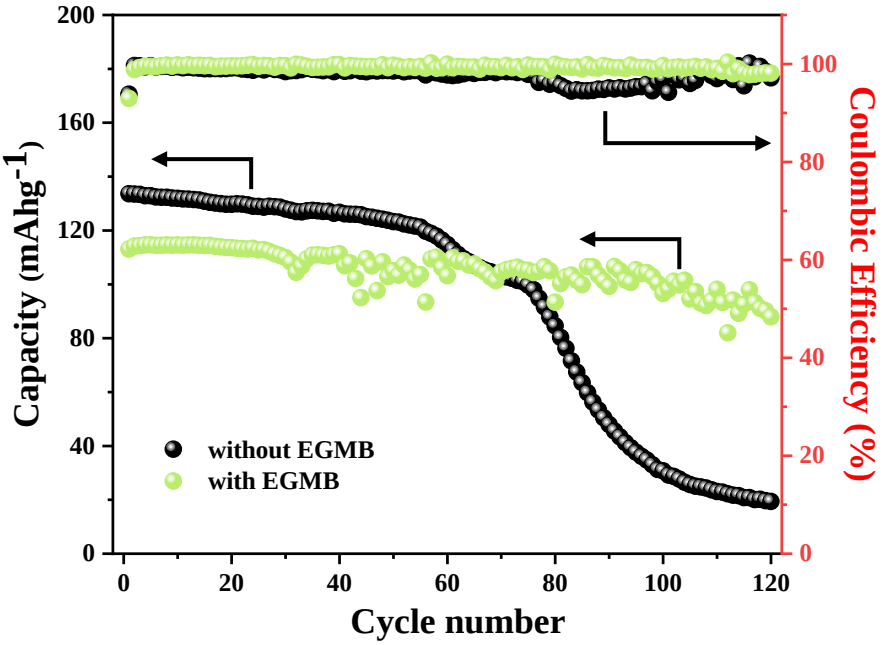

Figure 8. Cycling performance of Li||NMC111 with commercial electrolyte and EGMB-containing electrolyte from 2.8 V to 4.2 V at 1C rate.

For Li||NMC111 cells shown in **Figure 8**, the EGMB-containing electrolyte significantly improves durability, maintaining a high capacity 100.39 mAh/g with a retention of 88% after 120 cycles. In contrast, the commercial electrolyte results in substantial capacity loss, remained 30.78 mAh/g with 23% retention after 120 cycles. As the performances of both NMC811 and NMC111 were optimized by EGMB, the application of modified electrolyte under extreme conditions were explored and compared to commercial electrolyte.

In Chapter 2, it was demonstrated that the incorporation of MDMB into the electrolyte improves durability and enhances lithium-ion transference ability. To explore the effects of a dual additive system, both MDMB and EGMB were introduced into a commercial electrolyte. The rate capability of this system from 1/4 C to 2 C is shown in **Figure 9**, while its cycling performance with NMC111 at a rate of 1C over 120 cycles is presented in **Figure 10**.

The rate capability study revealed outstanding performance of the dual additive system. Notably, when the rate was increased to 2C and subsequently returned to 1C, the discharge

capacity reached 137.23 mAh/g, surpassing the initial 1C discharge capacity of 136.16 mAh/g. This result indicates the dual additive system's ability to maintain and even enhance discharge capacity under varying rates, reflecting its robust electrochemical stability and adaptability.

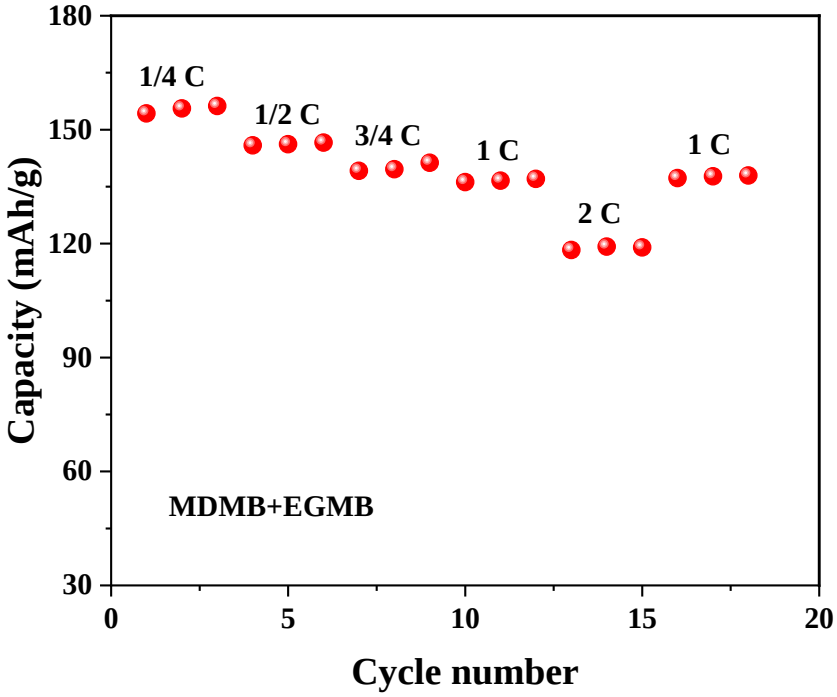

Figure 9. Rate capability of Li||NMC111 with electrolyte adding both MDMB and EGMB from 2.8 V to 4.2 V.

The long-cycle performance of the Li||NMC111 cell with the dual additive electrolyte was evaluated over a voltage range of 2.8 V to 4.2 V at a 1C rate for 120 cycles. Under 1C conditions, the dual additive system demonstrated a capacity reduction from 117.17 mAh/g to 85.99 mAh/g after 120 cycles, corresponding to a retention of 73%. While this retention significantly exceeds the 23% observed in the control system, it falls short of the performance achieved with the single EGMB-containing electrolyte. As illustrated in Figure 8, the EGMB-containing electrolyte maintained a high capacity of 100.39 mAh/g with a retention of 88% after 120 cycles. However, when MDMB was introduced alongside EGMB in the electrolyte, the capacity retention decreased from 88% to 73%. These findings underscore that electrolyte modification is not a simple additive process; the distinct properties and interactions of

individual additives critically influence the overall performance, highlighting the need for strategic design in electrolyte formulations.

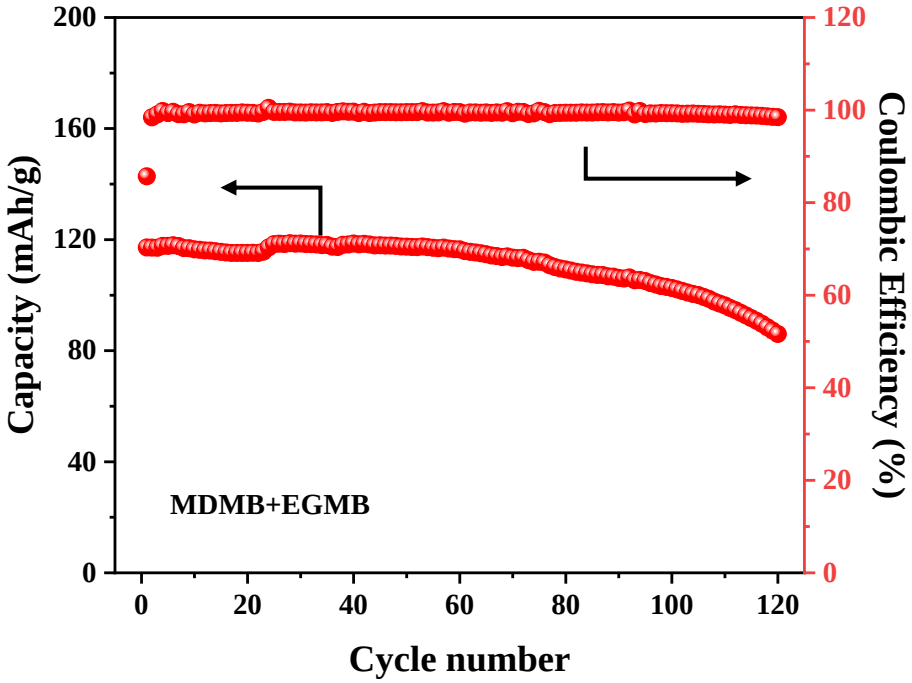

Figure 10. Cycling performance of Li||NMC111 with electrolyte adding both MDMB and EGMB from 2.8 V to 4.2 V at 1C rate.

3.3.3 Studies on NMC811 cathode under 4.8 V ultrahigh cut-off voltage

The energy density of LIBs is primarily determined by the Li^+ storage capacity and operating voltage of the electrode materials, making the selection of electrode materials critical to the overall performance of the battery system[30-32]. Over the years, various cathode materials, including $LiMn_2O_4$, $LiFePO_4$, and $LiNi_{0.8}Co_{0.1}Mn_{0.1}O_2$, have been extensively studied and applied in large-scale LIBs to replace $LiCoO_2$. Among the various cathode materials, NMC811, with its high nickel content (80%), exhibits a significantly higher theoretical capacity. This makes it one of the most widely studied and utilized materials in high-voltage lithium-ion

battery research. Its elevated nickel percentage contributes to increased energy density and better performance at higher voltages, leading to its growing popularity in applications requiring high energy storage and efficiency.

However, despite the promise of lithium-rich cathode material (LRCMs), several challenges persist. These include: (i) Low initial Coulombic efficiency (ICE), as many LRCMs experience poor efficiency during the first charge/discharge cycle; (ii) Voltage decay, where the discharge voltage decreases continuously with cycling, leading to a loss of energy density; (iii) Substantial capacity loss, which limits the long-term service life of these materials; (iv) Poor rate capability, caused by sluggish reaction kinetics and low electronic conductivity; and (v) Transition metal (TM) dissolution, where lattice distortion and Mn^{2+} dissolution, driven by the Jahn-Teller effect, cause significant capacity degradation over time [34].

Addressing these challenges is essential for advancing the development of high-performance cathode materials capable of delivering both enhanced energy densities and improved cycling stability, thereby enabling lithium-ion batteries (LIBs) with longer operational lifespans and superior overall performance. In the present study, initial investigations with NMC811 revealed that the incorporation of an EGMB-containing electrolyte significantly enhanced both the capacity and durability of the material. Building on these findings, the EGMB-containing electrolyte was further evaluated under ultrahigh voltage conditions to assess its potential for further performance improvements.

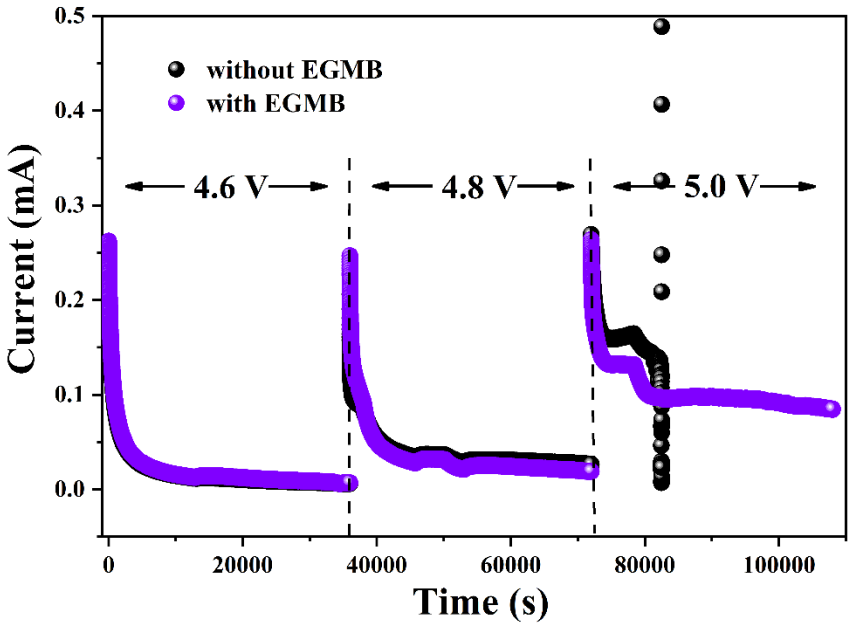

Figure 11. Floating test of Li||NMC811 cathodic half-cell from 4.6 V to 5.0 V.

As the $LiNi_{0.8}Co_{0.1}Mn_{0.1}O_2$ exhibits a high nickel content, which significantly enhances its capacity and energy density, it has become one of the most favored choices for applications involving ultra-high cutoff voltages. The electrochemical floating test method was utilized to evaluate the electrolyte oxidation stability under different high potential stages[35]. The cells were charged to 4.6 V at a current rate of 0.1 C and subsequently maintained at 4.6 V, 4.8 V, and 5.0 V for a duration of 10 hours respectively.

During this process, the leakage currents were monitored and recorded as illustrated in **Figure 11**. At an initial voltage of 4.6 V, the leakage currents for the EGMB-containing electrolyte and the blank system were comparable and exhibited similar current profiles. As the voltage was raised to 4.8 V, the leakage current for the control system was slightly higher than that for the EGMB-containing electrolyte. However, at 5.0 V, the blank electrolyte underwent significant decomposition and side reactions, leading to a cliffy increment in leakage current[36]. In contrast, the EGMB-containing electrolyte effectively passivated the NMC811 surface, thereby maintaining a relatively low leakage current, which demonstrates the potential for safe operation under extremely high voltages.

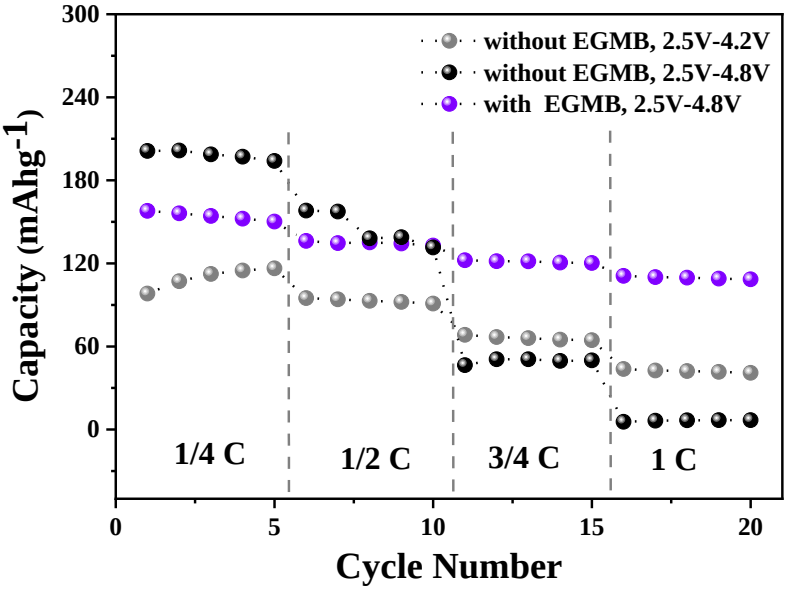

Figure 12. Rate studies for cells under 4.2 V or 4.8 V.

Figure 12 illustrates the discharge capacity of Li||NMC811 cathodic half-cells with different electrolytes and potential ranges (2.5 V–4.2 V or 2.5 V–4.8 V) under varying current rates. The performance of cells with commercial electrolytes was evaluated under both the 2.5 V–4.2 V and 2.5 V–4.8 V potential windows. For the cells operating within the 2.5 V–4.2 V range, the discharge capacities were measured as follows: 107.11 mAh/g at 1/4 C, 94.97 mAh/g at 1/2 C, 68.37 mAh/g at 3/4 C, and 43.71 mAh/g at 1 C. When the cutoff voltage was increased to 4.8 V, the capacities of the cells with commercial electrolyte were measured as 201.27 mAh/g at 1/4 C, 158.10 mAh/g at 1/2 C, 46.50 mAh/g at 3/4 C, and 5.55 mAh/g at 1 C.

A comparison of the performance under the two different cutoff voltages reveals that, at low rates (1/4 C and 1/2 C), the cells tested with a 4.2 V cutoff voltage exhibited lower capacity compared to those tested with a 4.8 V cutoff. However, when the current rate was increased to 3/4 C and 1 C, the cells with a 4.8 V cutoff voltage showed a significant decrease in capacity. This indicates that while higher cutoff voltages can improve capacity at low current rates, they lead to significant instability and poor performance at high rates.

In contrast, cells with an EGMB-containing electrolyte demonstrated both enhanced capacity and greater stability. The discharge capacities of these cells under the 2.5 V–4.8 V voltage range were 157.92 mAh/g at 1/4 C, 136.25 mAh/g at 1/2 C, 122.29 mAh/g at 3/4 C, and 110.97 mAh/g at 1 C. Notably, under high current rates (3/4 C and 1 C), the EGMB-containing electrolyte showed a marked improvement in capacity compared to the commercial electrolyte. This demonstrates the superior performance of the EGMB-based electrolyte, which provides a more stable and high-capacity solution under both low and high-rate cycling conditions.

Thus, while cells with commercial electrolytes demonstrate a capacity trade-off between voltage range and current rate, those with EGMB-containing electrolytes exhibit superior performance, especially at higher rates. This indicates that EGMB significantly enhances both capacity retention and rate capability in the Li||NMC811 system. Furthermore, this study underscores the importance of investigating the behavior of cells and cathodic active materials at high voltages for high energy-density applications. The stability of the electrolyte under elevated voltages remains a critical challenge that must be addressed in future research to ensure the long-term durability and operational efficiency of high-energy-density batteries.

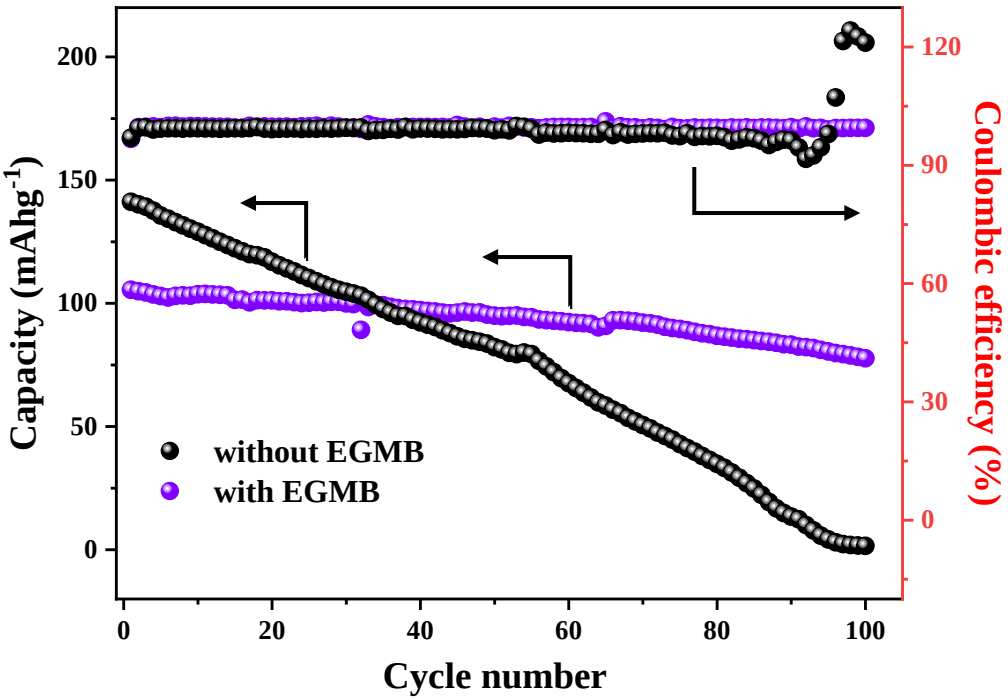

Figure 13. Cycling performance of Li||NMC811 cathodic half-cell with different electrolytes at 1C rate under 4.8 V high cut-off voltage.

Figure 13 illustrates the cyclability of Li||NMC811 cells with different electrolytes at an ultrahigh cutoff voltage of 4.8 V, demonstrating the significant improvements in the stability and durability of the NMC811 cathode material when using EGMB as an additive under 1C high-rate cycling conditions. Initially, the cell with the commercial electrolyte exhibited a higher discharge capacity of 141.17 mAh/g compared to the cell with EGMB-containing electrolyte, which showed a lower capacity of 105.50 mAh/g. However, after 100 cycles, the cell with EGMB maintained a capacity of 77.67 mAh/g and retained a high coulombic efficiency of 99.50%, indicating excellent cycling stability and minimal side reactions. In contrast, the cell with the commercial electrolyte experienced a dramatic capacity degradation, dropping to just 1.51 mAh/g, accompanied by an unusually high coulombic efficiency of 121.09%, suggesting significant side reactions (gas evolution) and electrolyte degradation within the cell[37]. In contrast, EGMB effectively stabilized both the electrolyte and the cathode, enhancing the safety of the batteries during operation under high-voltage conditions.

The addition of EGMB significantly improved the capacity retention of the Li||NMC811 cell, which increased from a mere 1.07% to 73.97% after 100 cycles at the 1C rate under the high 4.8 V cutoff voltage. These results highlight the crucial role of EGMB in enhancing the long-term performance and stability of high-energy-density cells, particularly at ultrahigh voltages, where conventional electrolytes tend to undergo rapid degradation.

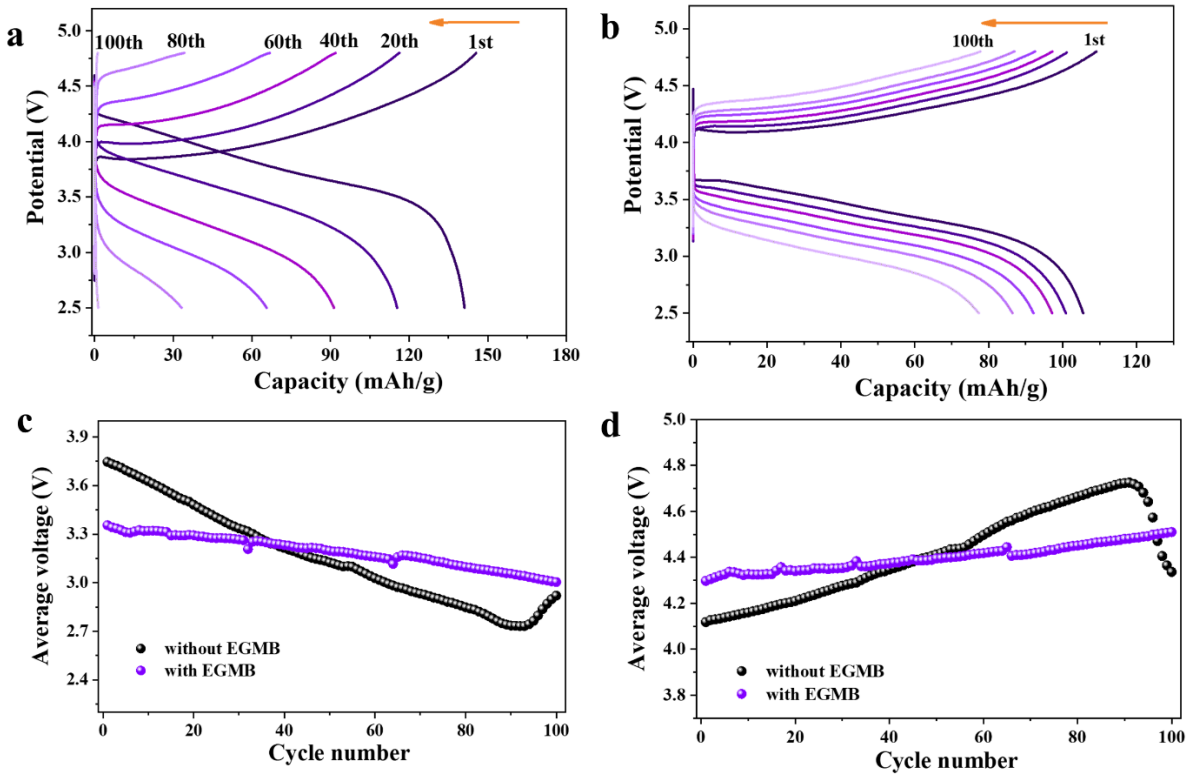

Figure 14. Voltage profiles of cells under 4.8 V using (a) commercial electrolyte and (b) EGMB electrolyte. Average voltage during (c) charging process and (d) discharging process.

The capacity degradation of the cells is further illustrated by the profiles depicted in **Figure 14a and 14b**. The capacity loss of NMC811 is reduced from 98.93% to 26.03% by EGMB modified battery. Compared to the rapid capacity decay with reference electrolyte, the EGMB-containing electrolyte effectively protected the NMC811 cathode and significantly reduced the rate of degradation[38]. The results underline the importance of electrolyte stability in high-energy-density systems, particularly when operating at elevated cutoff voltages like 4.8 V. The commercial electrolyte, while offering a high initial capacity, is prone to rapid

degradation under such conditions, resulting in poor capacity retention and significant side reactions. In contrast, the EGMB-containing electrolyte stabilizes the electrolyte/electrode interface, effectively preventing degradation and maintaining both capacity and coulombic efficiency over extended cycles.

Figure 14c and 14d present the average charging and discharging voltages for the Li||NMC811 cells with different electrolytes under high-voltage cycling conditions. During both the charging and discharging processes, the cell with the commercial electrolyte exhibited significant fluctuations in the average voltage. These fluctuations reflect a notable increase and decrease in voltage, which can be attributed to the buildup of undesirable internal resistance[39]. This resistance is likely caused by the continuous decomposition of the electrolyte, leading to the formation of a thick and unstable CEI, which increases the cell's internal impedance and introduces additional voltage losses during cycling.

In contrast, the cell with the EGMB-containing electrolyte demonstrated a more stable and consistent average voltage during both charge and discharge cycles. The addition of EGMB facilitated the formation of a robust and stable CEI, which effectively prevented the excessive buildup of CEI layers. This stable CEI minimized the formation of additional resistance within the cell, thereby preserving a constant average voltage throughout the cycling process. The ability of the EGMB-modified electrolyte to maintain a stable voltage profile indicates a significant reduction in side-reactions and electrolyte degradation, further demonstrating the superior performance of EGMB in enhancing the stability and efficiency of high-voltage cycling in Li||NMC811 cells, which suggest that the EGMB-containing electrolyte not only improves the cycling stability but also minimizes unwanted voltage variations that are typically associated with electrolyte decomposition, providing more efficient and reliable battery operation under high-energy-density conditions[40].

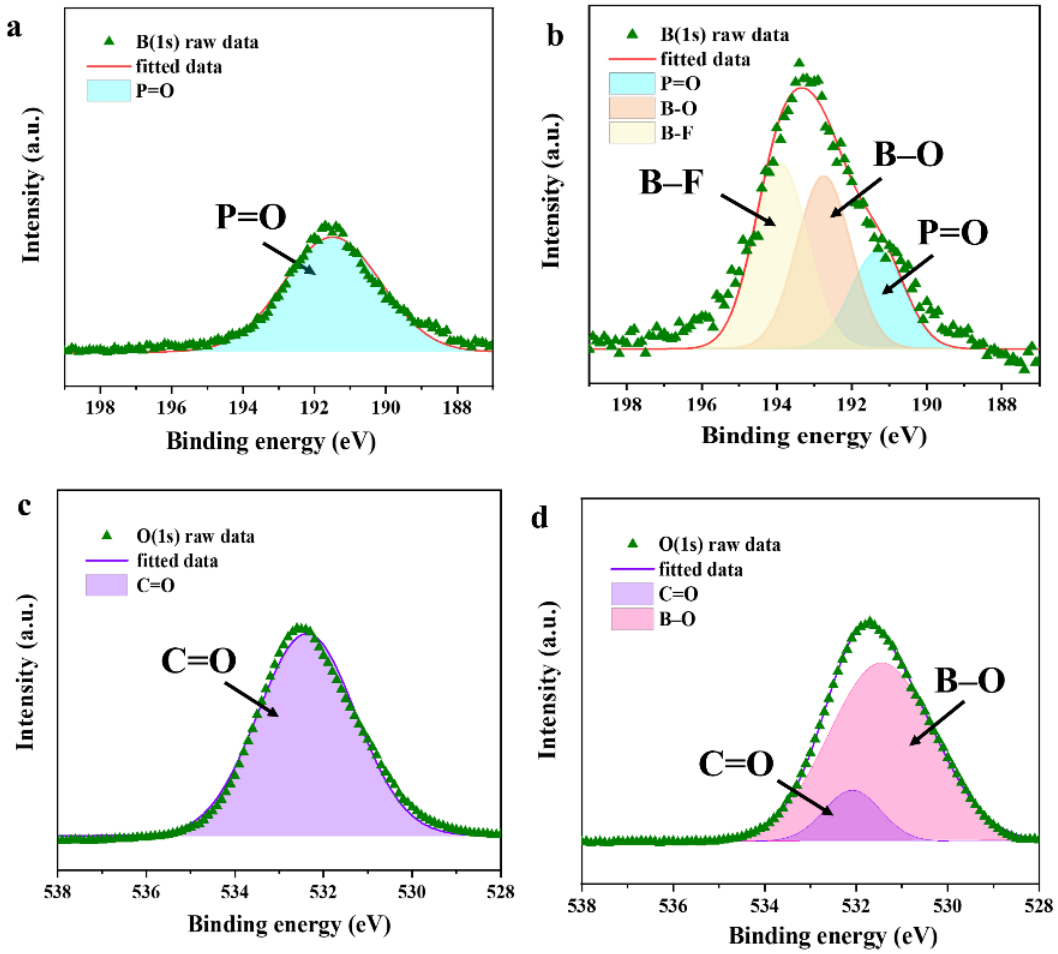

Figure 15. Post-studies on NMC811 after cycled under 4.8V high cut-off voltage. XPS spectra of B 1s on NMC811 surface cycled in electrolyte (a) without EGMB, (b) with EGMB, O 1s for (c) without EGMB and (d) with EGMB.

The X-ray photoelectron spectroscopy (XPS) was performed to further investigate chemical components of the interface on cycled NMC811 cathodes in different electrolytes. The XPS analysis identifys the presence of P=O, B–O, and B–F signals in the B 1s spectra[20, 39, 41], and C=O and B–O signals in the O 1s spectra, indicating the formation of specific components in the CEI resulting from electrolyte decomposition. As comparison of **Figure 15a** and **15b**, the B–O, B–F bonds were detected at 192.5 eV and 194.0 eV in the EGMB containing electrolyte[42]. Its presence confirms the role of boron in the formation of a robust CEI film on the surface of the cathodes.

On the one hand, the substantial formation of B–O bonds demonstrates that effective stabilization of reactive lattice oxygen on the surface of NMC811, which aligns with the improved durability was observed due to reduced oxygen release and its subsequent oxidation reactions with carbonate electrolyte components, resulting in production of CO, CO_2, H_2O and H^+ species[43]. Furthermore, H_2O and H^+ species can react with $LiPF_6$ lithium salt, resulting in the formation of HF, OPF_3, and $PO_2F_2^-$, which will corrode the surface and dissolve TM and contribute to the capacity decay during cycling[44,45].

On the other hand, B–O bonds peaks suggest the formation of an in-situ formed boron-rich CEI film[46], which can enhance the ionic conductivity and reduces interphase impedance. The reactions of EGMB on the surface of NMC811 provides robust protection for the TMs, effectively preventing their detachment from the cathode and subsequent dissolution into the electrolyte. This protective layer helps stabilize the cathode material, reducing the risk of capacity degradation caused by the loss of transition metals during cycling. Additionally, the electron-withdrawing nature of the boron atom promotes the formation of B–F bonds. The substantial consumption of free fluorine by boron effectively eliminates HF, thereby reducing the dissolution of transition metals. Consequently, the incorporation of boron improves both the durability and rate capability of NMC811 cathodic half cells.

In the O 1s spectra, the peak corresponding to the C=O bond at 532.5 eV exhibited a significantly stronger response in **Figure 15c** compared to the signal produced by boron-rich CEI in **Figure 15d**. This peak originates from the polymerization of carbonate components in the electrolyte. The substantial presence of B–O bonds replacing C=O bonds indicates that boron participates in the formation of the film as an adhesive material. As a result, the incorporation of boron leads to the formation of a more stable and robust in-situ formation artificial CEI.

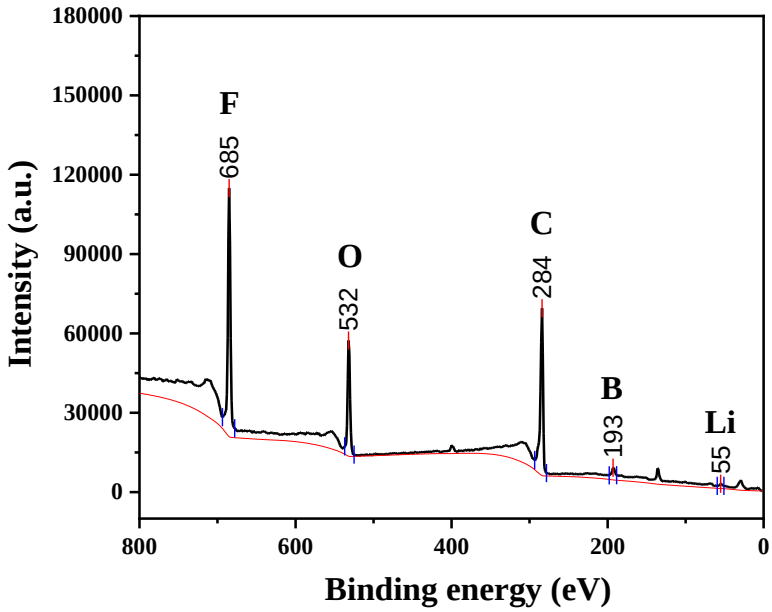

Figure 16. XPS survey spectrum of C, O, F, B elements on NMC811 after cycled under ultrahigh voltage.

X-ray photoelectron spectroscopy (XPS) was performed over a binding energy range of 0 eV to 800 eV, encompassing the elements Li, B, C, O, and F, to determine the boron content in the cathode-electrolyte interface (CEI). As shown in **Figure 16** and detailed in **Table 1**, the boron content in the CEI was found to be 8.4% at the cathodic surface. Despite the low concentration of EGMB in the electrolyte (only 2 mg/mL), its presence had a significant impact on the composition of the CEI. The results indicated that EGMB substantially altered the components of the CEI, highlighting its influence on the interface chemistry and suggesting its role in stabilizing the electrolyte/electrode interaction.

Table 1. Components of Li, C, O, F, B elements on NMC811

element	peak center	peak area	ASF	Percentage in CEI
Li	55	11317.11	0.025	20.7%
B	193	29035.47	0.159	8.4%
C	284	273167.1	0.296	42.0%
O	532	168917.7	0.711	10.8%
F	685	396585.5	1	18.1%

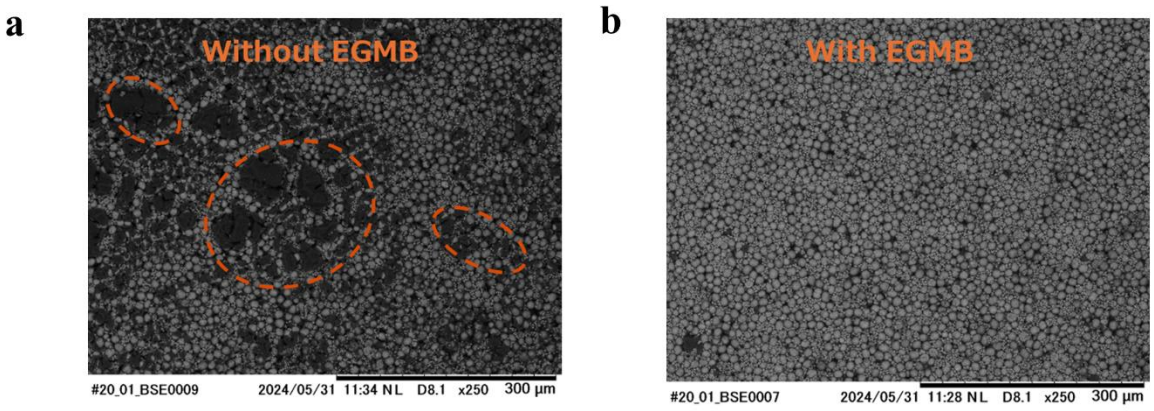

Figure 17. Scanning electron microscopy (SEM) of NMC811 surface after cycled (a) without EGMB and (b) with EGMB.

To investigate the degradation of cathodes induced by different electrolytes, NMC811 cathodes cycled in half-cells for 100 cycles under 4.8 V high cut-off voltage were examined using scanning electron microscopy (SEM). **Figure 17a** shows significant transition metal leaching when the cells were cycled with a commercial electrolyte under extreme conditions. This observation suggests substantial corrosion of the transition metals, driven by the presence of HF in the electrolyte, and highlights the insufficient protection provided by CEI formed through decomposition of the conventional electrolyte[53].

In contrast, **Figure 17b** reveals that the active particles of NMC811 are effectively protected when cycled with an EGMB-containing electrolyte. The decomposition of EGMB facilitates the formation of a robust, boron-containing CEI layer, which serves to mitigate the corrosion of the cathode surface and reduce the adverse effects of HF-induced degradation. This protective film enhances the stability of the cathode and improves its overall cycling performance.

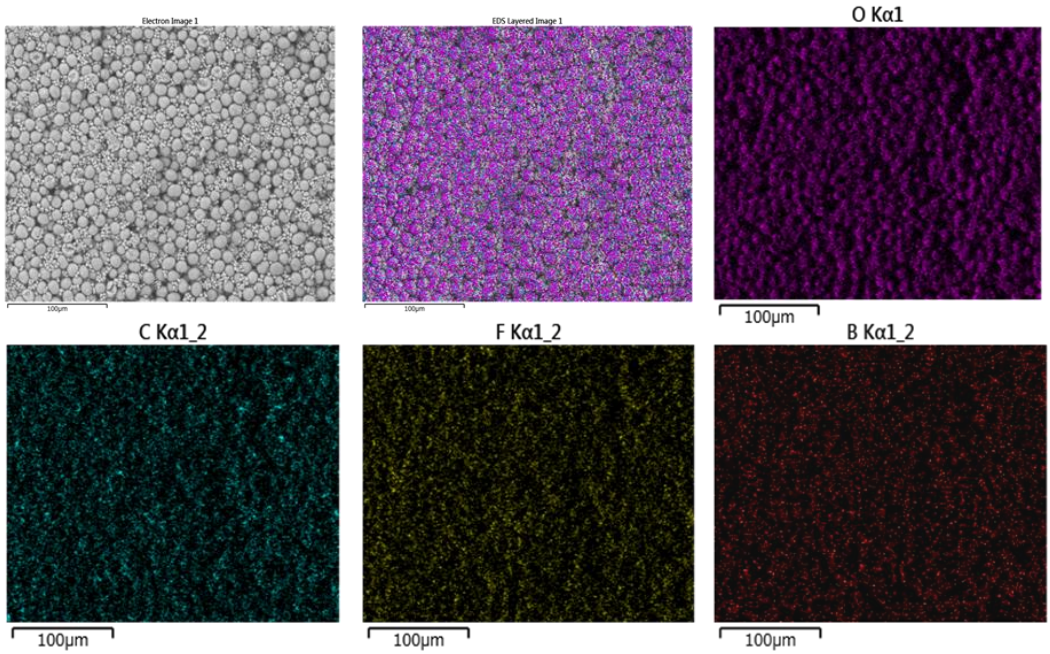

Figure 18. Energy dispersive X-ray spectroscopy (EDS) of O, F, C, B elements on cathodic surface after cycled with EGMB-containing electrolyte.

The distribution of C, O, F, B on NMC811 surface after cycled with EGMB under ultrahigh voltage was exhibited via energy dispersive X-ray spectroscopy (EDS) in **Figure 18**. After cycling, the electrolyte in the separator was vacuumed overnight to remove the DEC, forming a solid-state electrolyte with high-melting-point EC as the predominant component.

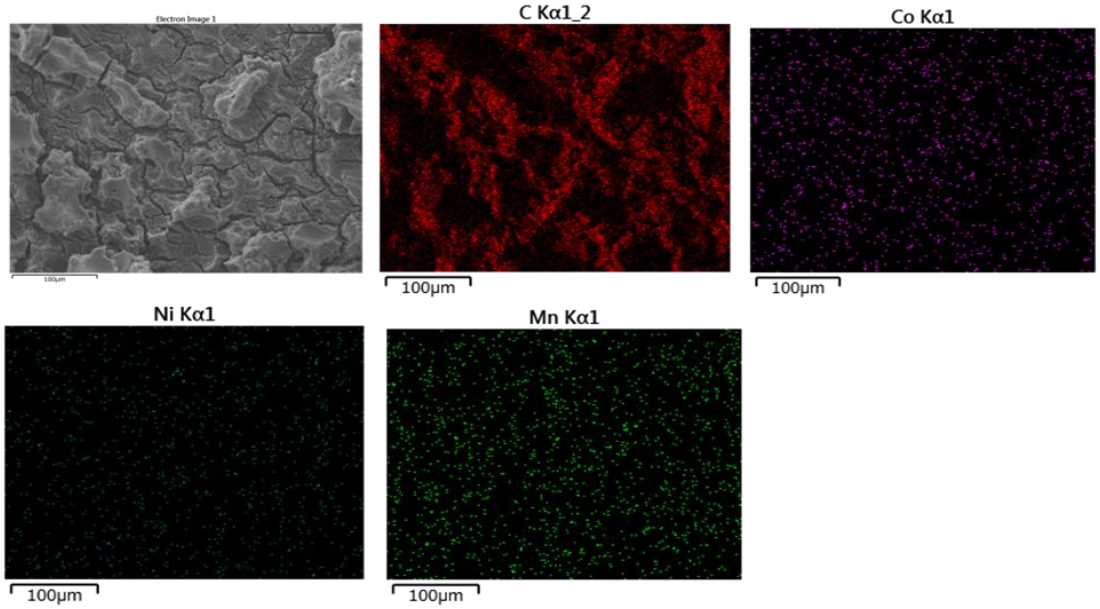

Figure 19. EDS of C, Co, Mn, Ni elements on cathodic surface with commercial electrolyte.

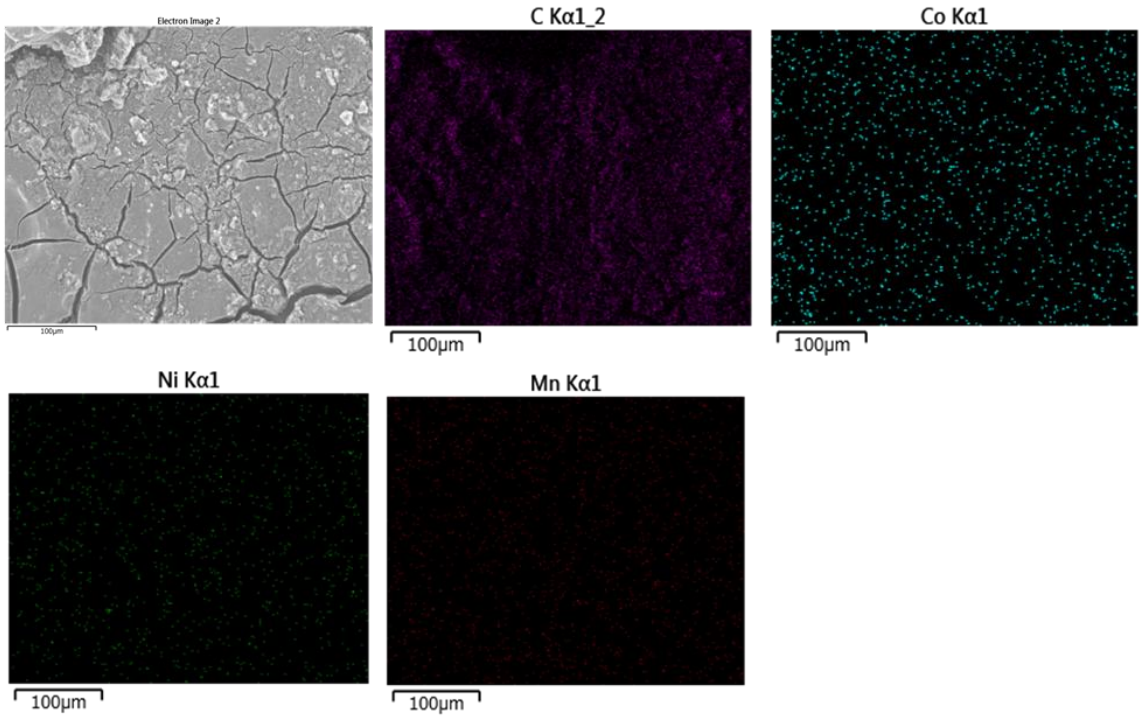

Figure 20. EDS of C, Co, Mn, Ni elements on cathodic surface with EGMB-containing electrolyte

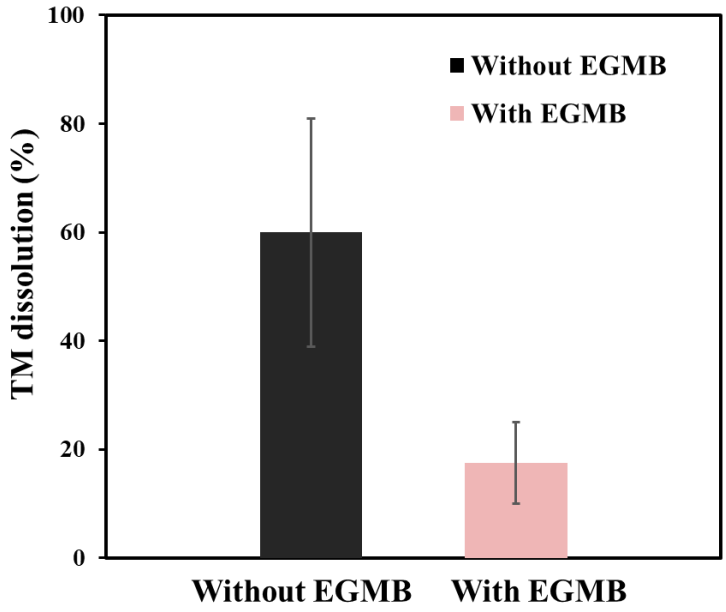

Figure 21. The percentage of Ni, Mn, Co in the vacuumed solid electrolyte.

The transition metal content in this solid-state electrolyte was then analyzed using EDS to evaluate the dissolution of TM into the electrolyte, as depicted in **Figures 19 and 20**.

Statistical results in **Figure 21** indicated that the dissolution of TM (Ni, Mn, Co) was significantly reduced with the addition of EGMB from 60.0% to 17.5%. It clearly reflects the serious dissolution situation of cathodic active metal during charging and discharging process under high voltage conditions and highlights the mitigating effect achieved by adding EGMB. The reduction of TM dissolution in EGMB-containing electrolyte is attributed to the impact of B–O and B–F bonds in CEI, which eliminates HF in the electrolyte, thus offering enhanced protection to the transition metals.

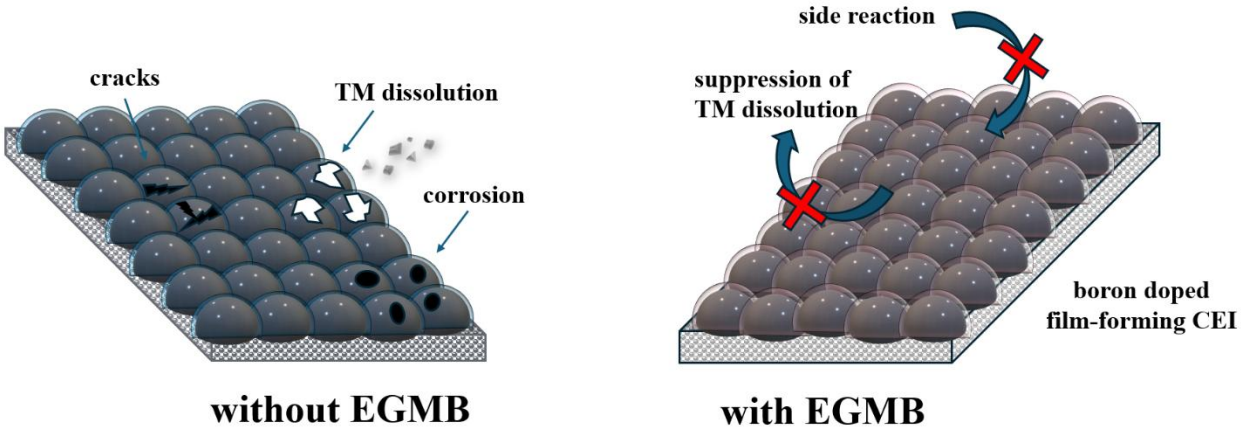

Figure 22. Schematic illustration of NMC811 cycled under high voltage with the CEI formed in commercial electrolyte and boron-rich CEI in EGMB electrolyte.

Figure 22 further illustrates the contrasting effects between the boron-rich CEI and the traditional carbonate CEI. It clearly depicts the vicious circle of side reactions in the commercial electrolyte. And it is mitigated in the EGMB-containing electrolyte at its source by stabilizing the lattice oxygen on NMC811 surface. The study of Li||NMC811 under 4.8V at 1C reveals that EGMB could prevent the chain of side reaction on Ni-rich cathodic surface as the voltage increases over 4.4 V by forming boron rich CEI layer, leading to the improvement of cell durability.

3.3.4 Studies on NMC111 cathode under extreme fast charging and discharging

The extended charging times (>30 min) of electric vehicles (EVs), in comparison to the refueling time of gasoline vehicles, remain a significant barrier to the widespread adoption of EVs[46-48]. As a result, researchers are actively exploring strategies to achieve fast charging, targeting a 15-minute charge to reach 80% state of charge (SoC). However, the durability of batteries under such extreme high charging rates remains a critical challenge. Previous studies have demonstrated improvements in battery longevity at fast charging rates of 1C with the addition of EGMB. Building on these findings, this study further investigates the enhancements provided by EGMB in improving the durability of cells under extreme high charging rates (≥4C).

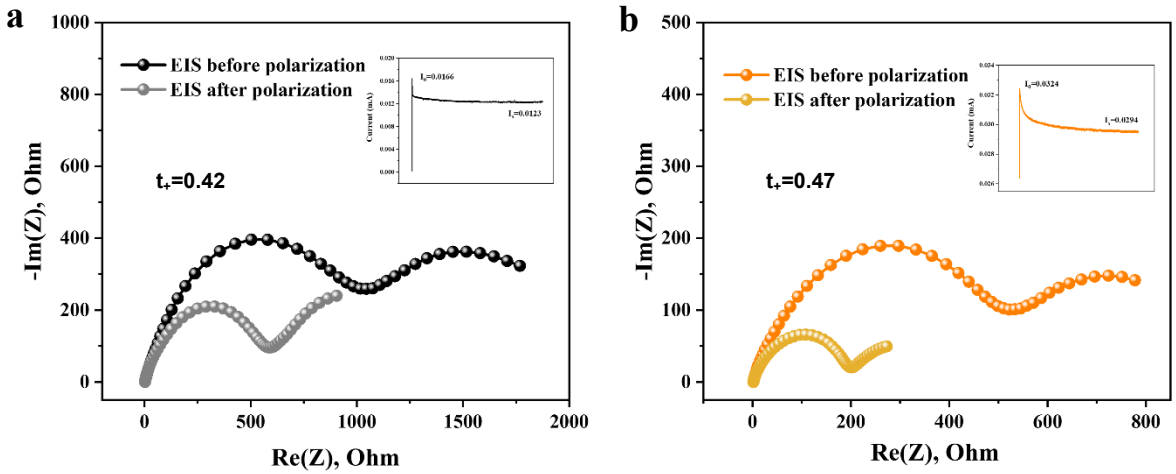

Figure 23. EIS before polarization and after polarization of Li||Li symmetric cells with (a) commercial electrolyte and (b) EGMB-containing electrolyte for Li-ion transference number calculation.

To further investigate the proposed working mechanism, the lithium-ion transference number was calculated for both the control system and the electrolyte containing EGMB, as shown in **Figure 23**. The lithium-ion transference numbers for the control system and the EGMB-containing electrolyte were found to be 0.42 and 0.47, respectively. These results suggest that the addition of EGMB to the electrolyte leads to only a marginal improvement in

lithium-ion transference number. In Chapter 2, a notable enhancement in lithium-ion mobility was observed upon incorporating MDMB into the electrolyte. MDMB significantly modified the solvent sheath and altered the interactions between the electrolyte components, which consequently facilitated a marked increase in lithium-ion transport. This improvement in the lithium-ion transference number resulted in a substantial enhancement of the electrochemical performance, leading to nearly double the capacity at high discharge rates compared to the control system. In contrast, the relatively small addition of EGMB did not significantly modify the solvent sheath or the interactions between the solvent components. As a result, the EGMB-containing electrolyte did not exhibit a substantial increase in lithium-ion transference or high-rate capacity, as evidenced by the rate capability tests in **Figure 24**.

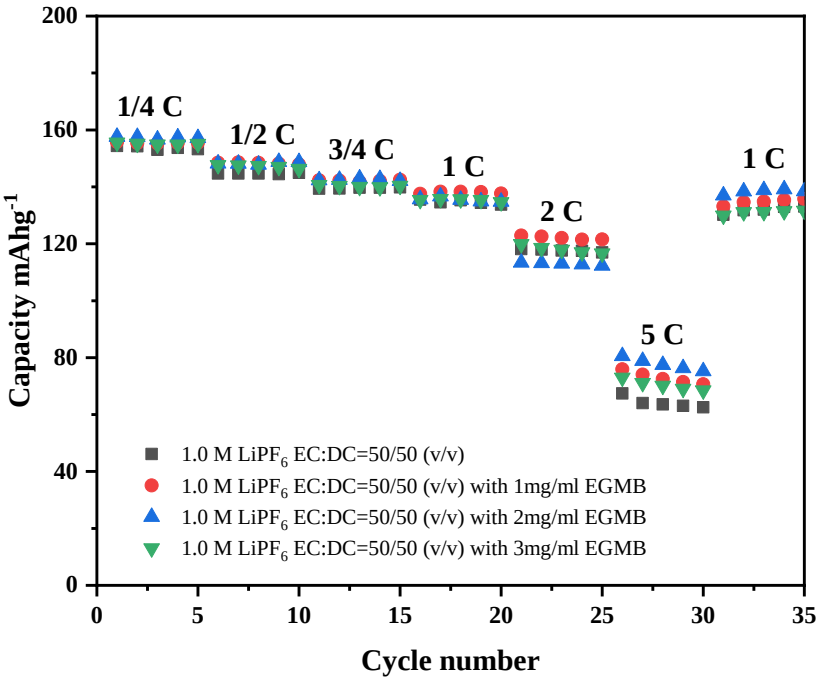

Figure 24. Rate study of Li||NMC111 cathodic half-cells with various concentrations of EGMB into electrolyte with a potential range from 2.8 V to 4.2 V.

The rate performance of Li||NMC111 cathodic half-cells is shown in **Figure 24**, which demonstrates minimal differences in the performance of cells with and without EGMB. It can be concluded that the addition of EGMB to the electrolyte does not significantly alter the key

properties of the bulk electrolyte, such as viscosity, polarity, lithium transference number, or ionic conductivity, which are critical factors influencing discharge capacity at high rates. Instead, the primary role of EGMB is to modify the composition of the CEI, stabilizing the cathodic active material and enhancing the overall durability of the battery. These findings highlight the value of incorporating EGMB as an electrolyte additive, particularly when combined with other electrolyte optimization strategies, to contribute to the development of the next generation of electric vehicle batteries. As shown in **Figure 25**, the long cyclability of two electrolytes was studied at 4C charging rate and 1C discharge rate. The cell with commercial electrolyte was dead at 29th cycle, in contrast, the EGMB-containing electolyte enable the cell cycled more than 100 times with slow degradation and high coulombic efficiency.

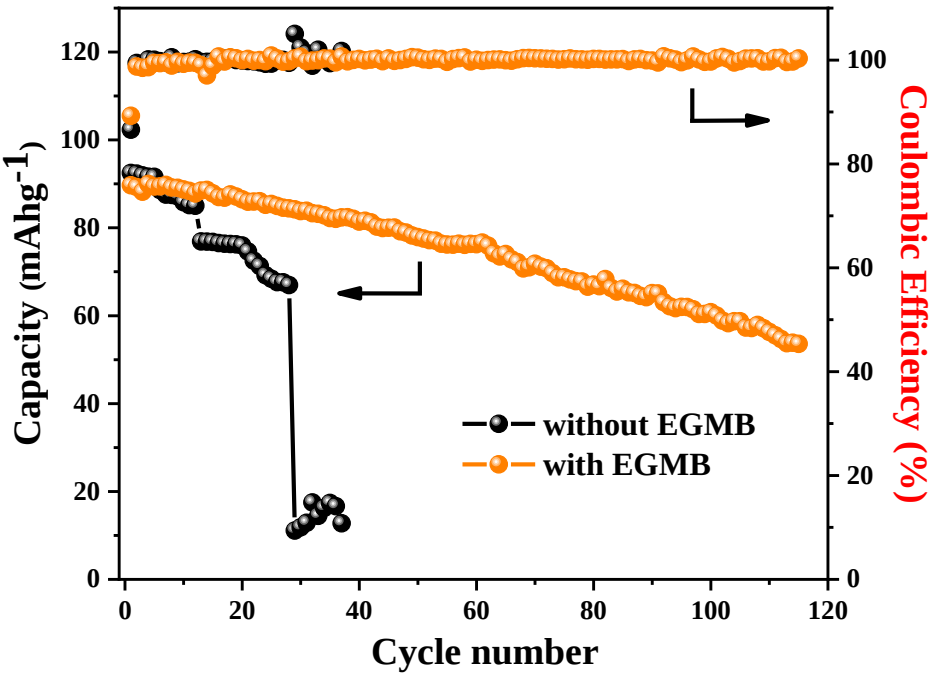

Figure 25. Long cycling study of Li||NMC111 cells charged at 4C and discharged at 1C with a potential range from 2.8 V to 4.2 V.

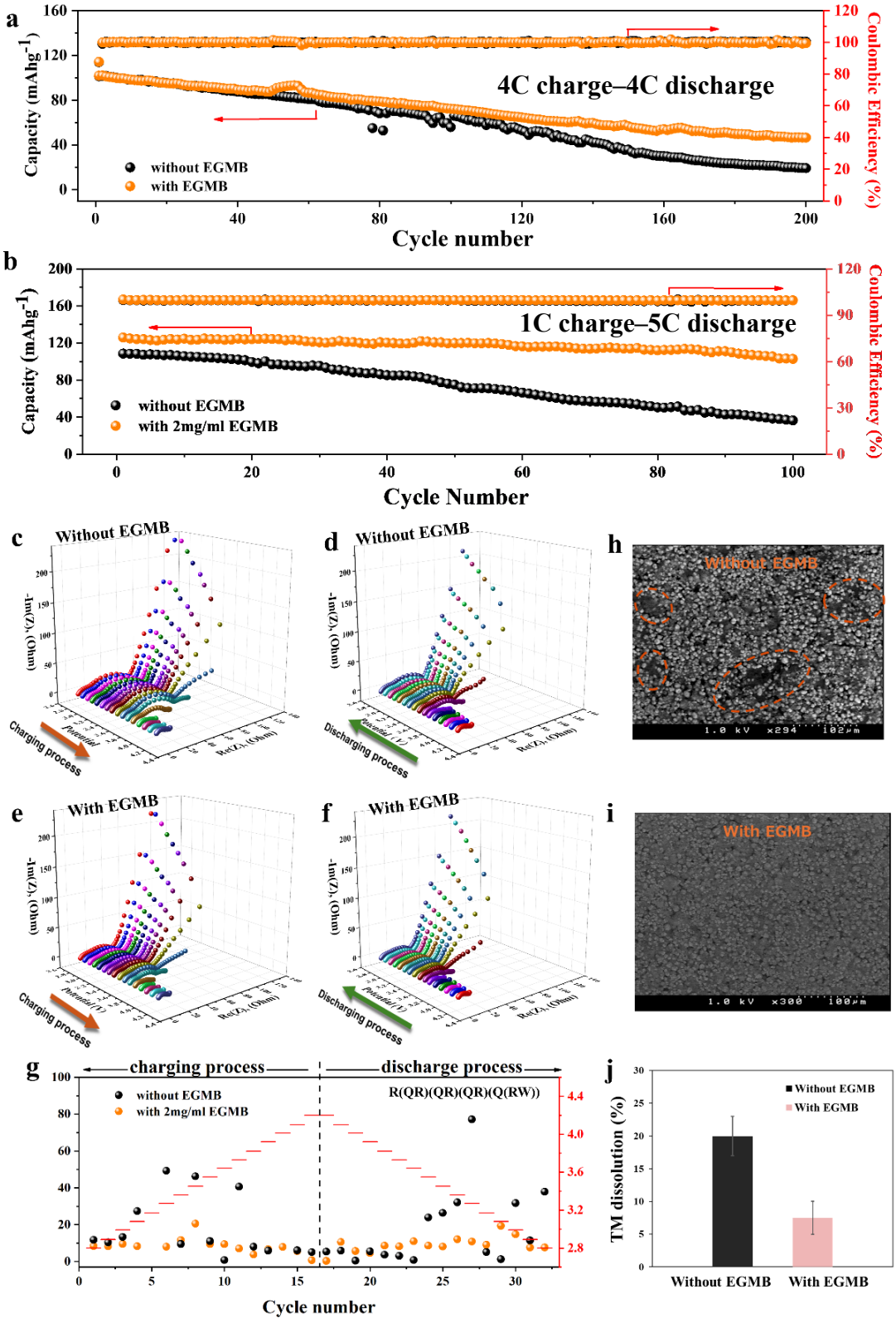

Figure 26. Studies on Li||NMC111 cathodic half-cells for high-rate applications. (a) Discharge capacity and coulombic efficiency of cells at 4C rate for both charging and discharging processes with a potential range from 2.8 V to 4.2 V. (b) discharge capacity and coulombic

efficiency of cells at 1C for charging and 5C for discharging with a potential range from 2.8 V to 4.2 V. (c) 3D DEIS Nyquist profiles for charging and (d) discharging process under 2.8V–4.2V of cycled cathodic half-cell with commercial electrolyte. (e) 3D DEIS Nyquist profiles for charging and (f) discharging process under 2.8V–4.2V of cycled cathodic half-cell with 2 mg/ml EGMB electrolyte. (g) R_{CEI} obtained via Equivalent circuit fitting under different voltage from charging to discharging. (h) scanning electron microscopy (SEM) of NMC111 surface after cycled without EGMB and (i) with EGMB. (j) the percentage of Ni, Mn, Co in the vacuumed solid electrolyte.

NMC111, as a more mature cathodic active material which integrates the benefits of various transition metals, shows improved performance under diverse conditions. Consequently, it was employed in this study to investigate the enhancements provided by the EGMB additive under high charge-discharge rates and wide temperature range. **Figure 26a** demonstrates the cyclability of NMC111 in cathodic half-cell with different electrolytes at extreme 4C rate for both charging and discharging process via constant current (CC) mode. The capacity loss of NMC111 was reduced from 80.96% to 54.43% with the addition of EGMB after 200 cycles. Although capacity degradation is inevitable, the incorporation of trace quantities of EGMB slows the rate of capacity loss to a certain extent. In **Figure 26b**, the cells were cycled at charging rate of 1C and discharging rate of 5C. The cell with EGMB exhibits a capacity of 125.93 mAh/g in the initial cycle and remains 102.91 mAh/g after 100 cycles with a retention of 81.72%. In contrast, the capacity of control system decreases from 108.55 mAh/g to 36.47 mAh/g with a retention of 33.59%. Due to the intricate degradation mechanisms associated with extreme charging and discharging rates, capacity decay is influenced by multiple factors. Notably, the dissolution of transition metals and the formation of the CEI layer are critical determinants of the rate of decay. Dynamic electrochemical impedance spectroscopy (DEIS) was employed to assess resistances of CEI under each potential during

the charging and discharging processes. Impedance measurements of the cycled cathodic half-cells were conducted over a potential range of 2.8 V to 4.2 V and a frequency range of 0.01 Hz to 1.0 MHz. **Figure 26c–26f** and **Table 2–5** display the 3D Nyquist plots and DEIS-fitted parameters for cells with different electrolytes. The circuit used for fitting the plots includes $R_{int}(QR_{ct})(QR_{CEI})(QR_{pre\text{-}diff})(Q(R_{complex\ diffusion}W))$[49]. This circuit model provides component impedance values within the cathodic half-cell, where the resistances correspond to internal resistance, charge transfer resistance, CEI resistance, pre-diffusion resistance, and complex diffusion resistance, respectively. The symbol W represents the Warburg diffusion coefficient, while Q denotes the constant phase element[50].

Table 2. DEIS data obtained by Nyquist plot fitting of charging process in control system.

V (V)	R_{int} (Ω)	R_{ct} (Ω)	R_{CEI} (Ω)	$R_{pre\text{-}diff}$ (Ω)	$R_{com\text{-}diff}$ (Ω)	W ($\Omega s^{-1/2}$)	chi2
2.8V	2.001	11.77	3846	43.38	0.9688	0.02926	1.36E-05
2.89V	1.179	10.34	306.5	42.61	0.4647	6.37E-13	4.07E-05
2.99V	2.481	13.32	148.3	48	9.958	3.47E-08	5.25E-04
3.08V	1.644	27.33	6.42E+12	66.91	0.3532	7.88E-08	1.16E-04
3.17V	2.446	3493	13.52	42.54	10.42	0.01183	8.44E-04
3.27V	2.484	49.19	0.5349	10.64	0.123	1.48E-09	6.63E-04
3.36V	1.378	9.461	44.66	9.701	3.63E+04	3.63E+04	2.96E-05
3.45V	2.066	46.23	0.8308	10.84	4532	1.94E+05	1.97E-05
3.55V	2.171	10.97	44.7	0.6094	761.8	17.42	1.26E-05
3.64V	2.093	0.7401	45.22	10.63	70.85	0.04789	1.06E-05
3.73V	2.063	40.6	10.2	0.7738	16.5	0.2738	1.03E-05
3.82V	1.705	7.978	19.29	18.99	20.33	1.49E-05	9.62E-05
3.92V	1.929	5.956	0.9488	1.635	8.855	0.7198	3.01E-05
4.01V	1.91	8.57E+06	5.363	8.719	3.63E+19	6.30E+13	1.02E-04
4.1V	1.911	6.03	7.514	1.48E+10	0.2435	0.7558	8.01E-05
4.2V	1.831	5.058	9.19	1.98E+06	2685	0.00211	1.04E-04

Table 3. DEIS data obtained by Nyquist plot fitting of discharging process in control system.

V (V)	R_{int} (Ω)	R_{ct} (Ω)	R_{CEI} (Ω)	$R_{pre-diff}$ (Ω)	$R_{com-diff}$ (Ω)	W ($\Omega s^{-1/2}$)	chi2
2.8V	1.975	37.85	1.117	11.73	1.83E+04	2.45E+04	4.30E-05
2.89V	1.722	11.36	1.56E+00	34.21	6372	1.825	4.76E-05
2.99V	2.316	31.68	4.513	13.88	1.06E+04	0.01326	3.67E-05
3.08V	1.813	1.233	33.93	11.77	3432	1.07E-01	2.22E-05
3.17V	0.1209	5.098	2177	1.81	1.654	7.11E+02	7.00E-05
3.27V	4.378	77.12	10.93	29.82	1096	1.52E+08	5.73E-04
3.36V	0.05391	32.1	10.03	8.643	0.2673	0.004565	5.53E-05
3.45V	2.34	26.36	368.7	15.22	153.2	5.12E-09	5.46E-04
3.55V	1	23.9	2.952	11.72	63.97	3.61E-01	3.34E-04
3.64V	2.064	0.7363	11.26	21.92	9.277	1.87E+16	7.33E-05
3.72V	1.657	3.051	8.002	14.54	0.1727	8.85E+03	2.02E-04
3.82V	2.334	3.602	2.51	11.16	787.9	5.15E-13	8.95E-04
3.92V	1.929	5.554	11.97	24.91	0.03461	1.14E+14	1.34E-04
4.01V	1.855	0.4123	10.05	5.934	0.01174	1.10E-03	9.06E-05
4.1V	1.816	5.853	0.3785	9.492	6.14E+04	5.84E+09	8.51E-05
4.2V	0.3467	5.324	1.651	9.418	9.195	2.32E+06	1.06E-04

Table 4. DEIS data obtained by Nyquist plot fitting of charging process in EGMB electrolyte.

V (V)	R_{int} (Ω)	R_{ct} (Ω)	R_{CEI} (Ω)	$R_{pre\text{-}diff}$ (Ω)	$R_{com\text{-}diff}$ (Ω)	W ($\Omega s^{-1/2}$)	chi2
2.8V	1.373	8.32	20.23	2.47E+04	4.11E+03	18.69	5.83E-05
2.89V	1.393	8.21	21.34	1.65E+06	6.56E+03	7.88E+04	6.60E-05
2.99V	2.308	9.509	29.89	0.06208	0.02387	2.74E-10	1.12E-04
3.08V	1.367	8.229	20.95	1.54E+08	5191	7.48E+04	6.39E-05
3.17V	1.266	4446	21.59	7.919	6.76E-01	2.86E-20	8.06E-05
3.27V	1.404	8.048	21.54	4398	1.66E-02	3.49E-05	6.10E-05
3.36V	2.233	11.6	25.99	20.42	2.59E+03	2.26E+06	5.48E-04
3.45V	2.237	20.6	11.4	8.67E+11	5.08E+02	5.80E-03	5.40E-04
3.55V	2.058	9.418	24.07	0.5354	4.34E+01	5.40E-09	4.58E-05
3.64V	2.094	9.39	22.99	27.75	4.89E-01	6.34E-02	1.68E-05
3.73V	1.696	7.037	12.73	26.54	1.52E-01	2.21E-06	1.87E-04
3.82V	2.227	3.782	10.1	5.686	3.44E+14	3.32E-05	5.91E-04
3.92V	1.647	6.597	3.08	3.833	1.01E+03	7.84E-05	7.62E-05
4.01V	2.162	7.9	0.9807	1.023	1.476	9.63E-01	2.41E-05
4.1V	1.878	5.667	0.28	5.419	1.87E+03	1.48E+01	5.94E-05
4.2V	1.763	0.6732	1.031	5.568	3.51E+00	7.54E-01	4.69E-05

Table 5. DEIS data obtained by Nyquist plot fitting of discharging process in EGMB electrolyte.

V (V)	R_{int} (Ω)	R_{ct} (Ω)	R_{CEI} (Ω)	$R_{pre-diff}$ (Ω)	$R_{com-diff}$ (Ω)	W ($\Omega s^{-1/2}$)	chi2
2.8V	1.099	7.572	17.95	5135	9.96E+04	1.76E-16	1.83E-04
2.89V	1.066	7.555	16.60	3030	710.1	1.44E-09	8.23E-05
2.99V	2.173	14.73	11.11	28.39	2545	3.63E+04	4.18E-04
3.08V	1.938	19.32	9.087	1128	0.8303	2.40E-02	1.99E-05
3.17V	1.955	9.021	20.49	8.93E+19	0.3139	1.98E-10	2.20E-04
3.27V	1.716	10.82	14.09	8.23E+04	1.94E+04	2.25E-03	5.15E-05
3.36V	2.237	12.02	18.16	1.00E+16	0.01306	3.53E-05	3.17E-04
3.45V	2.006	8.078	20.21	0.7349	1675	2.49E+06	8.37E-05
3.55V	1.126	8.599	13.09	89.11	0.006537	4.01E-10	2.67E-04
3.64V	1.977	10.94	7.886	0.7534	11.27	1.00E+20	1.32E-04
3.72V	1.931	8.189	0.5899	2.891	4.339	2.96E+00	3.51E-05
3.82V	1.927	8.574	0.01	10.51	6.056	8.83E+13	1.33E-04
3.92V	1.444	4.582	142.3	7.818	3.32E+04	1.09E-03	1.24E-04
4.01V	0.2312	5.673	2.027	6.231	106.2	9.65E+03	6.57E-05
4.1V	1.813	10.58	7.495	4.526	3.25	4.22E-06	1.20E-04
4.2V	1.86	5.827	0.2911	5.25	9.666	9.05E+06	6.44E-05

Figure 26g presents R_{CEI}, obtained from fitted results under various potentials during the charging and discharging processes. The fitted data result of R_{CEI} in the control system exhibits significant value fluctuations across both processes, driven by the persistent decomposition and reformation of the CEI. The instability of CEI not only induces the overgrowth of layer, but also exposes the underlying cathodic active material to the decomposed electrolyte with acidic components such as HF. This exposure can potentially lead to further degradation or other negative effects on the system. In contrast, the boron-rich CEI formed using EGMB demonstrates superior stability and exhibits a relatively low resistance value, offering robust

protection to the CAM against TM dissolution. The SEM images of NMC111 surface after cycled in cathodic half-cells for 100 times with different electrolytes are shown in **Figure 26h and 26i**. The SEM of the control system shows numerous signs of etching correlating with degraded CEI performance and significant capacity loss. In comparison, the NMC111 in EGMB electrolyte demonstrates better integrity of surface. In the evaluation of TM dissolution, the percentage of Ni, Co and Mn in commercial electrolyte is 3 times higher than EGMB electrolyte, as depicted in **Figure 26j**. This finding underscores the critical role of EGMB in forming an effective and robust interface that mitigates TM loss.

Compared to the relatively straightforward degradation caused by lattice oxygen release under high voltage conditions, improving battery performance under extreme fast charging and discharging typically necessitates a redesign of the electrolyte to enhance various properties critical to the lithium-ion transfer process, including ionic conductivity, polarity, transference number, solvation structure, and so on[51-55]. In this study, EGMB, used as a sacrificial additive at a concentration of 2 mg/ml (0.16 wt%), is primarily oxidized during the CEI formation process in the initial cycles, resulting in only a small residual amount in the electrolyte. This negligible residue does not significantly affect the electrolyte's properties, meaning that the electrolyte's characteristics remain largely unchanged. Consequently, the addition of EGMB does not substantially increase the charge and discharge capacity of NMC111 under high-rate conditions. Therefore, the purpose of applying EGMB under extreme high-rate conditions is not aimed at meeting the U.S. Department of Energy's objective of achieving 'Extreme Fast Charging' (XFC)—charging to 80% capacity in 15 minutes or less. The primary role of EGMB in Li||NMC111 cells is to protect transition metals, thereby reducing the dissolution of active material particles and mitigating capacity degradation. However, EGMB can be used in conjunction with other electrolyte designs to improve the durability of NMC materials.

3.3.5 Studies on NMC111 cathode with wide temperature range

Given the wide range of climate variability, understanding how rechargeable lithium batteries adapt to extreme conditions has become a key area of research[56]. In particular, applications that require reliable battery performance in extreme temperatures, such as subsurface exploration, emergency rescue missions, and etc. have driven interest in developing more resilient rechargeable lithium batteries. This challenge is present in both aqueous and nonaqueous RLB systems. At low temperatures, batteries experience significant obstacles due to slowed ion transfer at the interface[57]. This results in increased impedance and polarization, leading to sharp declines in capacity. In more severe cases, electrolyte freezing or the precipitation of lithium salts can obstruct ion transport, causing internal open circuits and ultimately leading to battery failure[58]. Conversely, at high temperatures (HT), while the electrochemical reaction kinetics of the electrode materials are enhanced, this can also exacerbate undesirable side reactions, potentially causing gas accumulation and posing serious safety risks.

The Li||NMC111 cathodic half-cell was further used to assess the effectiveness of the EGMB-modified electrolyte under both low (0 °C) and high (60 °C) temperatures. As shown in **Figure 27a**, the cells were initially cycled at 20 °C at a C/3 rate. The initial discharge capacity was taken as the baseline value to evaluate capacity retention during subsequent discharge cycles. As the temperature was reduced to 0 °C, the capacity retention of both cells decreased. Under low temperature conditions, the batteries experience hindered interfacial ion transfer, leading to increased overall impedance and interface polarization, which result in a sharp decline in battery capacity. However, the cell with the EGMB-modified electrolyte maintained a higher retention of 84.0%, compared to 80.7% for the conventional electrolyte. This modest improvement in discharge capacity is attributed to the enhanced ionic conductivity of CEI due to the abundant B–O bonds. Although the dynamics of the bulk electrolyte were

not significantly enhanced due to the minimal applied amount of EGMB, its benefits to the lithium-ion transference capability within the CEI contributed to better discharge performance at low temperatures. As the temperature was raised back to 20 °C and further increased to 60 °C, the capacity retention of the EGMB-modified electrolyte consistently remained higher than that of the conventional electrolyte.

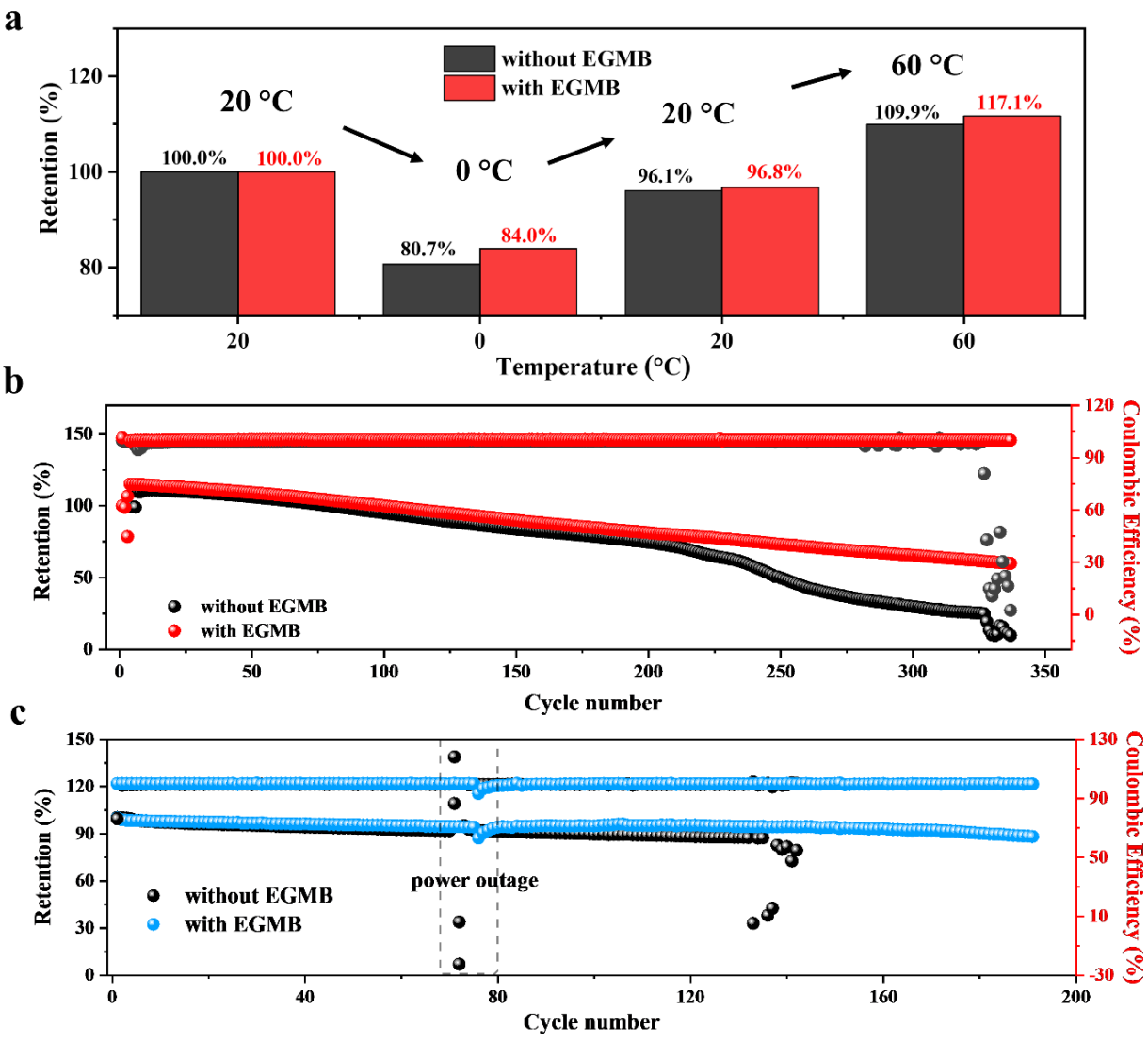

Figure 27. Electrochemical studies on Li||NMC111 cathodic half-cell with different electrolytes under wide temperature range. (a) The discharge retention at C/3 rate under wide temperature range. Both charging and discharging process were conducted from 20 °C, 0 °C, 20 °C, and to 60 °C. long term cycling stability at C/3 rate at (b) 60 °C and (C) 0 °C.

The long-term cycling performance of Li||NMC111 cathodic half-cells was evaluated at 60 °C and 0 °C to investigate the impact of EGMB across a broad temperature range. In **Figure 27b**, the capacity retention of the cell with the commercial electrolyte declines sharply after 200 cycles, ultimately failing by the 337th cycle with a remaining capacity of 9.7 mAh/g and a coulombic efficiency of 2.48%. This is attributed to high temperature accelerating side reactions at the electrolyte–electrode interface, including transition metal ion dissolution, gas evolution, and CEI decomposition and regeneration. These accelerated reactions increase thermal risks and are closely related to the thermodynamics and kinetics of the CEI. In contrast, the cell with the EGMB-containing electrolyte exhibits resistance to rapid degradation, retaining a capacity of 60.2 mAh/g and a coulombic efficiency of 99.91%. Due to the significant modification of the CEI by EGMB, both durability was extended and coulombic efficiency was improved under 60 °C high temperature condition. The cyclability of Li||NMC111 at 0 °C is shown in **Figure 27c**. Under low temperature conditions, capacity decay was significantly reduced due to the slowdown of side reactions. However, in the cell with commercial electrolyte, electrolyte freezing, or lithium salt precipitation obstructed ion transport, leading to internal open circuits and eventual battery failure, with the cell abruptly failing after 136 cycles at 0 °C. In contrast, the cell with the EGMB-modified electrolyte maintained a discharge capacity of 88.20 mAh/g and a coulombic efficiency of 99.67%.

Under three different extreme conditions, capacity degradation was significantly reduced in both Li||NMC811 and Li||NMC111 cathodic half-cells with the trace addition of 2 mg/ml EGMB. As a sacrificial additive in the electrolyte, EGMB is largely oxidized and participates in the formation of the CEI, which enhances ionic conductivity and stability. Although the enhancement of the CEI by EGMB provides modest improvements in rate capacity, the minimal residual EGMB means that the bulk electrolyte's properties—such as lithium transference ability for high-rate charging and freezing point at low temperatures—remain

largely unchanged. Therefore, the primary role of EGMB is not to significantly increase high-rate capacity but to improve the stability and cyclability of NMC cathodes under extreme conditions, preventing rapid capacity decay and sudden failure. The application of EGMB in both NMC811 and NMC111 cathodic half-cells demonstrated improved durability under ultrahigh voltage, extreme high rates, 60 °C high temperatures, and 0 °C low temperatures. This underscores EGMB's effectiveness in reducing the degradation of cathodic active materials and mitigating side reactions. Given that EGMB is used in a very small amount (0.16 wt%), it can be combined with other electrolyte design strategies to address the challenges faced by rechargeable lithium batteries under extreme conditions.

3.4 Conclusion

In conclusion, the addition of EGMB to the traditional carbonate electrolyte facilitates the formation of a boron-rich, robust CEI with low and stable impedance. The abundant B–O bonds formed from EGMB oxidation in the CEI not only stabilize transition metals but also prevent the release of reactive lattice oxygen, thereby mitigating side reactions. Additionally, the B–F bonds help eliminate HF from the electrolyte, further protecting transition metals from corrosion. These enhancements provided by EGMB result in the following improvements in battery electrochemical performance: (1) Increased the capacity of Li||NMC811 from 1.51 mAh/g to 77.67 mAh/g at a 1C rate under a 4.8 V ultrahigh cut-off voltage; (2) Improved the capacity retention of Li||NMC111 from 19.04% to 45.57% after 200 cycles under 4C extreme high-rate charging-discharging conditions; (3) Enhanced the capacity from 9.7 mAh/g with a coulombic efficiency of 2.48% to 60.2 mAh/g with a coulombic efficiency of 99.91% at 60 °C; and (4) Prevented sudden failure at 0 °C. Therefore, EGMB can be regarded as a potent additive for NMC-based cathodes, contributing to the development of next-generation batteries capable of withstanding various extreme conditions.

Reference

(1) Li, W., Erickson, E.M. & Manthiram, A. High-nickel layered oxide cathodes for lithium-based automotive batteries. *Nat. Energy* **2020**, *5* (1), 26–34.

(2) Liu, J., Bao, Z., Cui, Y., Dufek, E. J., Goodenough, J. B., Khalifah, P., ... & Zhang, J. G. Pathways for practical high-energy long-cycling lithium metal batteries. *Nat. Energy* **2019**, *4* (3), 180-186.

(3) Wu, F., Maier, J., & Yu, Y.. Guidelines and trends for next-generation rechargeable lithium and lithium-ion batteries. *Chem. Soc.Rev.* **2020**, *49* (5), 1569-1614.

(4) Feng, Y., Zhou, L., Ma, H., Wu, Z., Zhao, Q., Li, H., ... & Chen, J. Challenges and advances in wide-temperature rechargeable lithium batteries. *Energ. Environ. Sci.* **2022**, *15* (5), 1711-1759.

(5) Hou, J., Yang, M., Wang, D., & Zhang, J. Fundamentals and challenges of lithium ion batteries at temperatures between −40 and 60° C. *Adv. Ener. Mater.* **2020**, *10* (18), 1904152.

(6) Ahmed, S., Bloom, I., Jansen, A. N., Tanim, T., Dufek, E. J., Pesaran, A., ... & Zhang, J. Enabling fast charging–A battery technology gap assessment. *J. Power Sources* **2017**, *367*, 250-262.

(7) Weiss, M., Ruess, R., Kasnatscheew, J., Levartovsky, Y., Levy, N. R., Minnmann, P., ... & Janek, J. Fast charging of lithium-ion batteries: a review of materials aspects. *Adv. Ener. Mater.* **2021**, *11* (33), 2101126.

(8) Wang, C. Y., Liu, T., Yang, X. G., Ge, S., Stanley, N. V., Rountree, E. S., ... & McCarthy, B. D. Fast charging of energy-dense lithium-ion batteries. *Nature* **2022**, *611* (7936), 485-490.

(9) Li, G., Li, Z., Cai, Q., Yan, C., Xing, L., & Li, W. Construction of Low-Impedance and High-Passivated Interphase for Nickel-Rich Cathode by Low-Cost Boron-Containing Electrolyte Additive. *ChemSusChem* **2022**, *15* (11), e202200543.

(10) Li, T., Yuan, X. Z., Zhang, L., Song, D., Shi, K., & Bock, C. Degradation Mechanisms and Mitigation Strategies of Nickel-Rich NMC-Based Lithium-Ion Batteries. *Electrochem. Energ. Rev.* **2020**, *3*, 43–80.

(11) Markevich, E.; Salitra, G.; Aurbach, D. Fluoroethylene Carbonate as an Important Component for the Formation of an Effective Solid Electrolyte Interphase on Anodes and Cathodes for Advanced Li-Ion Batteries. *ACS Ener. Lett.* **2017**, pp 1337–1345.

(12) Lu, S. Q., Guo, S. J., Qi, M. Y., Li, J. Y., Cao, A. M., & Wan, L. J. Precise surface control of cathode materials for stable lithium-ion batteries. *Chem. Commun.* **2022**., *58* (10), 1454-1467.

(13) Ma, L., Tan, J., Wang, Y., Liu, Z., Yang, Y., Gray, T., ... & Shen, J. Boron-Based High-Performance Lithium Batteries: Recent Progress, Challenges, and Perspectives. *Adv. Ener. Mater.* **2023**, *13* (25), 2300042.

(14) Ma, L., Tan, J., Ren, Z., Feng, B., Liu, Z., Yi, P., ... & Shen, J. Designing Bilayer Heterostructure Functional Polymer Electrolytes with Interfacial Engineering Strategy for High-Performance Lithium Metal Batteries. *Adv. Funct. Mater.* **2024**, 2414816.

(15) Joshi, P., Vedarajan, R., & Matsumi, N. A crystalline low molecular weight cyclic organoboron compound for efficient solid state lithium-ion transport. *Chem. comm.* **2015**, *51* (81), 15035-15038.

(16) Li, J., Yang, J., Ji, Z., Su, M., Li, H., Wu, Y., ... & Zhang, Z. Prospective Application, Mechanism, and Deficiency of Lithium Bis (oxalate) Borate as the Electrolyte Additive for Lithium-Batteries. *Adv. Ener. Mater.* **2023**, *13* (35), 2301422.

(17) Li, W., He, Z., Jie, Y., Huang, F., Chen, Y., Wang, Y., ... & Jiao, S. Understanding and Design of Cathode–

Electrolyte Interphase in High-Voltage Lithium–Metal Batteries. *Adv. Func. Mater.* **2024**, 2406770.

(18) Lei, Y., Wang, K., Jiang, S., Xu, X., Zheng, J., Yin, J., & Gao, Y. Recent Progress on Multifunctional Electrolyte Additives for High-Energy-Density Li Batteries–A Review. *ChemElectroChem* **2024**, e202300702.

(19) Yue, H., Yang, Y., Xiao, Y., Dong, Z., Cheng, S., Yin, Y., ... & Yang, S. Boron additive passivated carbonate electrolytes for stable cycling of 5 V lithium–metal batteries. *Journal of Materials Chemistry A* **2019**, *7* (2), 594-602.

(20) Li, G., Li, Z., Cai, Q., Yan, C., Xing, L., & Li, W. Construction of Low-Impedance and High-Passivated Interphase for Nickel-Rich Cathode by Low-Cost Boron-Containing Electrolyte Additive. *ChemSusChem* **2022**, *15*(11), e202200543.

(21) Jung, R.; Metzger, M.; Maglia, F.; Stinner, C.; Gasteiger, H. A. Oxygen Release and Its Effect on the Cycling Stability of $LiNi_xMn_yCo_zO_2$ (NMC) Cathode Materials for Li-Ion Batteries. *J. Electrochem. Soc.* **2017**, *164* (7), A1361– A1377

(22) Freiberg, A. T. S.; Roos, M. K.; Wandt, J.; De Vivie-Riedle, R.; Gasteiger, H. A. Singlet Oxygen Reactivity with Carbonate Solvents Used for Li-Ion Battery Electrolytes. *J. Phys. Chem. A* **2018**, *122* (45), 8828– 8839.

(23) Jung, R.; Metzger, M.; Maglia, F.; Stinner, C.; Gasteiger, H. A. Chemical versus Electrochemical Electrolyte Oxidation on NMC111, NMC622, NMC811, LNMO, and Conductive Carbon. *J. Phys. Chem. Lett.* **2017**, *8* (19), 4820– 4825.

(24) Dose, W. M., Li, W., Temprano, I., O'Keefe, C. A., Mehdi, B. L., De Volder, M. F., & Grey, C. P. Onset potential for electrolyte oxidation and Ni-rich cathode degradation in lithium-ion batteries. *ACS Ener. Lett.* **2022**, *7* (10), 3524-3530.

(25) Wandt, J.; Freiberg, A. T. S.; Ogrodnik, A.; Gasteiger, H. A. Singlet Oxygen Evolution from Layered Transition Metal Oxide Cathode Materials and Its Implications for Lithium-Ion Batteries. *Mater. Today* **2018**, *21* (8), 825– 833, DOI: 10.1016/j.mattod.2018.03.037

(26) Jayawardana, C.; Rodrigo, N.; Parimalam, B.; Lucht, B. L. Role of Electrolyte Oxidation and Difluorophosphoric Acid Generation in Crossover and Capacity Fade in Lithium Ion Batteries. *ACS Ener. Lett.* **2021**, *6* (11), 3788– 3792, DOI: 10.1021/acsenergylett.1c01657

(27) Wiemers-Meyer, S.; Winter, M.; Nowak, S. Mechanistic Insights into Lithium Ion Battery Electrolyte Degradation-a Quantitative NMR Study. *Phys. Chem. Chem. Phys.* **2016**, *18* (38), 26595– 26601, DOI: 10.1039/C6CP05276B

(28) Metzger, M.; Strehle, B.; Solchenbach, S.; Gasteiger, H. A. Origin of H_2 Evolution in LIBs: H 2 O Reduction vs. Electrolyte Oxidation. *J. Electrochem. Soc.* **2016**, *163* (5), A798– A809, DOI: 10.1149/2.1151605jes

(29) Zhang, Z.; Hu, L.; Wu, H.; Weng, W.; Koh, M.; Redfern, P. C.; Curtiss, L. A.; Amine, K. Fluorinated Electrolytes for 5 v Lithium-Ion Battery Chemistry. *Energy Environ. Sci.* **2013**, *6* (6), 1806–1810. https://doi.org/10.1039/c3ee24414h.

(30) He, W., Guo, W., Wu, H., Lin, L., Liu, Q., Han, X., ... & Peng, D. L. Challenges and recent advances in high capacity Li-rich cathode materials for high energy density lithium-ion batteries. *Adv. Mater.* **2021**, *33*(50), 2005937.

(31) Okubo, M., Ko, S., Dwibedi, D., & Yamada, A. Designing positive electrodes with high energy density for lithium-ion batteries. *J. Mater. Chem. A* **2021**, *9*(12), 7407-7421.

(32) Lu, Y., & Chen, J. Prospects of organic electrode materials for practical lithium batteries. *Nat. Rev. Chem.* **2020**,

4 (3), 127-142. https://doi.org/10.1016/j.isci.2022.104910.

(33) Rosenbach, D.; Krimalowski, A.; Erabhoina, H.; Thelakkat, M. Solid Polymer Electrolytes from Polyesters with Diester Sidechains for Lithium Metal Batteries. *J. Mater. Chem. A* **2022**, *10* (16), 8932–8947. https://doi.org/10.1039/D2TA00800A.

(34) Zhao, S., Guo, Z., Yan, K., Wan, S., He, F., Sun, B., & Wang, G. Towards high-energy-density lithium-ion batteries: Strategies for developing high-capacity lithium-rich cathode materials. *Energy Storage Mater.* **2021**, *34*, 716-734.

(35) Li, Y.; Veith, G. M.; Browning, K. L.; Chen, J.; Hensley, D. K.; Paranthaman, M. P.; Dai, S.; Sun, X.-G. Lithium Malonatoborate Additives Enabled Stable Cycling of 5 V Lithium Metal and Lithium Ion Batteries. *Nano Energy* **2017**, *40*, 9–19. https://doi.org/10.1016/j.nanoen.2017.07.051.

(36) Sun, X. G., Wan, S., Guang, H. Y., Fang, Y., Reeves, K. S., Chi, M., & Dai, S. New promising lithium malonatoborate salts for high voltage lithium ion batteries. *J. Mater. Chem. A* **2017**, *5*(3), 1233-1241.

(37) Yi, M., Sim, R., & Manthiram, A. Electrolyte-Enabled High-Voltage Operation of a Low-Nickel, Low-Cobalt Layered Oxide Cathode for High Energy Density Lithium-Ion Batteries. *Small* **2024**, 2403429.

(38) Xue, W., Huang, M., Li, Y., Zhu, Y. G., Gao, R., Xiao, X., ... & Li, J. Ultra-high-voltage Ni-rich layered cathodes in practical Li metal batteries enabled by a sulfonamide-based electrolyte. *Nat. Energy* **2021**, *6* (5), 495-505.

(39) Li, G.; Liao, Y.; Li, Z.; Xu, N.; Lu, Y.; Lan, G.; Sun, G.; Li, W. Constructing a Low-Impedance Interface on a High-Voltage $LiNi_{0.8}Co_{0.1}Mn_{0.1}O_2$ Cathode with 2,4,6-Triphenyl Boroxine as a Film-Forming Electrolyte Additive for Li-Ion Batteries. *ACS Appl. Mater. Interfaces* **2020**, *12* (33), 37013–37026. https://doi.org/10.1021/acsami.0c05623.

(40) Li, J.; Liao, Y.; Fan, W.; Li, Z.; Li, G.; Zhang, Q.; Xing, L.; Xu, M.; Li, W. Significance of Electrolyte Additive Molecule Structure in Constructing Robust Interphases on High-Voltage Cathodes. *ACS Appl. Ener. Mater.* **2020**, *3* (3), 3049–3058. https://doi.org/10.1021/acsaem.0c00168.

(41) Feng, Y.; Qi, R.; Jiang, L.; Huang, Q.; Li, T.; Liu, G.; Li, W.; Yan, W.; Zhang, Z.; Wang, Z. Chemical modification of B_4C films and B_4C/Pd layers stored in different environments. *Materials* **2021**, *14*, 1319– 1330, DOI: 10.3390/ma14051319

(42) Sun, Z., Li, F., Ding, J., Lin, Z., Xu, M., Zhu, M., & Liu, J. High-voltage and high-temperature $LiCoO_2$ operation via the electrolyte additive of electron-defect boron compounds. *ACS Ener. Lett.* **2023**, *8* (6), 2478-2487.

(43) Streich, D.; Erk, C.; Guéguen, A.; Müller, P.; Chesneau, F. F.; Berg, E. J. Operando Monitoring of Early Ni-Mediated Surface Reconstruction in Layered Lithiated Ni-Co-Mn Oxides. *J. Phys. Chem. C* **2017**, *121* (25), 13481– 13486, DOI: 10.1021/acs.jpcc.7b02303

(44) Zhan, C.; Wu, T.; Lu, J.; Amine, K. Dissolution, Migration, and Deposition of Transition Metal Ions in Li-Ion Batteries Exemplified by Mn-Based Cathodes–a Critical Review. *Energy Environ. Sci.* **2018**, *11* (2), 243– 257, DOI: 10.1039/C7EE03122J

(45) Rinkel, B. L. D.; Hall, D. S.; Temprano, I.; Grey, C. P. Electrolyte Oxidation Pathways in Lithium-Ion Batteries. *J. Am. Chem. Soc.* **2020**, *142* (35), 15058– 15074, DOI: 10.1021/jacs.0c06363

(46) Tomaszewska, A.; Chu, Z.; Feng, X.; O'Kane, S.; Liu, X.; Chen, J.; Ji, C.; Endler, E.; Li, R.; Liu, L. Lithium-ion Battery Fast Charging: A review. *ETransportation* **2019**, *1*, 100011, DOI: 10.1016/j.etran.2019.100011

(47) Pradhan, A.; Badam, R.; Miyairi, R.; Takamori, N.; Matsumi, N. Extreme Fast Charging Capability in Graphite Anode via a Lithium Borate Type Biobased Polymer as Aqueous Polyelectrolyte Binder. *ACS Mater. Lett.* **2023**,

5 (2), 413–420. https://doi.org/10.1021/acsmaterialslett.2c00999.

(48) Sun, H. H.; Dolocan, A.; Weeks, J. A.; Rodriguez, R.; Heller, A.; Mullins, C. B. In Situ Formation of a Multicomponent Inorganic-Rich SEI Layer Provides a Fast Charging and High Specific Energy Li-Metal Battery. *J. Mater. Chem. A* **2019**, *7* (30), 17782–17789.

(49) Patra, A., & Matsumi, N. Densely Imidazolium Functionalized Water Soluble Poly (Ionic Liquid) Binder for Enhanced Performance of Carbon Anode in Lithium/Sodium-Ion Batteries. *Adv. Energy Mater.* **2024**, 2403071.

(50) Shi, Q.; Heng, S.; Qu, Q.; Gao, T.; Liu, W.; Hang, L.; Zheng, H. Constructing an Elastic Solid Electrolyte Interphase on Graphite: A Novel Strategy Suppressing Lithium Inventory Loss in Lithium-ion Batteries. *J. Mater. Chem. A* **2017**, *5* (22), 10885– 10894, DOI: 10.1039/C7TA02706K

(51) Colclasure, A. M., Dunlop, A. R., Trask, S. E., Polzin, B. J., Jansen, A. N., & Smith, K. Requirements for enabling extreme fast charging of high energy density Li-ion cells while avoiding lithium plating. *Journal of the electrochemical society* **2019**, *166* (8), A1412.

(52) Diederichsen, K. M., McShane, E. J., & McCloskey, B. D. Promising routes to a high Li+ transference number electrolyte for lithium ion batteries. *ACS Ener. Lett.* **2017**, *2* (11), 2563-2575.

(53) Logan, E. R., & Dahn, J. R. Electrolyte design for fast-charging Li-ion batteries. *Trends in Chemistry* **2020**, *2*(4), 354-366.

(54) Billaud, J., Bouville, F., Magrini, T., Villevieille, C., & Studart, A. R. Magnetically aligned graphite electrodes for high-rate performance Li-ion batteries. *Nat. Energy* **2016**, *1*(8), 1-6.

(55) Chen, K. H., Namkoong, M. J., Goel, V., Yang, C., Kazemiabnavi, S., Mortuza, S. M., ... & Dasgupta, N. P. Efficient fast-charging of lithium-ion batteries enabled by laser-patterned three-dimensional graphite anode architectures. *J. Power Sources* **2020**, *471*, 228475.

(56) Feng, Y., Zhou, L., Ma, H., Wu, Z., Zhao, Q., Li, H., ... & Chen, J. Challenges and advances in wide-temperature rechargeable lithium batteries. *Energy Environ. Sci.* **2022**, *15* (5), 1711-1759.

(57) Lin, X., Salari, M., Arava, L. M. R., Ajayan, P. M., & Grinstaff, M. W. High temperature electrical energy storage: advances, challenges, and frontiers. *Chem. Soc. Rev.* **2016**, *45* (21), 5848-5887.

(58) Hou, J., Yang, M., Wang, D., & Zhang, J. Fundamentals and challenges of lithium ion batteries at temperatures between− 40 and 60° C. *Adv. Ener. Mater.* **2020**, *10*(18), 1904152.

Chapter 4 Conclusion

This thesis focuses on addressing critical challenges in lithium-ion battery (LIB) performance by advancing electrolyte engineering, with a particular emphasis on the inclusion of boron-containing additives. Through a systematic investigation into the relationship between electrolyte composition, interfacial stability, and ionic transport, this work contributes to the development of more durable, efficient, and versatile LIBs. The findings across the three chapters collectively highlight the transformative potential of boron chemistry in tackling long-standing limitations such as high-voltage degradation, interfacial instability, and insufficient ionic conductivity.

The first chapter identifies the inherent limitations of conventional LIB cathodes, particularly high-energy-density materials like $LiNi_{0.33}Mn_{0.33}Co_{0.33}O_2$ (NMC111) and Ni-rich variants such as NMC811. While these materials offer promising energy densities, they are hindered by challenges such as metal dissolution, surface reactions, and structural instability during cycling at elevated voltages. This analysis sets the stage for exploring innovative electrolyte formulations to improve cathode durability and performance.

In the second chapter, mesityldimethoxyborane (MDMB) is introduced as a solvent component for enhancing LIB electrolyte performance. This compound was designed to address interfacial degradation by facilitating the formation of a boron-rich cathode-electrolyte interphase (CEI). MDMB also plays a key role in optimizing lithium-ion transport by modifying the solvation environment within the electrolyte, resulting in reduced resistance and improved ion mobility. The experimental findings demonstrate that MDMB significantly enhances discharge capacity and cycle stability, particularly under high-rate cycling conditions. Insights from computational studies provided further understanding of the molecular mechanisms underlying these improvements, validating MDMB's role as a multifunctional additive.

The third chapter builds on this foundation by introducing ethylene glycol-mesitylborane

(EGMB), a more advanced boron-containing additive tailored for challenging operating conditions. Unlike MDMB, EGMB incorporates additional fluorine functionality, which promotes the formation of a robust, fluorine-enriched CEI. This enhanced interphase minimizes detrimental reactions at the cathode surface, mitigates transition metal dissolution, and improves the mechanical resilience of the interfacial layer. EGMB-containing electrolytes demonstrated superior performance at ultrahigh voltages, fast cycling rates, and across a wide temperature range, highlighting their potential for demanding applications such as electric vehicles and energy storage systems.

A key takeaway from this thesis is the ability of boron additives not only to stabilize the cathode surface but also enhance the overall efficiency of the LIB system by improving lithium-ion conductivity and reducing interfacial resistance. By systematically designing and evaluating MDMB and EGMB, this work provides a clear pathway for addressing both short-term degradation and long-term stability concerns in LIBs.

Importantly, this research moves beyond theoretical insights and experimental validation by offering a practical framework for implementing boron-based additives in practical applications. The findings underscore the importance of tailoring electrolyte formulations to meet specific performance criteria, whether for improving high-rate capabilities, enhancing voltage stability, or extending operational temperature ranges.

Future directions for this research could include extending these strategies to other cathode chemistries or exploring the synergistic effects of combining boron additives with other functional components. Moreover, integrating advanced characterization methods with machine learning tools could accelerate the discovery and optimization of new electrolyte formulations, paving the way for even greater performance gains in LIBs.

In conclusion, this thesis establishes the potential of boron-containing electrolyte components as a game-changing solution for addressing some of the most pressing challenges

in LIB technology. By enhancing the stability of the cathode-electrolyte interphase and improving ionic transport, MDMB and EGMB exemplify the promise of chemistry-driven innovation in advancing energy storage systems. These findings mark an important step toward the realization of high-performance, reliable, and scalable LIBs capable of supporting the growing global demand for sustainable energy technologies.